

Aus der Abteilung für Klinische Pharmakologie

Direktor: Prof. Dr. med. S. Endres

Medizinische Klinik und Poliklinik IV

Klinikum der Universität

Ludwig-Maximilians-Universität München

Direktor: Prof. Dr. med. M. Reincke

**Identification and characterization of activators and modulators
in the antiviral RIG-I-like receptor pathway**

Dissertation

zum Erwerb des Doktorgrades der Humanbiologie

an der Medizinischen Fakultät der

Ludwig-Maximilians-Universität zu München



vorgelegt von

Viktoria Bothe

aus Altdöbern

2019

Mit Genehmigung der Medizinischen Fakultät
der Universität München

1. Berichterstatter: Prof. Dr. med. Simon Rothenfuß

Mitberichterstatte: Prof. Dr. rer. nat Reinhard Zeidler
Prof. Dr. med. Michael Hölscher
Prof. Dr. rer. nat. Karl-Klaus Conzelmann

Mitbetreuung durch die
promovierten Mitarbeiter: Dr. rer. biol. hum. Dharmendra Pandey

Dekan: Prof. Dr. med. dent. Reinhard Hickel

Tag der mündlichen Prüfung: 18.11.2019

Erklärung nach § 7 Abs. 4 der Promotionsordnung vom 16. Juli 2010

Hiermit versichere ich, dass diese Dissertation selbstständig angefertigt wurde, ich mich außer den angegebenen Hilfsmitteln keiner weiteren bedient habe und alle Erkenntnisse, die aus dem Schrifttum ganz oder annähernd übernommen wurden, als solche kenntlich gemacht und nach ihrer Herkunft unter Bezeichnung der Fundstelle einzeln nachgewiesen sind.

Des Weiteren versichere ich, dass die hier vorgelegte Dissertation nicht in gleicher oder in ähnlicher Form bei einer anderen Stelle zur Erlangung eines akademischen Grades eingereicht wurde.

München, den 04.06.2019

.....

Viktoria Bothe

Table of content

| | |
|--|-----------|
| 1 Introduction | 1 |
| 1.1 Pattern recognition by the innate immune system | 1 |
| 1.2 RIG-I-like receptors | 2 |
| 1.3 Virus detection by RIG-I-like receptors | 3 |
| 1.4 Replication cycle of vesicular stomatitis virus | 3 |
| 1.5 Origin and types of defective interfering genomes | 4 |
| 1.6 RIG-I activation and signal transduction | 6 |
| 1.7 MAVS and its activation | 7 |
| 1.8 Regulation of MAVS signaling | 9 |
| 1.9 RIG-I-like receptor signaling in health and disease | 13 |
| 1.10 Analysis of protein-protein interaction | 14 |
| 1.11 Proximity-based APEX-mediated live cell labeling | 16 |
| 1.12 Objectives and aims | 17 |
| 2 Material and methods..... | 19 |
| 2.1 Material | 19 |
| 2.1.1 Technical equipment..... | 19 |
| 2.1.2 Kits..... | 19 |
| 2.1.3 Chemicals | 19 |
| 2.1.4 Solutions and media for cell culture | 20 |
| 2.1.5 Antibiotics | 21 |
| 2.1.6 TLR agonists and cytokines | 21 |
| 2.1.7 Transfection reagent | 21 |
| 2.1.8 Enzymes | 21 |
| 2.1.9 Dyes | 21 |
| 2.1.10 Molecular weight markers | 22 |
| 2.1.11 Beads for pull-down | 22 |
| 2.1.12 Buffer and solutions | 22 |
| 2.1.13 Antibodies | 23 |
| 2.1.14 Cell lines | 24 |
| 2.1.15 Plasmids | 24 |
| 2.1.16 Software | 25 |
| 2.2 Methods for cell biology | 26 |
| 2.2.1 Cell culture | 26 |
| 2.2.2 Virus infection | 26 |
| 2.2.3 Transfection of plasmid DNA | 26 |
| 2.2.4 Stimulation with synthetic RNA molecules..... | 27 |
| 2.2.5 Transfection of RNA isolated from VSV-infected cells | 27 |
| 2.2.6 Transduction and generation of stable cell lines | 27 |
| 2.2.7 Tetracycline and doxycycline induction | 28 |

| | |
|--|-----------|
| 2.2.8 Generation of knockout cell lines using the CRISPR/Cas9 system | 29 |
| 2.2.9 Induction of biotin labeling with APEX..... | 30 |
| 2.2.10 Live cell staining with Mitotracker..... | 30 |
| 2.2.11 Isolation and cultivation of murine bone marrow-derived macrophages | 30 |
| 2.3 Methods for molecular biology | 31 |
| 2.3.1 Polymerase chain reaction | 31 |
| 2.3.2 T7 endonuclease digestion | 31 |
| 2.3.3 DNA gel electrophoresis | 32 |
| 2.3.4 Gel extraction of DNA | 32 |
| 2.3.5 Annealing of oligonucleotides encoding sgRNA | 32 |
| 2.3.6 Restriction enzyme digest..... | 33 |
| 2.3.7 Restriction-enzyme based ligation..... | 33 |
| 2.3.8 In-Fusion cloning | 33 |
| 2.3.9 Bacterial transformation | 33 |
| 2.3.10 Purification of plasmid DNA | 34 |
| 2.3.11 RNA purification..... | 34 |
| 2.3.12 Phenol-chloroform-based RNA purification | 34 |
| 2.3.13 RNA fragmentation | 34 |
| 2.3.14 cDNA synthesis | 34 |
| 2.3.15 Quantitative reverse transcriptase polymerase chain reaction..... | 35 |
| 2.4 Methods for protein biochemistry | 36 |
| 2.4.1 Immunoprecipitation of flag-RIG-I bound RNA..... | 36 |
| 2.4.2 Streptavidin pull-down of APEX-biotinylated proteins..... | 36 |
| 2.4.3 Preparation of cell lysates for Western blot..... | 37 |
| 2.4.4 Determination of protein concentration | 37 |
| 2.4.5 SDS-polyacrylamide gel electrophoresis (PAGE) analysis | 37 |
| 2.4.6 Western blot | 38 |
| 2.4.7 Immunofluorescence imaging by confocal microscopy | 38 |
| 2.4.8 Enzyme-linked immune-sorbent assay | 39 |
| 2.4.9 Luciferase assay | 39 |
| 2.5 Statistics | 39 |
| 3 Results | 40 |
| 3.1 Characterization of RIG-I ligands during infection with vesicular stomatitis virus | 40 |
| 3.1.1 Detection of a specific defective interfering genome in the VSV virus stock | 40 |
| 3.1.2 The defective interfering genome of VSV has a major impact on the immune response... | 41 |
| 3.1.3 The defective interfering genome and Leader/N sequences of VSV are enriched after RIG-I immunoprecipitation | 44 |
| 3.2 Identification of potential MAVS interaction partners by APEX- mediated proximity-based labeling | 45 |

| | |
|--|------------|
| 3.2.1 MAVS-APEX fusion proteins display MAVS and APEX activity | 45 |
| 3.2.2 Generation of a reproducible system by stable transduction of the fusion proteins..... | 48 |
| 3.2.3 APEX-MAVS specifically labels MAVS interaction partners upon RLR activation | 50 |
| 3.2.4 Mass spectrometry reveals new potential MAVS interaction partners | 53 |
| 3.2.5 Cell lines deficient in the newly identified potential MAVS-interaction proteins have a phenotype for antiviral signaling..... | 57 |
| 3.2.6 UBASH3B shows a negative regulatory function on RLR signaling..... | 59 |
| 3.2.7 Overexpression of UBASH3B has an inhibitory effect on RLR signaling in HEK293T cells but not in 1205 Lu cells..... | 66 |
| 3.2.8 The effect of UBASH3A/B deficiency on RLR signaling in murine bone marrow-derived macrophages varies depending on the strength of RLR signal..... | 70 |
| 4 Discussion | 72 |
| 4.1 The defective interfering genome is the main trigger of RIG-I during infection with VSV | 72 |
| 4.2 RIG-I ligands in the absence of defective interfering genomes | 74 |
| 4.3 Physiological role of defective interfering genomes | 75 |
| 4.4 The specificity of APEX in the MAVS-APEX fusion protein | 76 |
| 4.5 Control conditions for mass spectrometric analysis..... | 79 |
| 4.6 Analysis of the identified MAVS interaction network..... | 80 |
| 4.7 UBASH3B is a negative regulator of RLR signaling | 82 |
| 5 Summary | 89 |
| 6 Zusammenfassung | 91 |
| 7 References..... | 93 |
| 8 Appendices..... | 109 |
| 8.1 List of identified candidate proteins | 109 |
| 8.2 List of quantitative reverse transcriptase PCR primers and probes | 110 |
| 8.3 List of sgRNAs and its oligonucleotides | 111 |
| 8.4 List of primers for target site amplification | 112 |
| 8.5 List of abbreviations | 113 |
| 9 Acknowledgement | 116 |
| 10 Curriculum vitae | 117 |

1 Introduction

1.1 Pattern recognition by the innate immune system

The innate immune system is the first and immediate defense against diverse pathogens including bacteria, viruses, fungi and parasites. For a long time, its role was underestimated as an unspecific reaction, until 1989 Charles Janeway proposed pattern recognition to form a main characteristic of innate immunity. In his model pattern recognition receptors (PRRs) can distinguish between “self” and “non-self” by detecting conserved microbial components – the pathogen associated molecular patterns (PAMPs) - and can subsequently initiate an adaptive immune response (1,2). In the following years this model could be verified by identification and characterization of several PRRs.

Based on their structural features, the PRRs can be classified into five main families: Toll-like receptors (TLRs), NOD-like receptors (NLRs), C-type-lectine receptors (CLRs), AIM2-like-receptors (ALRs) and RIG-I-like receptors (RLRs).

The longest known and best characterized group are the TLRs. In most vertebrates 10 to 15 members are known. Nine of which (TLR1 to TLR9) are conserved in human and mice (3). Regarding their localization the TLRs can be subdivided into two groups. TLR1, TLR2, TLR4, TLR5 and TLR6 are localized in the cell membrane and detect membrane components of bacteria and fungi, such as lipids, proteins and lipoproteins in the extracellular space. TLR3, TLR7, TLR8 and TLR9 are predominantly expressed in the endosomal membrane and recognize nucleic acids derived from viruses or bacteria (3,4).

The NLRs include 22 known members in humans. But only a few of them have been functionally characterized so far. All of them are expressed in the cytoplasm where they detect a broad spectrum of PAMPs. This includes peptidoglycans of bacteria (NOD1 and NOD2), viral and bacterial nucleic acids, as well as metabolic changes induced by different toxins of bacteria and fungi (NLRP3) (5).

The CLRs are a group of PRRs that are expressed at the cell surface and recognize different carbohydrates, such as mannose, fucose and glucan allowing the detection of a variety of bacteria, fungi, viruses and parasites (6).

Four ALRs are known to exist in human (AIM2, IFI16, PYHIN1 and MDA5). They all recognize DNA derived from viruses or bacteria and are expressed in the cytoplasm or nucleus (IFI16) (7,8). The latest identified DNA sensor is the nucleotidyltransferase cyclic GMP-AMP synthase (cGAS). Although it does not belong to the ALRs it shares some common features and detects cytoplasmic microbial DNA. However, cGAS has the unique feature to signal via

the production of a second messenger called cyclic GMP-AMP (2'3'cGAMP) that triggers the adapter molecule STING (9).

An important family for detection of viral infection in the cell are the RLRs. They are composed of three members, namely melanoma differentiation antigen 5 (MDA5), retinoic acid inducible gene I (RIG-I) and laboratory of genetics and physiology 2 (LGP2) that detect different viral RNAs in the cytoplasm (4).

Although there is a great variety of PAMPs and PRRs, they all have in common that they activate immune responses through expression of diverse proinflammatory cytokines, chemokines and type I interferons which in turn results in the inhibition of the pathogen's ability to replicate and the recruitment of further immune cells (4).

1.2 RIG-I-like receptors

Viruses do not possess an own metabolism and thus, depend on the metabolic pathways of their hosts. Therefore, there are no virus specific structures of lipids or sugars that could be utilized as PAMP. The detection of viruses within the innate immune system is highly dependent on specific structures and the localization of their nucleic acids that differs from nucleic acids from their hosts and can be used to sense their presence.

RLRs detect viral RNA in the cytoplasm and play a pivotal role in virus recognition. Up to now there are three members of this receptor class known, namely RIG-I, MDA5 and LGP2 (10). Common features are the ATP-dependent helicase domain and the carboxy-terminal domain (CTD) that are responsible for binding of RNA. Additionally, RIG-I and MDA5 have an amino-terminal caspase recruitment domain (CARD) that is essential for the interaction with the downstream molecule mitochondrial antiviral signaling protein (MAVS) and subsequent activation of the antiviral signaling cascade (11,12).

Using synthetic RNA ligands, different studies could reveal the specific structure of RIG-I ligands: RIG-I binds preferentially short RNA molecules (18 to 20 bp) that have to bear a triphosphate on its 5' end and must be at least partially double-stranded to trigger downstream signaling (13,14). More recently it was found that RIG-I can also be activated by double-stranded RNA having a 5' diphosphate (15).

Specific requirements for MDA5 triggers are less well characterized besides its high affinity for long RNA molecules like the RNA analogon polyIC (polyinosinic:polycytidylic acid) that is often used to trigger MDA5 signaling. It is assumed that the lack of 2'-O-methylations and specific primary and secondary structures also play a certain role (16,17).

Due to the lack of CARD domains LGP2 is not able to activate the MAVS dependent signaling cascade. It has a regulatory role by modulating the binding of viral RNA by RIG-I or MDA5.

Originally it was identified as negative regulator of RIG-I (18,19), whereas more recent studies also described a positive regulatory function on RIG-I and MDA5 (20–22).

1.3 Virus detection by RIG-I-like receptors

Due to its preference for different RNA structures RIG-I and MDA5 recognize different groups of viruses (23). RIG-I is known to sense viruses of the order *Mononegavirales* that are characterized by a single stranded RNA genome of negative orientation [(-)ssRNA], e.g. influenza virus, Ebola virus, Sendai virus and vesicular stomatitis virus (VSV) (24–26). Typical sensors of MDA5 are members of the family *Picornaviridae* bearing a positive sense ssRNA genome [(+)ssRNA], e.g. hepatitis A virus, encephalomyocarditis virus (EMCV) and Mengo virus (26,27).

However, the detection of a virus is not exclusively limited to one of these receptors. For some of the (+)ssRNA viruses (e.g. *Flaviviridae* [hepatitis C virus, Dengue virus, West Nile virus]) and dsRNA viruses (reoviruses, e.g. rotavirus) both receptors have been shown to bind its RNA (28,29). Additionally, both receptors play a role in detection of different DNA viruses, like herpes viruses (e.g. herpes simplex virus-1, Epstein-Barr virus) or adenoviruses for RIG-I or the vaccinia virus detected by MDA5. This needs the transcription of AT-rich viral sequences by the RNA polymerase III leading to RNA intermediates with a triphosphate moiety on their 5' end (30,31). Although the responsible receptor for detection of many viruses is known, information about the precise viral RNA pattern that binds the receptor is often lacking or under discussion.

In the course of replication different viral RNA species are described to be responsible for the activation of RIG-I. For some members of *Mononegavirales* (i.e. Zaire Ebola virus, Nipah virus) the tri-phosphorylated full-length genome was found to be the ligand for RIG-I (24,32). Others claim short transcripts of the 3'-leader and 5'-trailer promoter regions and so called DI (defective interfering) genomes to be the main trigger of RIG-I during Sendai virus infection (33–35).

1.4 Replication cycle of vesicular stomatitis virus

VSV is a widely used model virus of the family *Rhabdoviridae* that belongs to the order *Mononegavirales* that has the common feature of a nonsegmented (-)ssRNA genome. It is well known that infection with VSV triggers the RIG-I signaling pathway. However, the exact RNA species that activates RIG-I during VSV infection is unknown. But there is evidence that its detection by RIG-I depends not only on the structure of the incoming genomic RNA of VSV but on viral RNA species generated during the viral replication cycle in the infected cell (36).

The genome of VSV has a size of 11.161 nucleotides (nt) that encodes for five proteins: the nucleoprotein (N), phosphoprotein (P), matrix protein (M), glycoprotein (G) as well as for the viral RNA-dependent RNA polymerase (L). These genes are separated by regulatory intergenic regions that act as transcriptional promoters. The genome is flanked by untranslated regions (UTR), that are called leader at the 3'UTR and trailer at the 5'UTR. The leader sequence serves as a promoter for the transcription and replication (37,38). During transcription the polymerase generates mRNA for each gene separately. It stops transcription after every transgenic region before continuing with the next gene. The mRNAs are modified by a cap structure at the 5' end and a polyA tail at the 3' terminus. The first transcript that is synthesized is the leader-transcript and in contrast to all others is not capped or polyadenylated. Since the viral polymerase is highly error-prone, it does not stop at every intergenic region leading to so-called leader-N read-through transcripts or bi- or tricistronic RNAs (39,40).

If enough N protein for encapsidation of the viral genome is synthesized, the polymerase switches from transcription to replication. In the process of replication, the polymerase skips the intergenic regions to generate a full-length antigenome. This in turn serves as template for replication of new full-length genomes, wherein the trailer sequence serves as a promoter (41). These are packed into virus particles for release of the cell and further infection.

Not only during transcription but also during replication the polymerase is prone to errors which can lead to deleterious variants of the full-length genome, the so-called defective interfering genomes.

1.5 Origin and types of defective interfering genomes

Defective interfering particles are spontaneously generated incomplete virus particles that are formed during replication and carry an incomplete (defective) genome. The reason for the production of such genomes lies in the high error-prone viral polymerase that has the ability to skip from one template to another or within one template. This leads to incomplete genomes or RNAs pieced together using more than one template (42,43).

Already 70 years ago, Henle and Henle made the observation, that inactive viral particles can interfere with the replication of influenza (44). Further studies by Magnus et al. could show, that incomplete viral particles are responsible for this phenomenon (45). He found that these defective viral particles are generated by undiluted passaging of the virus in embryonated chicken eggs. Further analyses of these incomplete viral particles lead to the following characteristics of the so-called defective interfering (DI) particles: they contain normal parental viral proteins, they contain only a part of the viral genome, they require a complete parental virus, the so-called helper virus for reproduction, because they provide the missing

proteins for replication and propagation and DI genomes interfere with the replication of the parental virus (46).

Most of the viruses, RNA as well as DNA viruses, have been found to generate DI genomes (47). However, the best studied DI genomes are derived from (-)ssRNA viruses, which have allowed the classification into three types. The simplest type is deletion defection, where a part within the genome is missing that can be up to 90 % of the total genome. A second variant is the snapback defect. That occurs when the viral polymerase transcribes one part of the template and then continues with transcription of the new strand. This leads to formation of a DI with a usual 5' end but an inverted repeat of the same terminus at the 3' end. Due to complementarity of the ends, they can form hairpin structures. The third type is known as copyback DI genome. The replicase carries a partially synthesized strand and skips back on the same strand to transcribe the 5' end leading to a panhandle structure (Figure 1) (42,48). Because of their smaller size and their two transcriptional start sites (for copyback and snapback DI genome) the DI genome has a replicative advantage compared to the full genome, causing an accumulation of DI genomes while the titer of parental virus is decreasing.

Besides their ability to interfere with the replication of the full-length viruses, DI genomes have been found years ago to also influence the immune response by increasing the IFN level (49). A main reason for that became clear in the recent years when DI genomes, especially copyback DIs, were found to bind to RIG-I, e.g. for Sendai virus, influenza and measles virus. Due to their double-stranded parts and their 5'triphosphorylated terminus, they have the required structural features for being a RIG-I ligand (50).

Since DI genomes were found to originate during multiple passaging at a high multiplicity of infection (MOI), it was believed that they are cell culture artefacts. However, the usage of high sensitive techniques, like deep sequencing, for detection of viral genomes, DI genomes have been identified in several human specimens after infection with different viruses *ex vivo*, like Dengue virus, influenza A virus and hepatitis A and C virus (51–54). Until now, it is under discussion what the role of the DI genomes under physiological conditions is.

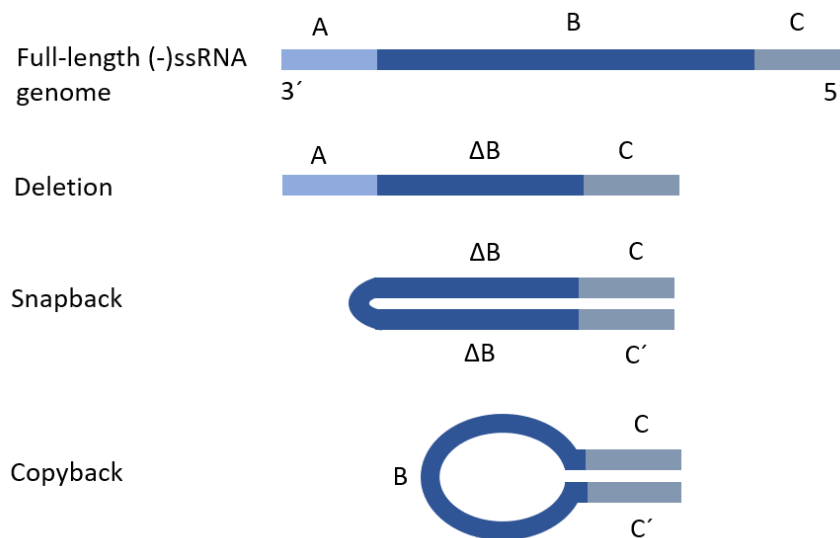


Figure 1: Types of defective interfering genomes. Scheme of different DI genomes generated in the replication cycle of (-)ssRNA viruses. The description of their origin is given in the text. Modified from (55).

1.6 RIG-I activation and signal transduction

The activation of RIG-I is highly regulated, since spontaneous signaling can cause inflammatory and autoimmune diseases, which is known from patients that carry RIG-I gain-of-function mutations (56). The tight regulation is achieved by the requirement of conformational changes and post-translational modifications for activation.

In an uninfected cell RIG-I is kept in an autoinhibited state that sterically keeps the CARD domain sequestered by the repressor domain (57,58). This inactive form is maintained in part through the phosphorylation of two specific sites in the CARD domain by conventional protein kinase α (PKC- α) and PKC- β and by phosphorylation within the repressor domain by casein kinase II (59,60). Due to the conformational change upon binding of viral RNA, the inhibitory phospho-residues are removed. The CARD phosphorylation sites are known to be removed by the phosphoprotein phosphatase 1- α (PP1 α) and PP1 γ (61). This dephosphorylation and conformational change lead to RIG-I oligomerization via their CARD domain allowing the E3 ligase TRIM25 (tripartite motif containing 25) to bind and generate K63-linked ubiquitin chains to the CARD domain of RIG-I (62). This further leads to the recruitment of the mitochondrial targeting chaperone protein 14-3-3 ϵ , which is an essential component of the “translocon” leading to translocation of RIG-I to the mitochondrial antiviral signaling protein MAVS (63). Besides these essential molecules further ubiquitin-ligases are described to either enhance the signaling (e.g. Riplet, Mex3c) by generating K63-linked ubiquitination or to dampen the signaling by marking RIG-I for degradation with K48-linked ubiquitination

(e.g. RNF122, RNF125) or by removing K63-linked ubiquitin chains (e.g. CYLD, USP3) (64–70).

However, once RIG-I is activated the exposed and oligomerized CARD domains interact with the central downstream adapter molecule MAVS via their CARD domains leading to transduction of the antiviral signaling.

1.7 MAVS and its activation

Shortly after RIG-I was discovered, MAVS - also known as IPS-1 (IFN- β promoter stimulator protein 1) , VISA (virus-induced signaling adapter) or Cardif (CARD adapter inducing IFN- β) - was identified by four different groups as an essential adapter molecule for the signal transduction by RIG-I-like receptors (RLRs) (71–74). MAVS, a 540 amino acid (aa) containing protein (in humans) is composed of a CARD domain at the N-terminus, a proline-rich region (PRR) and a transmembrane (TM) domain at the C-terminus (Figure 2A). The TM domain allows the integration of MAVS mainly into the outer mitochondrial membrane (OMM) but was also found to localize to peroxisomes (75) and to mitochondria-associated membranes (MAM) (76) which are subdomains of the endoplasmic reticulum (ER). Via CARD-CARD interaction MAVS is activated by RIG-I or MDA5 and is thus essential for their signaling. It was also found that the localization in membrane is required for signaling, since the deletion of the TM domain abolished the ability of MAVS to transmit RLR signaling (73). Another requirement for MAVS activation is its ability to form homo-oligomers that subsequently lead to the prion-like formation of MAVS oligomers. These aggregates form a signaling platform for the recruitment of downstream signaling molecules.

The first molecules associating with oligomerized MAVS are TNF receptor-associated factor 2 (TRAF2), TRAF3, TRAF5 and TRAF6, that interact via the PRR domain of MAVS (74,77,78). These E3 ubiquitin ligases generate ubiquitin chains that serve as scaffold for further signaling molecules. Liu et al showed that the TRAF molecules act redundantly, since the knockout of one of these molecules do not affect the signaling (79). There are three sites identified in MAVS that have binding motifs for TRAF molecules, the TRAF-interacting motifs (TIM). The region I (aa 138-152) containing a TRAF2/3/5- and a TRAF3/6-binding motif and region II (aa 451-465), that has only a TRAF3/6-binding motif, were shown to be important for the activation of the NF κ B (nuclear factor κ B) signaling branch, whereas the region III (aa 401-450) was shown to be indispensable to activate the IRF3 (interferon regulatory factor 3) signaling branch (see Figure 2A) (80) .

The interferon induction downstream of RLRs requires the activation of IRF3 or IRF7 that is mediated by its phosphorylation through TBK1 (TANK binding kinase 1). Therefore, TBK1 is an essential molecule in MAVS-mediated IRF3 signaling. However, how TBK1 is activated is

still a matter of debate. One model says, that NEMO (NF κ B essential modulator) is recruited after TRAF-binding. This acts as a scaffold for further recruitment and activation of TBK1 and IKK ϵ (I κ B kinase ϵ) to the MAVS signaling complex via the adapter molecule TANK (TRAF family member associated NF κ B activator) (81). In contrast, a recent study claims, that TBK1/IKK ϵ can also be activated independently of NEMO through direct interaction with TRAF molecules (82). As it was for a long time assumed, IRF3 is not directly phosphorylated by TBK1 but needs the interaction with MAVS as well. MAVS has a specific phosphorylation motif that is first phosphorylated by TBK1 and IKK ϵ . This in turn leads to recruitment of IRF3 to MAVS, which is essential for its subsequent phosphorylation by TBK1 (83). Activated IRF3 then dissociates from MAVS and dimerizes through the phospho-binding domain before it is translocated into the nucleus to drive the expression of type I interferons (IFNs).

The activation of the NF κ B branch, other than for IRF3 activation, is completely dependent on NEMO (82). After binding of NEMO through TANK, it recruits the subunits IKK α and IKK β . Together they form the classical IKK complex that is important for phosphorylation of I κ B α , that in turn releases the subunit p50 and p65 of NF κ B for translocation into the nucleus to drive transcription of proinflammatory cytokines such as interleukin 6 (IL-6) and IL-1 β (84) (Figure 2B).

Besides these essential players of the antiviral signaling via MAVS there is also a growing list of proteins and mechanisms that negatively or positively regulate the activity of MAVS.

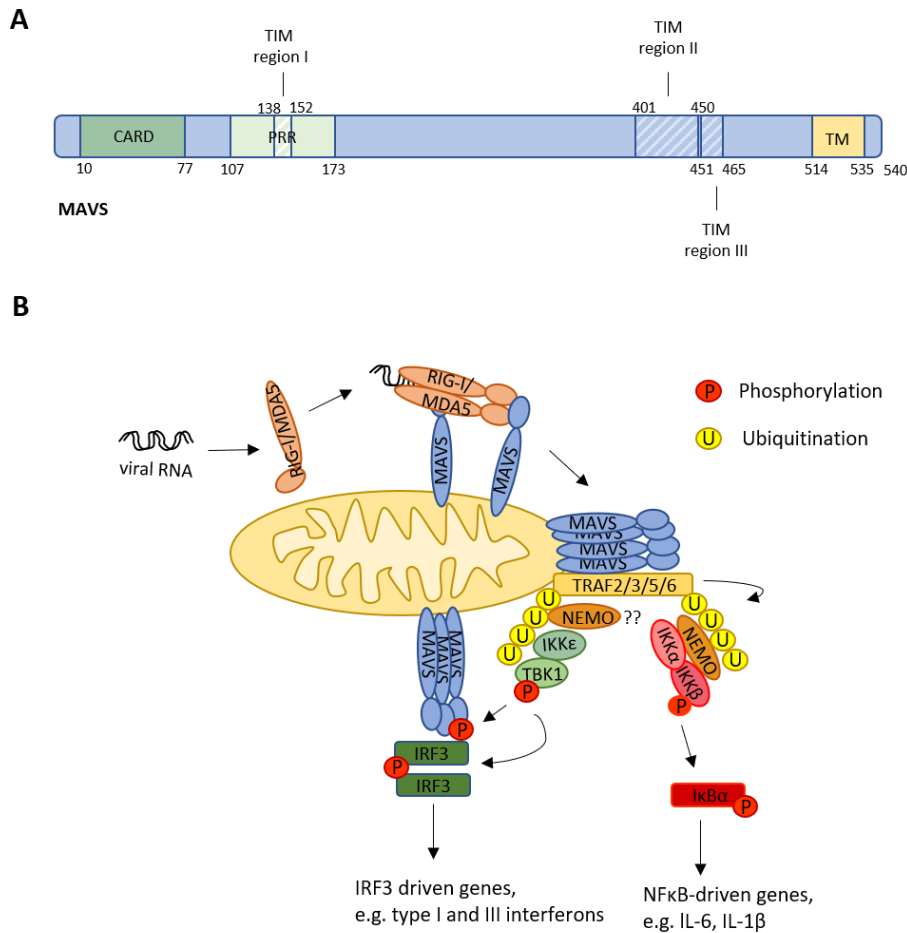


Figure 2: MAVS and the RIG-I-like receptor pathway. (A) Schematic representation of MAVS with important functional domains: caspase-recruitment domain (CARD), proline-rich region (PRR), transmembrane domain (TM) and TRAF-interacting motifs (TIM). (B) The RLR pathway is activated by binding of viral RNA to RIG-I or MDA5. Subsequently, they bind to MAVS via CARD-CARD interaction. The activation of MAVS leads to its polymerization and recruitment of several interaction partners that finally leads to transcription of IRF3- and NFκB-driven genes. Details are described in 1.6 and 1.7.

1.8 Regulation of MAVS signaling

In contrast to RIG-I, MAVS is not a classical interferon-stimulated gene (ISG) that is transcriptionally regulated by IRFs. Its expression level and activity are instead controlled by different transcriptional, post-transcriptional and post-translational mechanisms.

Protein phosphorylation is one well known mechanism by which protein activity is regulated, although for MAVS just a few phosphorylation-dependent modulations are described. The Polo-like kinase 1 (PLK1) was found to bind to MAVS and disrupt the binding of TRAF3 to MAVS thereby inhibiting the IFN induction (85). The protein kinase A (PKAC) subunits α and β were recently identified as further inhibitory kinases. They were shown to phosphorylate MAVS at threonine residue 54 (T54) to inhibit MAVS aggregation and prime it for degradation (86). C-Abl is a tyrosine kinase, that was described to phosphorylate MAVS and positively

regulate the RLR signaling. Its knockdown impaired the activation of IRF3 and NF κ B (87). In another report the tyrosine residue 9 (Y9) was identified as an important site for antiviral signaling. A phosphorylation-incompetent mutant of that site was not able to induce IFN- β anymore and showed highly diminished NF κ B signaling. Still, the kinase that phosphorylates Y9 needs to be identified (88). The first phosphatase that interacts with MAVS was described by Xiang et al. (89). They found that the protein phosphatase magnesium-dependent 1A (PPM1A), that was already described to regulate IKK β and STING activity, also dephosphorylates MAVS as well as the TBK1/IKK ϵ complex, thus dampening the IRF3 axis.

Another important post-translational regulation mechanism is ubiquitination. Ubiquitination is mediated by E3 ligases that can generate and transfer different types of ubiquitin chains. The most common ones are the K63- or K48-linked ubiquitin chain. Whereas the former causes protein activation, the latter mediates degradation. Besides the well-described activating ubiquitination by TRAFs, there are many more E3 ligases known that coordinate MAVS activity. For example the E3 ligase TRIM31 conjugates K63-linked ubiquitin to MAVS, that facilitates the formation of MAVS aggregates thereby enhancing the MAVS signal (90). However, there are also E3 ligases described that conjugate K48-linked ubiquitin chains to MAVS thereby leading to its degradation, e.g. RNF125, TRIM25, MARCH5 and AIP4 (67,91–93) and shut down of antiviral signaling.

Since MAVS is mainly localized to mitochondria, mitochondrial proteins are also involved in its regulation. The first identified regulatory protein of MAVS is the nucleotide-binding domain and leucine-rich repeat containing family member NLRX1. It inhibits the signaling by preventing the CARD-CARD interaction of RIG-I and MAVS (94). Since NLRX1 was found to be expressed in the mitochondrial matrix (95), it is not clear how it exerts its function. The translocase of outer membrane 70 (TOM70) is a positive regulator and facilitates the recruitment of TBK1/IRF3 to the mitochondria (96).

Moreover, proteins involved in mitochondrial dynamics can influence MAVS activity. Mitofusin 2 (Mfn2) is important for mitochondrial fusion and directly interacts with MAVS thereby inhibiting the downstream signaling (97). Whereas it is unclear if this function of Mfn2 is linked to its function in mitochondrial fusion another study provide evidence that mitochondrial fusion enhances RLR signaling. Here, it was shown that infection with Sendai virus induced elongation of the mitochondria and upon knockdown of Mfn1 and OPA1 (optic atrophy protein 1), both mediators of mitochondrial fusion, the activation of IFN- β and NF κ B signaling was inhibited. The opposite was true upon knockdown of Drp1 (dynamin 1 like protein) and Fis1 (mitochondrial fission 1 protein) that are important proteins for mitochondrial fission (98).

Besides mitochondrial dynamics, also metabolic functions are involved in antiviral signaling, like the production of reactive oxygen species (ROS) and the mitochondrial membrane potential ($\Delta\psi_m$). Koshiba et al. showed that Mfn1/Mfn2 double knockout cells had impaired $\Delta\psi_m$ and reduced antiviral signaling. Furthermore, they could show that chemically disrupting the $\Delta\psi_m$ with the protonophore CCCP had the same negative effect (99). Since the aforementioned fission and fusion process also influences the membrane potential it is unclear, what initially causes the effect.

The $\Delta\psi_m$ is also linked to the production of ROS, which was found to regulate RLR signaling as well. The treatment with antioxidant compounds reduced RLR signaling, whereas an increase of ROS production induced by rotenone increased the induction of interferon type I (100). In line with this, Soucy-Faulkner et al. found that ROS is required to active IRF3 after Sendai infection (101). Furthermore, the mitochondrial protein COX5B (cytochrome C oxidase 5B) that is part of the electron transport chain was described to directly interact with MAVS. The deletion of this protein lead to enhanced MAVS-dependent signaling, whereas overexpression caused its suppression. This effect was linked to the negative regulatory function of COX5B on ROS production (102). The group further showed that COX5B interacts with Atg5 (autophagy related 5), a protein that is important for autophagic signaling, upon MAVS activation. Signal enhancement or repression was observed after Atg5 knockdown or overexpression, respectively. This suggests that the negative regulation is mediated by autophagy.

Autophagy is also strongly linked to ROS production and mitochondrial dynamics. This is a process by which damaged organelles are removed from the cell, and in case of mitochondria specifically known as mitophagy. There are several autophagy-related proteins known to regulate RLR signaling. In line with Zhao et al. (102), another study showed that the knockout of Atg5 leads to increased MAVS expression and RLR signaling. The authors concluded that the loss of autophagy leads to accumulation of damaged mitochondria that increases the ROS production, thus the mitochondrial homeostasis is important for proper signaling (100). Sun et al. further showed that MAVS is directly involved in maintaining mitochondrial homeostasis via autophagy. They identified the LC3 interacting region (LIR domain) Y9xxI12 in MAVS and demonstrated direct interaction of LC3 via this domain (103). LC3 is a main player in autophagy and essential for the formation of autophagosomes. The same finding was made by another group, that specifically showed this interaction in microglial cells. They further found that the LC3-MAVS interaction is mediated by phosphorylation of MAVS via c-Abl (104). Ubiquitination is also a process that is highly important to transmit autophagic signaling. Recently, the autophagy receptor CALCOCO2 was shown to be recruited to ubiquitinated MAVS for autophagic degradation. Here a K27-linked ubiquitin chain was catalyzed by MARCH8 that was recruited to MAVS via BST2, a protein known to be a viral

restriction factor (105). All in all, autophagy is described as an important mechanism to avoid excessive inflammation by downregulating MAVS signaling.

Another specific feature of MAVS is its polycistronic mRNA allowing the translation of distinct proteins from a single mRNA. Brubaker et al. identified a truncated variant of MAVS, the so called miniMAVS, that is translated from the alternative start codon Met142 and has a size of approximately 50 kDa (106). By overexpression of miniMAVS together with full-length (FL) MAVS a decrease of IFN induction was observed. Whereas the formation of MAVS aggregates was unaffected, the authors claim that interaction of miniMAVS with TRAF molecules causes the negative regulation: The more TRAF molecules bind to miniMAVS, the less is available for binding of FL-MAVS and subsequent signal transduction. In contrast, another study describes truncated MAVS to be important for MAVS aggregation. Besides miniMAVS, they identified four more truncated MAVS variants, that are all capable for homotypic interaction of their TM-domain with the TM-domain of FL-MAVS. This interaction is important for the homeostasis of MAVS by preventing spontaneous aggregation of FL-MAVS (107). However, both studies imply a negative regulatory function of miniMAVS. Moreover, miniMAVS also displays an inhibitory function on the TLR3 pathway. They could show, that silencing of MAVS enhanced TLR3-driven signaling, whereas overexpression of miniMAVS lead to downregulation, indicating that there is crosstalk between these two antiviral signaling pathways (108) (see Figure 3).

A strong crosstalk also exists between the DNA-sensing pathway via STING and MAVS. Upon activation of RIG-I, STING interacts with the RIG-I-MAVS complex and facilitates the recruitment of TBK1 (109,110). This interaction was known before the actual function of STING, the downstream adapter of the DNA sensor cGAS, was identified.

There are many regulatory proteins and mechanisms known that orchestrates the antiviral immune response upon MAVS activation. This makes clear, that tight regulation of this signaling is necessary to integrate different signaling branches to produce an adequate antiviral immune response that restricts viral replication but also limits inflammation.

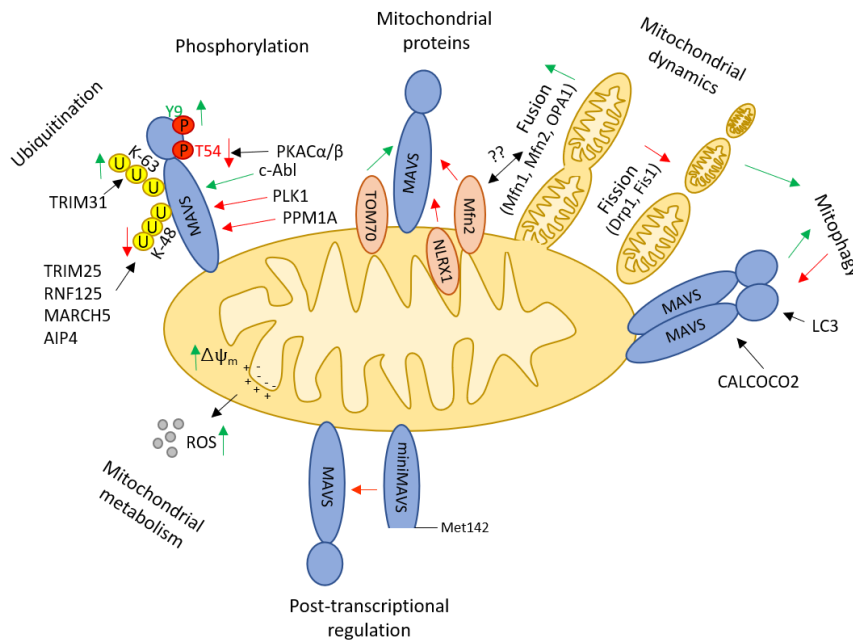


Figure 3: Regulation of MAVS activation. Different mechanism of the regulation of MAVS activity are shown. Arrows in green and red show positive and negative regulation, respectively. The details are described in section 1.8.

1.9 RIG-I-like receptor signaling in health and disease

The importance of a tight RLR signaling regulation becomes evident in patients with different mutations in RIG-I or MDA5. Regardless of viral infections, an abnormal activity of RIG-I or MDA5 can lead to autoimmune diseases. For MDA5 several gain-of-function mutations are described, that lead to hyperactive variants of MDA5 that causes different interferonopathies such as Aicardi-Goutières syndrome (AGS), systemic lupus erythematosus (SLE) and Singleton-Merten syndrome (SMS) (111,112). A gain-of-function mutation in RIG-I has been found to be causative for an atypical SMS (113). Vice versa there are mutations in MDA5 described that cause a loss-of-function and result in immunodeficiency disorders leading to higher susceptibility to respiratory viral infection such as respiratory syncytial virus (RSV) and rhinovirus (114–116). For MAVS, there is so far one loss-of-function mutation described that was found to be associated with lower IFN production in SLE patients because of inhibition of ROS-induced self-oligomerization of MAVS (117,118).

The RLR pathway is also an interesting target for cancer immunotherapy. Triggering this pathway in tumor cells can lead to direct IFN-independent tumor cell killing as well as to IFN-dependent activation of adaptive immunity. Although RLR ligands are not yet approved for treatment of cancer, there are many studies hinting towards a promising strategy to fight cancer. Besides using pIC as immunostimulatory agent, different siRNAs with a 5'triphosphate moiety have been tested (119). These bifunctional molecules are able to

induce RLR-dependent signaling as well as to silence a specific oncogene, as it was shown for TGF- β 1 to treat pancreatic cancer or with an bifunctional siRNA against Bcl-2 to treat melanoma in mice (120). Moreover, oncolytic viruses are attractive tools to trigger RLR-dependent signaling in tumor cells. These viruses selectively replicate in tumor cells and are able to directly induce tumor cell lysis and also to induce adaptive antitumor immunity. T-Vec (talimogene laherparepvec), a genetically engineered herpes simplex virus additionally encoding GM-CSF to further stimulate the immune system, is the first approved oncolytic virus to treat malignant melanoma (121). Another promising oncolytic vector is VSV, because it has a rapid replication cycle and is naturally selective for tumors, since it can only replicate in cells defective for IFN signaling, a typical feature of many tumor cells. Although many variants of engineered VSV have been successfully tested in the mouse model, there are still safety issues to overcome, because the wt VSV is neurotrophic and can cause encephalitis in humans (122).

1.10 Analysis of protein-protein interaction

The identification and characterization of protein-protein interactions (PPIs) is a major challenge in cell biology. PPIs are fundamental to understand biological processes and intracellular signaling pathways and help in understanding diseases. Conventional methods, like co-immunoprecipitation (IP) and yeast-two-hybrid (Y2H) assays have been used for years and most interaction networks that are known have been identified or verified by these methods.

In co-immunoprecipitation assays the protein of interest is isolated from a whole cell lysate with a specific antibody coupled to a matrix like agarose, sepharose or magnetic beads. To increase binding specificity the protein of interest is often marked with a tag (e.g. flag, myc, His) that is then used as the antigen for the IP. The IP can also be performed with purified proteins in a cell-free assay or after overexpression in a suitable cell line and cell lysis. The precipitated proteins can be analyzed by Western blot for expected proteins or via Mass spectrometry to identify all proteins in the complex. This method can be also applied to identify bound DNA (ChIP) or RNA (RIP) that just need another purification step after IP. Although this method is used broadly, it has some major limitations. It relies on in vitro handling of cell extracts and only allows the detection of high-affinity PPIs that are still intact after cell lysis. Conversely, after cell lysis new complexes can form, that are not present in living cells, leading to false positive candidates (123).

First described in 1989, the Y2H system is a method that is used for detection of two interacting proteins in the living yeast cell. Here, the two putative interactors are fused to different subunits of a transcription factor. Only when these proteins come in close proximity,

the transcription factor becomes functional and drives the expression of a reporter gene, e.g. LacZ. This method is extensively used in screening approaches by using a set of prey and a set of bait proteins that are systematically co-expressed. This method is suitable to detect direct physical interactions between two proteins. But, as for IP, does not represent a physiological situation, since modified proteins are used, that are most often not originated from the yeast (124).

The idea of tagging proteins to detect their interaction was also used for newly developed methods like fluorescence resonance energy transfer (FRET). Here, a prey and bait protein are fused to two different fluorescence tags with overlapping emission/excitation spectra. If both proteins are in close vicinity, the energy from the donor fluorophore is transferred to the acceptor fluorophore and can be visualized via confocal microscopy in living cells. This is similar to bioluminescence resonance electron transfer (BRET) that uses the combination of a fluorophore and luciferase. Other modifications of this method use split proteins like split-ubiquitin or split-GFP. Here the N-terminus and the C-terminus are fused to different proteins of interest and only if they come together the functional protein (Ubiquitin or GFP) is detectable. An advantage of these methods is, that interactions in the living cell can be detected. These techniques however are better suitable for verification of protein interactions, rather than for identification of new interactors. It further needs the modification of two proteins of interest, which bears the danger to artificially introduce functional and structural changes (125).

A new class of method for detection of PPIs is the enzyme-mediated proximity-based labeling. The basic principle is that an enzyme catalyzes a reaction that forms reactive biotin and can then covalently bind to nearby proteins. The main advantages are that these techniques are unbiased and can be applied to living cells, catching a physiological situation. Since all interacting proteins are tagged with biotin within the living cell, the cells can then be lysed with harsh condition and biotinylated proteins can specifically be enriched by Streptavidin pull-down, thus enabling for the detection of weak and transient interactors.

There are two new methods for this type of PPI detection. On the one hand it is the so called BioID, that uses a variant of the bacterial enzyme BirA and the APEX-mediated labeling, that uses an engineered ascorbate peroxidase (APEX). The main difference of these approaches is the enzyme kinetic. Whereas BirA needs to be active for 16 h the biotinylation reaction of APEX takes place in just one minute. For BirA, this leads to a history of proteins that interacted with the protein of interest in this time frame, whereas APEX is suitable to give a snapshot of a proteome at a defined time point (126,127).

1.11 Proximity-based APEX-mediated live cell labeling

The method of APEX-mediated labeling in living cells was first described by Rhee et al. in 2013 showing a highly specific proteome mapping of the mitochondrial matrix (128). The new striking feature of this method is the combination of spatial and temporal resolution of a proteome in the living cell.

APEX is derived from a 28 kDa cytosolic plant peroxidase. It was first discovered as a suitable tool for staining in electron microscopy. Here, it catalyzes the H_2O_2 -dependent polymerization of diaminobenzidine (DAB) for EM contrast, the same reaction that was usually induced using the horse radish peroxidase (HRP). One disadvantage of the HRP is that it is inactive when expressed in the cytosol, which could be overcome by APEX, showing activity in all cellular compartments (129).

Besides DAB, APEX can oxidize several phenol derivatives to phenoxyl radicals in the presence of H_2O_2 , that covalently react with electron-rich amino acids (i.e. Tyr, Trp, His, and Cys). These highly reactive radicals have a very short life-time of < 1 ms, allowing the covalent reaction to be restricted to the small labeling radius (< 20 nm) that these molecules can reach by diffusion during their reactive life time (128). By using biotin-phenol as a substrate, proteins in the near surrounding of APEX get biotinylated.

In the mentioned proof-of-principle study Rhee et al. showed by targeting APEX to the mitochondrial matrix, that they were able to specifically label matrix proteins. The MS data of biotinylated proteins revealed, that 80 – 90% of the described matrix proteome was detected. They could further detect proteins, that had not been described as matrix protein yet (128).

Rhee et al. established the following workflow for this method: The first requirement is a fusion protein of APEX with either a specific targeting sequence (e.g. nucleus, mitochondrial matrix, OMM) or with a defined protein of interest. After expression of the fusion protein, the cells are incubated with biotin-phenol for 30 min. To activate the APEX-mediated biotinylation H_2O_2 is added. Since APEX possesses a fast kinetic, 1 min incubation was found to be sufficient. Afterwards the reaction is immediately stopped by removing the H_2O_2 -containing medium and addition of antioxidants (sodium ascorbate, Trolox and sodium azide). The biotinylated proteins can then be visualized by confocal microscopy or Western blot or they can be purified with streptavidin beads for MS analysis (130).

In a following study they used directed evolution to screen for a more sensitive variant of APEX and found that a single mutation (A134P) strongly increased APEX' activity (APEX2) (131). This variant was used in further studies and also in the present thesis.

Up to now, this method was used in different settings, most often to analyze a proteome of a subcellular compartment, like the mitochondrial intermembrane space (IMS), OMM, mammalian cilia, the Golgi proteome in yeast or mammalian ER-plasma junctions (132–136). A more recent study used APEX for the first time to resolve a protein network. They fused a G-protein-coupled receptor (GPCR) to APEX and were able to track the dynamics and interactors of this receptor in a spatially and temporally-dependent manner (137). Another study could recently show, that APEX also works in the extracellular space to identify specific interaction partners during signaling. They fused the enzyme to FGF1 (fibroblast growth factor 1) and could identify two new receptors of this protein (138). Another interesting advancement of this method is the combination with the CRISPR/Cas9 system. A catalytically dead Cas9, that is still able to target a specific DNA locus but does not cut the DNA, was fused to APEX. This allowed the identification of proteins binding to specific DNA sites and is a promising alternative to the conventional ChIP approach (139).

1.12 Objectives and aims

Activation of the RLR pathway is highly important to induce a proper immune response against many clinically relevant viruses. The RLR-induced response is tightly controlled since an inadequate response can allow an unlimited spread of the invading virus while an exaggerate response can lead to excessive inflammation causing autoimmunity. RLR ligands are under development as anti-tumor agents and vaccine adjuvants and gain-of-function mutations in the RLR pathway have been identified as the cause of inborn autoinflammatory syndromes. A better understanding of the characteristics of RNAs that trigger an RLR signal physiologically and of the factors that modulate and terminate signal transduction will help to optimize the therapeutic manipulation of the RLR pathway.

In the presented thesis two of these aspects were addressed to better understand the RLR signaling pathway. In the first part, the project aims to characterize natural ligands in the replication cycle of the model virus VSV that trigger RIG-I. Preliminary studies in our group had found that a specific defective interfering genome bound to RIG-I during VSV infection. Here, the present study continued and addressed the following questions:

1. Is the DI genome indeed detectable during VSV infection and what is the kinetic of DI genome production?
2. Is the DI genome the trigger of RIG-I activation and how does it influence the immune response?
3. Are there additional ligands for RIG-I, if the virus stock is free of DI genomes and does the depletion of DI genomes have an impact on the immune response?

The second part of the thesis focused on MAVS, the key player in the RLR pathway, and aimed to identify new interaction partners of this molecule and thereby characterize new regulatory mechanisms of the RLR signaling pathway. To achieve this goal the method of APEX-mediated proximity labeling of proteins was used, that enables the mapping of a proteome in living cells in a spatially and time-restricted manner. The experimental setup thereby aimed to label proteins in the proximity of MAVS in the steady state and after triggering of the pathway with an RLR ligand. Analysis of these MAVS proteomes by mass spectrometry should reveal candidate proteins that interact directly or indirectly with the MAVS-complex upon RLR activation. Specifically, the study thereby tackled the following questions:

1. Is there a fusion protein of MAVS and APEX that is suitable in terms of protein activity and specificity?
2. Since APEX is localized at the cytosolic part, is the biotinylation restricted to mitochondria-associated proteins?
3. Does APEX-MAVS fusion protein label MAVS interaction partners after signal activation?
4. Are there significantly altered biotinylated proteins detectable in MS after signal activation?
5. If new candidate proteins can be detected, do they play a role in MAVS signaling and what is their function?

2 Material and methods

2.1 Material

2.1.1 Technical equipment

| | |
|-----------------------------|------------------------------------|
| Alpha Imager HP | Alpha Innotech (San Leandro, USA) |
| ChemiDoc Imaging system | Bio-Rad (Munich, DE) |
| TCS SP5 confocal microscope | Leica (Wetzlar, DE) |
| LightCycler 480 | Roche (Mannheim, DE) |
| NanoPhotometer | Implen (Munich, DE) |
| Digital Sonifier 450 | Branson Ultrasonics (Danbury, USA) |
| Trans Blot Cell | Bio-Rad (Munich, DE) |

2.1.2 Kits

| | |
|--------------------------------|----------------------------------|
| Clarity Western ECL substrate | Bio-Rad (Munich, DE) |
| DC TM protein assay | Bio-Rad (Munich, DE) |
| ECL Western blotting substrate | Thermo Scientific (Waltham, USA) |
| GeneJET Plasmid Miniprep kit | Thermo Scientific (Waltham, USA) |
| Human IL-6 ELISA set | BD Biosciences (San Diego, USA) |
| Human IP-10 ELISA set | BD Biosciences (San Diego, USA) |
| In-Fusion HD cloning kit | Clontech (Mountain view, USA) |
| miRNeasy kit | Qiagen (Hilden, DE) |
| Total RNA kit | VWR (Radnor, USA) |
| Zymoclean Gel DNA Recovery | Zymo Research (Irvine, USA) |

2.1.3 Chemicals

| | |
|---------------------------------------|-----------------------------------|
| Agarose | Biozym Scientific (Oldendorf, DE) |
| Ammoniumpersulfate (APS) | Sigma-Aldrich (Steinheim, DE) |
| Biotin-phenol | Iris Biotech (Marktredwitz, DE) |
| Bromphenol blue | Roth (Karlsruhe, DE) |
| Bovine serum albumin (BSA) | Roth (Karlsruhe, DE) |
| Coelenterazine H | Promega (Madison, USA) |
| Cycloheximide (CHX) | Sigma-Aldrich (Steinheim, DE) |
| Ethylendiaminetetraacetic acid (EDTA) | Roth (Karlsruhe, DE) |
| Flag peptide | Sigma-Aldrich (Steinheim, DE) |
| Formamide | Sigma-Aldrich (Steinheim, DE) |
| Glycerol | Roth (Karlsruhe, DE) |

| | |
|---|-------------------------------|
| Glycine | Roth (Karlsruhe, DE) |
| Hydrogen peroxide (H ₂ O ₂) | Merck (Darmstadt, DE) |
| Magnesium chloride | Sigma-Aldrich (Steinheim, DE) |
| Methanol | Merck (Darmstadt, DE) |
| β-Mercaptoethanol (BME) | Bio-Rad (Munich, DE) |
| Milk powder | Roth (Karlsruhe, DE) |
| Mowiol-488 | Roth (Karlsruhe, DE) |
| Nonidet P-40 (NP-40) | Fluka Biochemika (Buchs, CH) |
| Paraformaldehyde (PFA) | Sigma-Aldrich (Steinheim, DE) |
| Passive lysis buffer (5x) | Promega (Madison, USA) |
| Polybrene | Sigma-Aldrich (Steinheim, DE) |
| Protease Inhibitor Cocktail | Sigma-Aldrich (Steinheim, DE) |
| Sodium ascorbate | Sigma-Aldrich (Steinheim, DE) |
| Sodium azide (NaN ₃) | Sigma-Aldrich (Steinheim, DE) |
| Sodium chloride (NaCl) | Roth (Karlsruhe, DE) |
| Sodium deoxycholate | Sigma-Aldrich (Steinheim, DE) |
| Sodium dodecyl sulfate (SDS) | Roth (Karlsruhe, DE) |
| Sodium fluoride (NaF) | Sigma-Aldrich (Steinheim, DE) |
| Sodium hydroxide (NaOH) | Roth (Karlsruhe, DE) |
| Sodium orthovanadate (Na ₃ OV ₄) | Sigma-Aldrich (Steinheim, DE) |
| Sodium pyruvate | Sigma-Aldrich (Steinheim, DE) |
| Rotiphoresis Gel 30 (37,5:1) | Roth (Karlsruhe, DE) |
| Tetramethylethylenediamine (TEMED) | Roth (Karlsruhe, DE) |
| Trichlorethanol | Sigma-Aldrich (Steinheim, DE) |
| Tris hydroxymethylaminomethan (Tris) | Roth (Karlsruhe, DE) |
| TRIS hydrochloride (Tris-HCl) | Roth (Karlsruhe, DE) |
| Triton X-100 | Sigma-Aldrich (Steinheim, DE) |
| Trolox | Sigma-Aldrich (Steinheim, DE) |
| Tween 20 | Roth (Karlsruhe, DE) |

2.1.4 Solutions and media for cell culture

| | |
|---|------------------------------------|
| Dulbecco's Modified Eagle Medium (DMEM) | Sigma-Aldrich (Steinheim, DE) |
| Fetal calf serum (FCS) | Gibco Products (Grand Island, USA) |
| L-Glutamine | Sigma-Aldrich (Steinheim, DE) |

| | |
|---------------------------------|------------------------------------|
| Opti-MEM | Gibco Products (Grand Island, USA) |
| Penicillin-Streptomycin | Lonza (Basel, CH) |
| Phosphate-buffered saline (PBS) | Sigma-Aldrich (Steinheim, DE) |
| RPMI | Sigma-Aldrich (Steinheim, DE) |
| Trypsin (10x) | Lonza (Basel, CH) |

2.1.5 Antibiotics

| | |
|----------------------------|--------------------------------|
| Blasticidin | Invivogen (San Diego, CA, USA) |
| Doxycycline | Sigma-Aldrich (Steinheim, DE) |
| Geneticin (G418) | Invivogen (San Diego, CA, USA) |
| Puromycin | Invivogen (San Diego, CA, USA) |
| Tetracycline hydrochloride | Sigma-Aldrich (Steinheim, DE) |

2.1.6 TLR agonists and cytokines

| | |
|--|--|
| Poly(I:C), HMW | Invivogen (San Diego, CA, USA) |
| Macrophage colony-stimulating factor (M-CSF) | Miltenyi Biotech (Bergisch Gladbach, DE) |

2.1.7 Transfection reagent

| | |
|--------------------|----------------------------------|
| TransIT X2 | Mirus Bio (Madison, USA) |
| Lipofectamine 2000 | Thermo Scientific (Waltham, USA) |
| RNAimax | Thermo Scientific (Waltham, USA) |

2.1.8 Enzymes

| | |
|---|------------------------------------|
| T7 Endonuclease | New England Biolabs (Ipswich, USA) |
| Phusion DNA polymerase | New England Biolabs (Ipswich, USA) |
| RevertAid H Minus Reverse Transcriptase | Thermo Scientific (Waltham, USA) |
| BbSI | New England Biolabs (Ipswich, USA) |
| Fast Alkaline Phosphatase (AP) | Thermo Scientific (Waltham, USA) |
| T4 polynucleotide kinase | New England Biolabs (Ipswich, USA) |
| RiboLock RNase Inhibitor | Thermo Scientific (Waltham, USA) |

2.1.9 Dyes

| | |
|------------------------|----------------------------------|
| DNA loading dye (6x) | Thermo Scientific (Waltham, USA) |
| DNA stain G | Serva (Heidelberg, DE) |
| Hoechst 33342 | Pierce Bioscience (Bonn, DE) |
| MitoTracker Red CMXRos | Thermo Scientific (Waltham, USA) |
| Trypan blue | Lonza (Basel, CH) |

2.1.10 Molecular weight markers

| | |
|---|--------------------------------------|
| PageRuler Plus prestained protein Ladder (10-250 kDa) | Thermo Scientific (Waltham, MA, USA) |
| RNA molecular weight marker, DIG labeled (0.5 -10 kb) | Roche (Mannheim, DE) |
| TriDye 2-log DNA ladder (0.1-10 kb) | New England Biolabs (Ipswich, USA) |

2.1.11 Beads for pull-down

| | |
|------------------------------------|----------------------------------|
| Sepharose CL-4B | Sigma-Aldrich (Steinheim, DE) |
| Anti-flag M2 affinity gel | Sigma-Aldrich (Steinheim, DE) |
| Pierce Streptavidin magnetic beads | Thermo Scientific (Waltham, USA) |

2.1.12 Buffer and solutions**Lysis buffer**

| | |
|---|--|
| Lysis buffer for flag-IP | 20 mM Tris HCl (pH 7.5), 150 mM NaCl, 0.25%NP-40, 1.5 mM MgCl ₂ , 1 mM NaF, 400 U/ml RiboLock RNase inhibitor, protease inhibitor cocktail (1:100) |
| Lysis buffer for streptavidin pull-down | 50 mM Tris (pH 7.5), 150 mM NaCl, 0.1% SDS, 0.5% sodium deoxycholate, 1% Triton X-100, 10 mM NaN ₃ , 10 mM sodium ascorbate, 5 mM Trolox, protease inhibitor cocktail (1:100) |
| RIPA buffer | 50 mM Tris HCl (pH 8.0), 150 mM NaCl, 1% Triton X-100, 0.05% sodium deoxycholate, 10 mM EDTA, 2mM Na ₃ OV ₄ , protease inhibitor cocktail (1:100) |
| Erylysis buffer | 166 mM NH ₄ Cl, 0.29 mM KHCO ₃ , 3.4 mM EDTA, adjust to pH 7.2 |

SDS-PAGE and Western blot

| | |
|------------------------|---|
| TBS-T | 50 mM Tris (pH 7.6), 150 mM NaCl, 0.1%Tween 20 |
| Stacking buffer (4x) | 0.5 M Tris (pH 6.8), 0.1% SDS, 0.01% bromophenol blue |
| Separation buffer (4x) | 1.5 M Tris (pH 8.8), 0.1% SDS |
| Running buffer | 25 mM Tris, 200 mM glycine, 0.1% SDS |
| Transfer buffer | 25 mM Tris, 200 mM glycine, 20% methanol |

Loading dyes

| | |
|------------------------|--|
| Laemmli buffer (6x) | 300mM Tris HCl (pH 6.8), 60% glycerol, 12% SDS, 0.03% bromophenol blue, 5% BME |
| RNA loading dye (1,5x) | 98% formamide, 0.025% bromophenol blue, 50 mM EDTA |

Substrates

| | |
|------------------------------|--|
| Firefly-luciferase substrate | 20 mM tricine, 2.67 mM magnesium sulfate heptahydrate, 0.1mM EDTA (pH 8.0), 33.3 mM DTT, 0.53 mM ATP, 270 μ M Acetyl-coenzyme A, 131.6 μ g/ml Luciferin, 5 mM NaOH, 0.265 mM magnesium carbonate hydroxide |
|------------------------------|--|

2.1.13 Antibodies

| Antibody | Dilution | | Supplier |
|------------------------------------|----------|-------|----------------------------------|
| | WB | IF | |
| Primary antibodies | | | |
| Mouse anti-Cas9 | 1:1000 | | Cell signaling (Cambridge, UK) |
| Mouse anti-GAPDH | 1:30000 | | Merck Millipore (Darmstadt, DE) |
| Mouse anti-MAVS (E-3) | 1:1000 | 1:200 | Santa Cruz (Santa Cruz, USA) |
| Mouse anti-Phospho-IκBα (Ser32/36) | 1:1000 | | Cell signaling (Cambridge, UK) |
| Mouse anti-RIG-I (Alme-1) | 1:1000 | 1:100 | Adipogen (San Diego, USA) |
| Rabbit anti-flag | 1:1000 | 1:100 | Sigma-Aldrich (Steinheim, DE) |
| Rabbit anti-NAK (TBK1) | 1:500 | 1:100 | eBioscience (Waltham, USA) |
| Rabbit anti-Phospho-IRF3 (Ser396) | 1:500 | | Cell signaling (Cambridge, UK) |
| Rabbit anti-Phospho-TBK1 (Ser172) | 1:500 | | Cell signaling (Cambridge, UK) |
| Rabbit-anti-TRAF3 | 1:500 | | Santa Cruz (Santa Cruz, USA) |
| Rabbit-anti-UBASH3B | 1:1000 | | Abcam (Cambridge, UK) |
| Secondary antibodies | | | |
| Alexa Fluor 488 goat anti-mouse | | 1:400 | Thermo scientific (Waltham, USA) |
| Alexa Fluor 488 goat anti-rabbit | | 1:400 | Thermo scientific (Waltham, USA) |
| Alexa Fluor 568 goat anti-mouse | | 1:400 | Thermo scientific (Waltham, USA) |
| Alexa Fluor 568 goat anti-rabbit | | 1:400 | Thermo scientific (Waltham, USA) |
| Alexa Fluor 647 goat anti-mouse | | 1:400 | Thermo scientific (Waltham, USA) |
| Alexa Fluor 647 goat anti-rabbit | | 1:400 | Thermo scientific (Waltham, USA) |
| Goat anti-mouse IgG-HRP | 1:3000 | | Bio Rad (Munich, DE) |

| | | |
|-------------------------|--------|--|
| Goat ant-rabbit IgG-HRP | 1:3000 | Bio Rad (Munich, DE) |
| Streptavidin-FITC | 1:400 | BD Bioscience (Franklin Lakes, USA) |
| Streptavidin-HRP | 1:1000 | Jackson ImmunoResearch (Pennsylvania, USA) |

2.1.14 Cell lines

| | |
|--------------------------------|--|
| 1205 Lu cells | provided by Dr. Robert Besch (LMU, Munich) |
| HEK293T | ATCC (Manassas, USA) |
| PlatA | Cell biolabs (San Diego, USA) |
| HEK-Flip-In (Flp-In TREX™-293) | Invitrogen |
| HEK-flag-RIG-I | modified Flp-In TREX™ -293 with flag-RIG-containing pcDNA5 (frt-to) under Tet-inducible promoter |
| Fibroblasts | provided by Prof. Ania Muntau (LMU, Munich) |

2.1.15 Plasmids

Table 1: List of plasmids. All plasmids used in the thesis are listed with backbone vector, promoter and important characteristics.

| Name | Vector | Promoter | Characteristics |
|-------------------------|----------------|---------------------------|---|
| Luciferase assay | | | |
| RIG-I | pcDNA5/FRT /TO | CMV | |
| MAVS | pcDNA3.1 | CMV | |
| TBK-I | pcDNA3 | CMV | |
| IRF3-5D | pcDNA3.1 | CMV | Constitutively active variant of IRF3; Mutations: S396D, S398D, S402D, T404D, and S405D |
| UBASH3B | pcDNA3.1 (Zeo) | CMV | Flag at N-terminus |
| UBASH3B-H391A | pcDNA3.1 (Zeo) | CMV | Phosphatase-dead mutant of UBASH3B with point mutation H391A; flag at N-terminus |
| p125-firefly-luciferase | pGL3 | p125 (IFN β) | Reporter plasmid; Firefly luciferase expression controlled by IFN β promoter |
| pRL-TK-Renilla | pRL | HSV-thymidine kinase (TK) | Control reporter; Renilla luciferase expression controlled by TK promoter; purchased from Promega |
| APEX constructs | | | |
| APEX2-NES | pcDNA3 | CMV | Expresses APEX2 with flag at the N-terminus fused to NES sequence; used for cloning of APEX-MAVS constructs (131) |

| | | | |
|--------------------------|--------------------------------|--|--|
| APEX _N MAVS | pCDNA3 | CMV | APEX2 fused to the N-terminus of MAVS |
| APEX ₈₄ MAVS | pCDNA3 | CMV | APEX2 with flag at N-terminus or not fused into MAVS at AA 84 |
| APEX ₂₆₄ MAVS | pCDNA3 | CMV | APEX2 with flag at N-terminus or not fused into MAVS at AA 264 |
| APEX ₅₁₀ MAVS | pCDNA3 | CMV | APEX2 with flag at N-terminus or not fused into MAVS at AA 510 via the linker N`GGAAS`C |
| APEX-TM | pCDNA3 | CMV | APEX2 with flag at N-terminus fused to the TM domain of MAVS (AA 510) via the linker N`GGAAS`C |
| Mito-APEX | pCDNA3 | CMV | Expresses APEX fused to mitochondrial localization site (128) |
| APEX ₅₁₀ MAVS | pMXs-Puro | 5`LTR derived from MMLV | Retroviral expression of APEX ₅₁₀ MAVS |
| APEX-TM | pMXs-Puro | 5`LTR derived from MMLV | Retroviral expression of APEX-TM |
| Reconstitution | | | |
| UBASH3B | pLVX-Tight-Puro | P-tight, Tet-responsive promoter | Dox-inducible lentiviral expression of UBASH3B |
| UBASH3B-H391A | pLVX-Tight-Puro | P-tight, Tet-responsive promoter | Dox-inducible lentiviral expression of UBASH3B-H391A |
| tTA Advanced | pLVX-Tet-On Advanced | | Lentiviral vector for expression of tetracycline-controlled transcriptional activator; purchased from Clontech |
| Other | | | |
| hTERT | pBABE-puro | 5`LTR derived from MMLV | Retroviral expression of human telomerase reverse transcriptase; for generation of immortalized cell lines |
| eSpCas9 | eSpCas9(1.1)-2A-Puro or -Hygro | CBh (CMV enhancer + chicken β -actin promoter) | Expression of enhanced Cas9 with the respective inserted sgRNA (see Table 4) |

2.1.16 Software

| | |
|-----------------------|--|
| Microsoft Office 2016 | Microsoft (Redmont, USA) |
| GraphPad Prism 7 | GraphPad Software Inc. (California, USA) |
| Perseus 1.5.5.3 | Max Planck Institute (Munich, DE) |
| Corel Draw X7 | Corel (Ottawa, Canada) |

2.2 Methods for cell biology

2.2.1 Cell culture

All human cell lines were cultivated at 37°C, 95% humidity and 5% CO₂ concentration in DMEM supplemented with 10% FCS, 1.5 mM L-glutamine and 1% penicillin-streptomycin. Sub-cultivation was done every 3 to 4 days. The medium was removed, and cells were washed once with PBS before addition of trypsin to lift the cells off the flasks surface. After 5 min incubation at 37°C the reaction of trypsin was neutralized by addition of cell culture medium. For ensuing experiments, the cells were counted with a “Neubauer” cell counter and the viability was controlled by trypan blue staining. The cells were plated in a defined number one day prior to start of the experiment.

| Format | Cell line | Cell number |
|---------------------------|-------------------|---------------------|
| 96-well | 1205 Lu | 1×10 ⁴ |
| 24-well | | 5×10 ⁴ |
| 6-well | | 3×10 ⁵ |
| 10 cm ² dish | | 1.5×10 ⁶ |
| 20 cm ² dish | | 5×10 ⁶ |
| 96-well | HEK293T, PlatA | 3×10 ⁴ |
| 6-well | | 8×10 ⁵ |
| 10 cm ² dish | | 4×10 ⁶ |
| 175 cm ² flask | | 1×10 ⁷ |
| 24-well | Human fibroblasts | 2.5×10 ⁴ |
| 6-well | | 1×10 ⁵ |

2.2.2 Virus infection

For viral infection assays vesicular stomatitis virus (VSV) Indiana strain provided by Prof. Dr. Anne Krug (LMU München) was used.

One day after plating, the cells were infected with VSV using a multiplicity of infection (MOI) of 1. The MOI reflects the amount of virus particles present per cell in an infection assay. The infection was performed in a minimal volume of Opti-MEM medium and 2 to 4 h after infection the supernatant was removed and replaced by growth medium. At indicated time points after infection (hpi) the cells were processed for further analyses.

2.2.3 Transfection of plasmid DNA

Plasmid DNA was transfected using TransIT X2. For transfection of 1 µg DNA 2.5 µl transfection reagent was used and diluted together in Opti-MEM (20 % of the total growth medium). The mix was incubated for 5 – 10 min at room temperature (RT) and pipetted drop-

wise onto the cells. Expression of the indicated protein was allowed for 24 h before proceeding with the experiment.

2.2.4 Stimulation with synthetic RNA molecules

To activate antiviral signaling, the cells were stimulated with different RNAs. A commercially available high molecular weight polyinosinic:polycytidic acid (pIC) was used to activate TLR3 signaling by supplying the RNA without transfection. pIC was diluted in Opti-MEM (20 % of the total growth medium) for a final concentration of 5 µg/ml and directly added into the cells medium.

A synthetic short RNA molecule of 44 bp with a hairpin structure and a triphosphate moiety at the 5' end (3p-RNA) synthesized in our group by in-vitro transcription with the sequence 3p-GCGCUAUCCAGCUUACGUA GAGCUC loop UACGUAAGCUGGAUAGCGC-5' was used as a RIG-I specific stimulus. The RNA was diluted in Opti-MEM (20 % of the total cell culture medium) to have a final concentration of 500 ng/ml. Per 1 µg RNA 3 µl RNAimax was added incubated for 10 min at RT and transferred drop-wise onto the cells. The cells were stimulated for the indicated time points before proceeding with the experiment.

2.2.5 Transfection of RNA isolated from VSV-infected cells

For determination of the immunostimulatory capacity of the RNA species generated after a certain time after infection and replication of VSV, total cellular RNA of infected cells was isolated (see 2.3.12), fragmented (see 2.3.13) and re-transfected into 1205 Lu cells. This allowed to determine the immune response to the naked RNA without the influence of viral replication or viral proteins.

1205 Lu cells plated in a 96-well were either transfected with 250 ng of the total cellular RNA or 10 µl of the fragmented RNA. For that the RNA was diluted in Opti-MEM in a total volume of 20 µl and mixed with 0.3 µl Lipofectamine RNAimax diluted in 20 µl Opti-MEM. After 10 min at RT the transfection mix was added to the cells and 24 h later the supernatant was taken for determination of IP-10 release via ELISA.

2.2.6 Transduction and generation of stable cell lines

Transduction is the process of integrating foreign DNA sequences into the genome of cells via viral vectors. To do this, lenti- or retroviral expression plasmids are used, that encode the gene of interest within a replication-incompetent viral genome.

For generation of viral particles derived from retroviral expression vectors, PlatA cells were used. This cell line is derived from HEK293T cells and stably expresses the retroviral proteins (*gag*, *pol*, *env*) needed for replication and packaging of the viral genome. Three 6-wells of these cells were transfected with 4 µg/ well of the retroviral expression vector. After 24 h the virus-containing supernatant was taken, flushed through a 0.45 µm pore-size filter,

supplemented with 4 µg/ml polybrene and applied to three 6-wells of the cell line to be modified. The PlatA cells were covered with 2 ml/well of fresh growth medium to produce more viral particles. After further 24 h the virus-containing supernatant was taken again and the transduction was repeated. 24 h after this second transduction hit the selection process of the cells was started. All retroviral expression plasmids used, additionally encode for puromycin resistance. For 1205 Lu cells and fibroblasts 2 µg/ml of puromycin was used as selection pressure and the medium was exchanged every second day with medium containing fresh antibiotics until the untransduced control cells were dead. Transduced cells were kept always under selection pressure with 1 µg/ml of puromycin.

Lentiviral particles were used for generation of cell lines, that express the gene of interest under a doxycycline-inducible promoter. For production of viral particles, HEK293T cells were transfected with plasmids encoding the viral envelope proteins VSV-G (250 ng/ml) (*env*) and the plasmid dR8.91 (250 ng/ml) encoding for *gag* and *pol* along with the lentiviral expression plasmid (500 ng/ml) encoding the gene of interest (pLVX-tight-puro) or the doxycycline-controlled transactivator (pLVX-Tet-on). The expression of both plasmids in a cell allows the tight regulation of gene expression for the gene of interest by the doxycycline concentration in the cell medium.

Both virus supernatants were taken 24 h after transfection, cleared through a 0.45 µm filter and supplemented with 4 µg/ml polybrene. The supernatants were mixed in a ratio of 5:1 (pLVX-tight-puro:pLVX-Tet-on) and 2 ml were added onto a 6-well of the cells to be modified. In total three 6-wells were transduced per cell line and gene of interest. 48 h after transduction the cells were selected with puromycin (2 µg/ml) and G418 (1 mg/ml) as the corresponding resistance genes are encoded on pLVX-tight-puro and on pLVX-Tet-on respectively. After all untransduced control cells died, transduced cells were further cultivated under constant selective pressure with 1 µg/ml puromycin and 0.25 mg/ml G418.

2.2.7 Tetracycline and doxycycline induction

For induction of flag-RIG, HEK293T-flag-RIG-I and control cells HEK293T-Flip-In were cultivated with 1 µg/ml tetracycline.

Cells transduced with pLVX-Tet-on inducible system were treated with the tetracycline derivate doxycycline in concentrations of 10 – 1000 ng/ml.

Each antibiotic was diluted in fresh growth medium and added to the cells to allow expression of the induced protein 24 h before the experiment started.

2.2.8 Generation of knockout cell lines using the CRISPR/Cas9 system

The CRISPR/Cas9 system is a method that allows the targeting and modification of a specific DNA sequence of a cell's genome. The modification induced at the target site by Cas9 includes random insertions or deletions of bases that can lead to missense mutations, thus leading to the knockout (KO) of the targeted gene.

Cas9 is a bacterial protein, that originally belongs to the bacterial adaptive immune system and removes foreign DNA. This endonuclease is able to bind a specific RNA sequence (crRNA) and cut DNA in the close surrounding. By fusing the crRNA to a target-specific sequence of 23 bp (sgRNA) including the specific motif `NGG`, the so-called PAM (protospacer adjacent motif) that is needed to activate Cas9, the enzyme cuts the DNA at the desired site in the genome that is complementary to the sgRNA.

Hence, the first step for generating KO cells was to find a suitable gene-specific sgRNA. For this purpose, the online tool <http://chopchop.cbu.uib.no/> was used. From the suggested sequences by the software, sgRNAs were chosen that have no or low off-target sites, that are in one of the early exons and that bears the nucleotide G at the 5' end, a feature needed for the enhanced Cas9 (eCas9) to bind highly specific. The eCas9 is an optimized Cas9 that has an enhanced specificity with reduced off-target effects. The cloning of the sgRNA encoding oligonucleotides into the eSpCas9 vector was done as described in 2.3.5.

Per plasmid three 6-wells were transfected with 250 ng/ml of the respective sgRNA encoding eSpCas9 plasmid. After 24 to 48 h the selection was started by addition of fresh growth medium supplemented with 2 µg/ml puromycin or 10 µg/ml blasticidin, depending on the resistance encoded on the plasmid. The medium was replaced by fresh antibiotics containing medium every day until the untransfected control cells were dead. Subsequently the cells were washed with PBS and further cultivated in medium without the selective antibiotic.

Either all surviving cells were expanded and used as a KO batch or they were collected and plated in 96-well plates in a concentration of 1 cell/well to generate single cell clones (SCC). These SCC were analyzed whether their DNA sequences were modified at the target site by T7 digestion (see 2.3.2) and positive clones were checked by Sanger sequencing for the kind of inserted mutation. Only clones showing one or two defined modifications that cause a biallelic frame shift were called a complete KO and used for further experiments.

In the second round of generation of UBASH3B-KO cells, the SCC were analyzed by deep sequencing in the group of Prof. Veit Hornung (Gene center, Munich) and the online tool outknocker.org was used to identify SCC that have frame shift mutations on both alleles.

2.2.9 Induction of biotin labeling with APEX

For the labeling, APEX-expressing cells were incubated with 500 μ M biotin-phenol dissolved in culture medium for 30 min at 37°C, that served as substrate for APEX. To induce the APEX reaction 100 mM H₂O₂ solution was directly pipetted into the medium to a final concentration of 1 mM and incubated for 1 min at RT. Immediately, the medium was removed and the cells were strongly washed three times with PBS containing the quenchers (10 mM NaN₃, 10 mM sodium ascorbate, 5 mM Trolox) to stop the enzymatic reaction of APEX. The labeled cells were either analyzed by immunofluorescence, Western blot or were processed for streptavidin pull-down (see 2.4.2).

2.2.10 Live cell staining with Mitotracker

Co-staining of mitochondria for subsequent confocal imaging (see 2.4.7) was performed with Mitotracker red that accumulates in living mitochondria due to its membrane potential.

100 nm MitoTracker Red CMXRos was diluted in pre-warmed growth medium and added to the cells 30 min prior to fixation.

2.2.11 Isolation and cultivation of murine bone marrow-derived macrophages

For isolation of bone marrow cells, the femurs of the mice were used. The bones of UBASH3A/B-KO mice were kindly provided by the group of Prof. Christian Brandts (University hospital, Frankfurt). Wt mice of the same background strain C57BL/6 were used as controls. The bones delivered in PBS were washed in 70% Ethanol for 2 min and transferred into cell culture medium (RPMI supplemented with 10 % FCS, 1 mM L-glutamine, 1% Sodium pyruvate, 1% Penicillin-Streptomycin and 100 μ M BME) in a 10 cm² dish. A 5 ml syringe was used to flush the bones with PBS through a 0.45 μ m filter into a 50 ml falcon. The cells were centrifuged at 400 g for 5 min and the supernatant was discarded. 3 ml erylisis buffer was added, mixed and incubated for 3 min before PBS was added to a total volume of 25 ml. The cells were centrifuged (400 g, 5 min) and resuspended in 1 ml cell culture medium.

For differentiation of macrophages (BMDMs) 8x10⁶ cells were seeded in a 10 cm² dish and 20 ng/ml M-CSF was added. After three days the medium was completely exchanged with fresh medium containing newly added M-CSF.

Three days later the cells were collected and plated in a 96-well plate with 2x10⁴ BMDMs/well in medium containing fresh M-CSF. The experiment was started one day after seeding.

2.3 Methods for molecular biology

2.3.1 Polymerase chain reaction

The polymerase chain reaction (PCR) was used to either amplify gene coding cDNA sequences from plasmids for further sub-cloning or to amplify the target locus of sgRNA from total cell DNA. For quantitative reverse transcriptase PCR see 2.3.15.

The standard PCR mix was as follows:

| Component | Volume |
|------------------------|------------|
| 5x Phusion HF buffer | 10 µl |
| dNTPs (10 mM) | 1,0 µl |
| Forward primer (10 µM) | 2,5 µl |
| Reverse Primer (10 µM) | 2,5 µl |
| Phusion DNA Polymerase | 0,5 µl |
| Plasmid/ genomic DNA | 20/ 100 ng |
| H ₂ O | ad 50 µl |

The PCR mix did run in the thermocycler under the following standard cycling conditions:

| Step | Temperature | Time | |
|----------------------|--|-----------|-----------|
| Initial denaturation | 98°C | 30 sec | |
| Denaturation | 98°C | 10 sec | |
| Annealing | 60 – 72°C (Primer melting temp + 3°C) | 30 sec | 25 cycles |
| Elongation | 72 °C | 30 sec/kb | |
| Final extension | 72°C | 5 min | |
| Hold | 4°C | hold | |

2.3.2 T7 endonuclease digestion

The T7 endonuclease is an enzyme that recognizes and cleaves mismatched DNA and was used to detect the presence of CRISPR/Cas9- generated genomic changes at the target site (see 2.2.8).

First, an app. 500 bp DNA sequence including the sgRNA-target site was amplified via PCR (see 8.4). The PCR products of wt cells and of the CRISPR/Cas9 treated cell clone in question were pooled (10 µl each) and annealed under the following conditions in the thermocycler:

95°C, 10 min

95°C to 85°C, -2°C/s

85°C to 25°C, -0.1°C/s

4°C, hold

Afterwards 0.5 µl T7 Endonuclease, 1x NEB buffer 2 and H₂O was added to a total volume of 30 µl. The reaction was incubated at 37°C for 1 h and analyzed for cleavage by gel electrophoresis.

2.3.3 DNA gel electrophoresis

For size-dependent separation of PCR products and digested plasmids agarose gel electrophoresis was performed. Depending on the size of the expected fragment 0.8 – 2 % agarose gels were used supplemented with 3.5 µl DNA stain per 100 ml gel. For loading, the samples were mixed with 1x DNA Loading dye and run at 100 V for 20 – 60 min. A 10 kb DNA ladder was used for size determination.

2.3.4 Gel extraction of DNA

To purify PCR products and digested plasmids the Gel extraction kit of Zymoresearch was used according to the manufacturers protocol. The resulting DNA concentration and purity was determined by photometric measurement in a nanodrop TM instrument.

2.3.5 Annealing of oligonucleotides encoding sgRNA

Synthetic DNA oligonucleotides coding for positive and negative strand of the sgRNA flanked by the restriction site of the enzyme BbsI (see 8.3) were ordered and annealed as follows:

| Component | Volume |
|--------------------------|----------|
| Oligo-top (100 µM) | 1 µl |
| Oligo-bottom (100 µM) | 1 µl |
| 10x T4 DNA ligase buffer | 1 µl |
| T4 Polynucleotide kinase | 1 µl |
| Phusion DNA Polymerase | 0.5 µl |
| H ₂ O | ad 10 µl |

The reaction was incubated in the thermocycler at 37°C for 30 min, heated up to 95°C for 5 min before it was slowly (1°C/min) cooled down to 4°C.

The annealed oligonucleotides were diluted 1:200 and 3 µl were used for subsequent cloning (see 2.3.7) into 100 ng BbsI-linearized eSpCas9 vector.

2.3.6 Restriction enzyme digest

For cloning of protein coding cDNA into a vector, the vector and the purified PCR product were cut with two restriction enzymes to allow a subsequent ligation. The primers for the PCR therefore had the specific restriction sites at their 5' end.

The standard reaction was as follows:

| Component | Volume |
|------------------------------------|----------------------|
| 10x Appropriate restriction buffer | 3.0 µl |
| Restriction enzyme I | 1.0 µl |
| Restriction enzyme II | 1.0 µl |
| Plasmid/ PCR product | 1-2 µg/ 100 – 500 ng |
| H ₂ O | ad 30 µl |

The reaction was incubated for 1 – 3 h at 37°C. To avoid re-ligation of the linearized plasmid, 1 µl FastAP (Alkaline Phosphatase) was added to the reaction mix and incubated another 30 min at 37°C. The cut plasmid was isolated via gel electrophoresis and purified with gel extraction kit, whereas the digested PCR product was only column-purified.

2.3.7 Restriction-enzyme based ligation

To insert the cDNA of interest into a recipient vector, the digested and purified fragments were ligated. The vector and insert were mixed in a molar ratio of 1:3 to 1:10 (vector:insert), 1 x ligase buffer and 1 µl ligase was added to a total volume of 20 µl. The ligation run for 4 to 16 h at RT.

2.3.8 In-Fusion® cloning

The conventional molecular cloning relies on restriction sites to fuse fragments together, which is often a limiting factor for cloning. To overcome this, the so-called In-fusion cloning was performed, that works independent of any restriction site. It relies on the In-fusion enzyme that recognizes complementary 15 bp overhangs of the vector and insert and ligates it. The vector can be opened at any desired position by inverse PCR and the primers for amplification of the insert are designed with 15 bp overhang complementary to the linearized vector site.

This method was used to generate the MAVS-APEX fusion constructs, where APEX was inserted into different sites of the cDNA of MAVS. The cloning was performed with the In-Fusion® HD cloning kit according to the manufacturers protocol.

2.3.9 Bacterial transformation

After ligation, the plasmid DNA was introduced into bacteria for amplification of the plasmid. 5 µl of the ligation mix was added to 50 µl of competent E. coli bacteria (used strains: DH5α

and MACH1) and incubated for 30 min on ice. Subsequently, the bacteria were heat shocked for 60 sec at 42°C and immediately put back on ice for 5 min. For recovery of the cells, 500 µl LB growth medium was added and incubated under shaking conditions for 1 h at 37°C. Afterwards the cells were plated on Agar plates supplemented with the required antibiotic.

2.3.10 Purification of plasmid DNA

For isolation of plasmid DNA, distinct bacterial colonies were picked and incubated in 5 ml LB growth medium containing antibiotic for selection at 37°C under shaking overnight.

The grown bacteria were pelleted, and plasmid DNA was isolated with the kit GeneJET Plasmid Miniprep Kit from Thermofisher as described in the manufacturer's protocol.

2.3.11 RNA purification

Total RNA was isolated from cells grown in a 24-well using an RNA isolation kit (PeqLab). The kit was used according to the manufacturer's protocol.

2.3.12 Phenol-chloroform-based RNA purification

To analyze the VSV-derived RNA molecules, either after immunoprecipitation, for re-transfection or for fragmentation, the RNA was isolated with the miRNeasy Kit from Qiagen. This kit is suitable to isolate high amounts of pure RNA, including small molecules >18 bp. It relies on the phenol-chloroform precipitation, that separates the RNA from DNA and proteins.

The RNA isolation was performed as described in the provider's manual.

2.3.13 RNA fragmentation

HEK293T cells grown in a 10 cm² dish and infected with VSV for 24 h were lysed and RNA was isolated by phenol-chloroform precipitation (see 2.3.12). 8 µg of the RNA was supplemented with 1.5 x RNA loading dye, heated for 10 min at 70°C and immediately put on ice. After 10 min the RNA was separated on 0.8 % agarose gel at 60 V for 2.5 h. For size determination a 10 kb RNA ladder was used. After separation the RNA was cut size-dependently into 10 fractions.

The gel extraction of the RNA was done with the *Zymoclean Gel RNA Recovery* kit according to the manufacturer's protocol and used for re-transfection of 1205 Lu cells (see 2.2.5).

2.3.14 cDNA synthesis

First-strand cDNA was generated from 200 ng of total RNA or from 10 µl re-isolated RNA after fragmentation and purification. For analyzes of viral genome sequences the transcription was performed with Random Hexamer Primer. If only mRNA transcription was desired, Oligo(dT) primer were used.

The reaction mix was composed as follows:

| Component | Volume |
|---|-----------------------|
| 5x Reverse Transcriptase buffer | 4,0 µl |
| dNTPs (10 mM) | 2,0 µl |
| OligodT/ Random Hexamer Primer (10 µM) | 2,0 µl |
| Ribolock RNase Inhibitor | 0,5 µl |
| RevertAid H Minus Reverse Transcriptase | 0,5 µl |
| RNA | 200 ng or as required |
| H ₂ O | ad 20 µl |

2.3.15 Quantitative reverse transcriptase polymerase chain reaction

For quantification of the relative amount of specific mRNAs or of viral genome sequences, quantitative reverse transcriptase polymerase chain reaction (qRT-PCR) was used. Relative gene expression was calculated as the ratio of gene of interest to the house-keeping gene both determined in the same sample. For all runs the standard Roche protocol for mono color hydrolysis probes with 45 amplifications were used and run with the LightCycler 480 instrument. The primers and probes are listed in 8.2. The reaction mix was composed as follows:

| Component | Volume |
|-------------------------------|---------------|
| 2x Kappa Probe Fast mastermix | 5,0 µl |
| Forward primer (10 µM) | 0,2 µl |
| Reverse primer (10 µM) | 0,2 µl |
| Fluorescent hydrolysis probe | 0,1 µl |
| cDNA (diluted 1:3) | 3,0 µl |
| H ₂ O | ad 20 µl |

2.4 Methods for protein biochemistry

2.4.1 Immunoprecipitation of flag-RIG-I-bound RNA

For the analysis of RIG-I bound RNA, HEK293T cells that overexpress flag-tagged RIG-I under the control of a tetracycline inducible promoter (HEK-flag-RIG-I) were infected with VSV. HEK293T cells that only bear the empty plasmid without the flag-RIG-I insertion (HEK-Flip-In) served as negative control. For each condition 4×10^7 cells were plated in $4 \times 175 \text{ cm}^2$ flasks. The expression of flag-RIG-I was induced by addition of tetracycline ($1 \mu\text{g/ml}$) and 24 h later the cells were infected with VSV (MOI 1). Another 24 h later the cells were collected, washed 2x with PBS and resuspended in 1 ml lysis buffer. After centrifugation (14000 g , 15 min, 4°C) the supernatant was collected and added to 500 μl of sepharose beads, that were washed 2x with lysis buffer prior to usage (5000 g , 1 min). This pre-clearing step was performed for 1 h at 4°C with permanent rotation and should clean the lysate from all unspecific binding partners. The beads were centrifuged at 5000 g for 1 min and the supernatant was added to 250 μl of anti-flag coupled beads, that were washed 2 x with lysis buffer before. The incubation was proceeded for 2 h at 4°C under constant rotation. Subsequently, the beads were centrifuged (1000 g , 1 min) and washed 5 x with lysis buffer (1000 g , 30 sec). In between the beads were incubated for 5 min under rotation at 4°C .

For elution of the flag-bound proteins and nucleic acids the beads were resuspended in 200 μl lysis buffer and put onto a column. To dry the beads, they were centrifuged for 30 sec at 5000 g . The column was transferred into a clean tube and 10 μl of 3x flag-peptide and 3 μl RiboLock was added directly on the beads and incubated for 10 min under shaking at room temperature (RT). Afterwards 3 x flag-peptide was diluted in TBS (1:50) and 137 μl were added to the beads and again was incubated for 10 min under shaking. Due to competitive binding of the flag-peptide the flag-bound proteins and nucleic acids were released into the solution. Finally, the eluate was collected by centrifugation (4000 g , 3 min, 4°C) and used for further isolation of RNA (see 2.3.12) that was used for the analysis of viral genomic sequences by qRT-PCR.

2.4.2 Streptavidin pull-down of APEX-biotinylated proteins

For enrichment of proteins biotinylated by APEX, a streptavidin pull-down was performed.

After induction of APEX-labeling for 1 min (see 2.2.9), the cells grown in a 10 or 20 cm^2 dish were washed three times with PBS supplemented with quenchers (10 mM NaN_3 , 10 mM sodium ascorbate, 5 mM Trolox). To get rid of free biotin that could interfere with streptavidin it was important to use a big volume of wash buffer for each wash step (20 ml per 20 cm^2 dish and 10 ml per 10 cm^2 dish).

Afterwards the cells were lysed in lysis buffer containing quencher (1 ml for 10 cm² dish and 2 ml for 20 cm² dish). For further lysis of the nucleus and solubilization of protein aggregates the sample was sonicated three times for 10 sec with 10 sec break on ice. Since the quenchers interfere with the DCTM protein assay, reference cells were lysed in lysis buffer without quenchers to determine the protein concentration. The protein concentration was adjusted to 1 mg/ml. Prior to pull-down, the magnetic streptavidin beads were washed two times with lysis buffer using a magnetic rack for Eppendorf tubes. Afterwards 600 µg protein per 100 µl magnetic streptavidin beads were added and incubated for 1 h at RT under rotation. The beads were washed three times with lysis buffer.

For further mass spectrometric analysis 3 mg protein derived from two 20 cm² dishes were used for pull-down and the beads were stored in 500 µl lysis buffer at -80°C. They were further processed by on-bead digestion in the group of Prof. Axel Imhof and analyzed via LC/MS.

For Western blot analysis the pull-down was performed from 300 µg protein derived from a 10 cm² dish. After washing the beads, they were incubated with 50 µl 3x Laemmli buffer containing 5 % BME for 10 min at 95 °C. Finally, the beads were removed using the magnetic rack.

2.4.3 Preparation of cell lysates for Western blot

For Western blot analysis, the cells were grown in a 6-well plate, washed once with PBS, lysed in 150 µl RIPA buffer and incubated for 10 to 30 min at 4°C. The lysed cells were collected with a cell scraper. For complete lysis, the samples were further treated by sonification for three times 10 sec with 10 sec break on ice.

For detection of MAVS aggregates the samples were not sonicated, thus the pellet still contains unlysed cell organelles and protein aggregates. The samples were further centrifuged at 14000 g for 10 min at 4°C and the lysate was separated from the pellet. After determination of the protein concentration the lysate and pellet were incubated at 95°C with 1x Laemmli buffer containing 5 % BME for 5 or 30 min, respectively.

2.4.4 Determination of protein concentration

The protein concentration of cell lysates was measured using the DCTM protein assay from Bio-Rad. This is a colorimetric assay based on the Lowry protein assay. The assay was performed according to the manufacturer's protocol.

2.4.5 SDS-polyacrylamide gel electrophoresis (PAGE) analysis

Size-dependent separation of proteins by sodium dodecyl sulfate polyacrylamide gel electrophoresis (SDS-PAGE) was performed using 10 % separation and a 5 % stacking gels (for ingredients of the gels see the table below). 10 – 40 µg of protein sample (see 2.4.3) were

loaded on the gel and electrophoresis was performed in 1x running buffer starting with 100 V for 30 min followed by 150 V until complete separation. The 250 kDa PageRuler was used as a marker for protein size.

| Component | 5 % stacking gel | 10 % resolving gel |
|------------------------------|-------------------------|---------------------------|
| H ₂ O | 2.26 ml | 4.1 ml |
| Rotiphoresis Gel 30 (37,5:1) | 0.68 ml | 3.3 ml |
| Stacking buffer (4x) | 1.0 ml | - |
| Resolving buffer (4x) | - | 2.5 ml |
| 10 % APS | 0.04 ml | 0.1 ml |
| TEMED | 0.004 ml | 0.004 ml |
| Trichlorethanol | - | 0.05 ml |

2.4.6 Western blot

After protein separation, a wet blot was performed. The proteins were electrophoretically moved from the gel onto a PVDF membrane with a pore size of 0.45 µm or 0.2 µm (for detection of phosphorylated proteins) in 1x transfer buffer containing 20 % methanol at 250 mA for 2 h.

Subsequently, the membrane was washed once in TBS-T. To avoid unspecific antibody binding the membrane was blocked in 5% milk or 3% BSA in TBS-T for 2 h at RT or overnight at 4°C. For protein staining, the membrane was probed with the primary antibody for 2 h, washed three times for 10 min and the HRP-linked secondary antibody was added for 1 h at RT. Again, the membrane was washed three times. Addition of the ECL substrate (ECL-Pico chemiluminescence kit or the ECL reagent of Bio-Rad) started the HRP reaction, that was detected with the alpha imager HP-system or Chemidoc system of Bio-Rad.

2.4.7 Immunofluorescence imaging by confocal microscopy

For confocal microscopy the cells were plated on 12 µm glass cover slips in a 24-well plate. The samples were fixed with 4% PFA for 10 min at RT, washed three times in PBS and permeabilized for 10 min in 0,1% Triton-X-100. After washing, the samples were blocked with 3% BSA for 2 h at RT or overnight at 4°C.

The cells were washed again and incubated with the primary antibody diluted in PBS for 2 h at RT or overnight at 4°C. The secondary antibody conjugated with a fluorophore and diluted in PBS was added after another washing step and incubated for 1 h at RT.

The nucleus was stained by addition of 5 μ M DNA binding dye Hoechst 33342 in PBS for 5 min, before the cells were finally washed. The cover slips were mounted on a glass slide with Mowiol-488, dried overnight and imaged using a Leica TCS SP5 confocal microscope.

2.4.8 Enzyme-linked immunosorbent assay

The release of the cytokines IP-10 and IL-6 into the cell cultures medium was measured via enzyme-linked immune-sorbent assay (ELISA). The assay was performed according to the manufacturers protocol. For measuring cytokines, the supernatants were collected and measured directly or stored at -20°C.

2.4.9 Luciferase assay

HEK293T cells were plated in a 96-well plate. Each well was transfected with a total DNA amount of 219 ng complexed with 0.55 μ l Lipofectamine 2000 in 20 μ l Opti-MEM, incubated for 10 min at RT and applied dropwise onto the cells.

The DNA amount was composed of 40 ng luciferase reporter plasmid, 4 ng renilla plasmid, 25 ng of the signaling protein encoding plasmid and 0 – 150 ng UBASH3B encoding plasmid. To keep the total DNA amount constant in every condition, the empty pcDNA3 vector was used to stuff up the DNA amount if necessary. Each condition was done in four technical replicates.

After 24 h of transfection the cells were lysed in 50 μ l 1x passive lysis buffer and incubated 10 min at RT. 20 μ l/well of the lysate was then transferred onto two different white microtiter plates. On one plate 20 μ l/well of the luciferase substrate and on the other 20 μ l/well of the renilla substrate coelenterazine h (1:800 in H₂O) was added and the luminescence was measured with a microplate reader.

2.5 Statistics

The data are presented as mean \pm SEM. Statistical significance was calculated by unpaired Student's t-test and kinetic data were additionally corrected for multiple comparison using the Holm-Sidak method (* $p \leq 0,05$; ** $p \leq 0,01$ und *** $p \leq 0,001$).

3 Results

3.1 Characterization of RIG-I ligands during infection with vesicular

stomatitis virus

3.1.1 Detection of a specific defective interfering genome in the VSV virus stock

Preliminary work in our group done by Andreas Linder aimed to identify the specific ligand of RIG-I in the replication cycle of VSV. HEK293T cells bearing a tetracycline (Tet)-inducible flag-tagged RIG-I or only the backbone vector Flip-In (negative control), were Tet-induced for 24 h followed by VSV infection for 9 h. Subsequently, the cells were lysed and a flag-IP was performed. The RNA was isolated and analyzed by next generation sequencing. These data revealed, that on the one hand in the flag-RIG condition the whole (-)ssRNA genome was enriched by 5-fold. On the other hand, there was a 23-fold enrichment at genomes position 6497 until the 5'end of the genome. The trailer region in (+)ssRNA orientation showed the same high enrichment. These enriched sequences show typical features of a so-called copy-back DI genome: it has a highly shortened genome and the reverse complementary trailer sequence at the 3'end (Figure 4A). This result raised the hypothesis that this DI genome is the major ligand of RIG-I (140).

The precise analysis of the deep sequencing data allowed the reconstruction of this specific DI genome with a length of 4719 bp. Based on the reconstructed sequence, a specific set of primers was designed that binds in the trailer region and at the boarder of the reverse complement trailer/L-gene (Figure 4 A). A qRT-PCR assay based on these primers allowed the detection of this identified DI genome and to follow its expression over time after infection with VSV. The observed increase of the DI genome up to 24 h after infection followed the same kinetics as the increase of the viral N protein and the IFN- β level, reflecting transcription of the full-length genome and the induction of the immune response, respectively. Cycloheximide (CHX) is an inhibitor of translation and by blocking the translation of the viral polymerase indirectly also an inhibitor of viral replication. Addition of CHX completely abolished the increase of the mRNA of the N protein as well as of the DI genome, suggesting that its propagation depends on the translation of VSV-N and the viral polymerase (Figure 4 B - D). In addition, the CHX data confirm that the interferon induction by VSV requires newly translated proteins and seems to depend on replication of the full-length or DI genome.

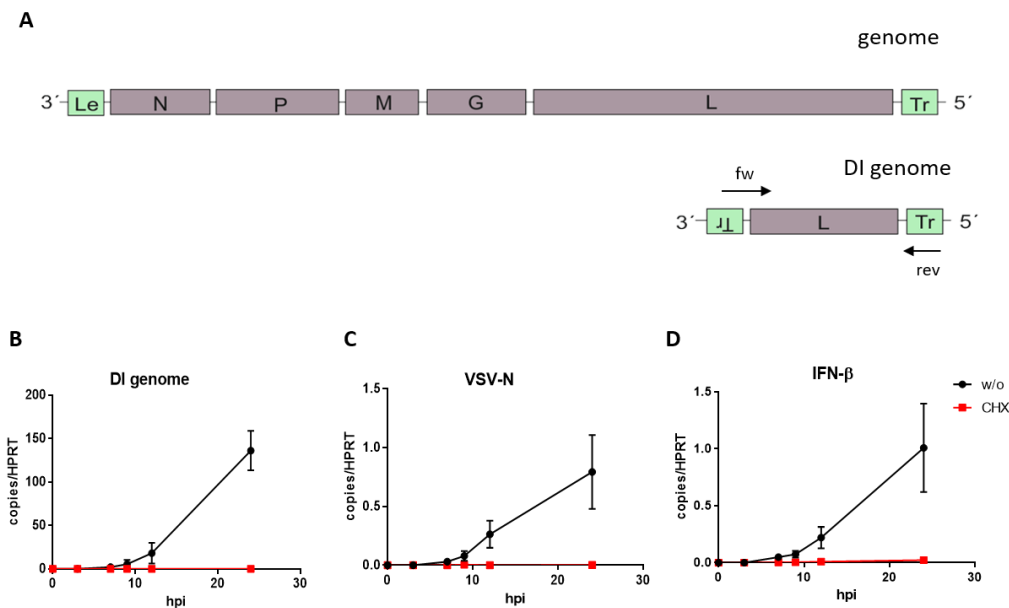


Figure 4: Detection of a specific DI genome in the VSV virus stock. (A) The copy-back DI genome was identified by deep sequencing analyses of RIG-I bound RNA. It bears a reverse complement trailer sequence at the 3' end, has a size of 4719 nucleotides and can be detected with a specific set of primer. HEK293T cells plated in 96-well plate were either treated with CHX (100 µg/ml) or not and infected with VSV (MOI 1). The RNA was isolated at the indicated time points. After cDNA synthesis the samples were analyzed via qRT-PCR for (B) the specific DI genome (C) the N protein of VSV and (D) the IFN-β level normalized to HPRT. Data are shown as mean ± SEM (n=3).

3.1.2 The defective interfering genome of VSV has a major impact on the immune response

After proofing the existence of the specific DI genome in our standard VSV stock and its replication after infection, its impact on the immune response was determined.

To achieve this, a virus stock was generated that is free of detectable DI genomes. A common method to do so, is to infect cells with a very low MOI over several passages. In fact, BHK cells grown in a 6-well plate were infected with an MOI of 10^{-6} and after 24 h the supernatant was collected and reused for a repetitive infection, each time with an MOI of 10^{-6} . This procedure was repeated for 5 passages until the DI genome was nearly completely diluted out as confirmed by qRT-PCR (P5) (Figure 5 B).

Compared to the original virus stock (P0), the infection with the stock containing low amounts of DI genome (P5) showed a highly decreased IFN-β-level measured 24 h post infection (hpi) by qRT-PCR (Figure 5 C). This was in line with the decreased immunostimulatory effect of the total RNA isolated at this time point from the infected cells and used for re-transfection of uninfected 1205Lu cells. In this assay, that measures the amount of immunostimulatory RNA in a cell at a certain time point, the IP-10 amount in the supernatant 24 h post transfection was strongly decreased when the RNA was isolated from cells infected with the

P5 stock compared to cells infected with the P0 stock (Figure 5 D). These results are in accordance with the hypothesis that DI genomes are the main trigger of the interferon response after VSV infection.

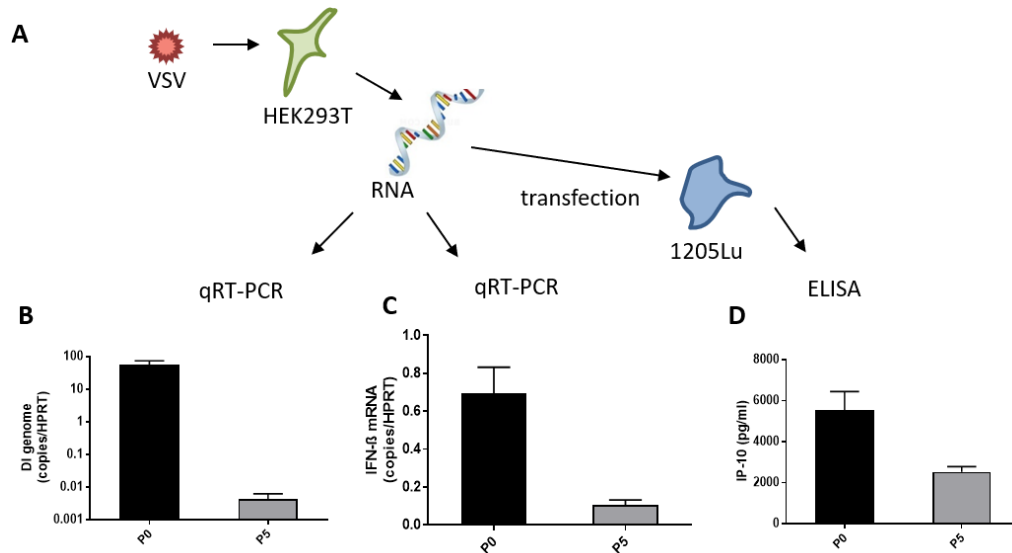


Figure 5: The DI genome of VSV has a major impact on the immune response. The generation of P5 was performed by serial dilution of the original VSV stock P0 on BHK cells. (A) HEK293T cells grown in a 24-well plate were infected with either VSV stock P0 or P5 (MOI=1). 24 h later the cells were lysed and RNA was isolated. The RNA was analyzed by qRT-PCR for (B) DI genome and (C) IFN- β mRNA level normalized to HPRT. (D) The isolated RNA was further used for transfection of 1205Lu cells in a 96-well plate and the amount of IP-10 in the supernatant was measured by ELISA 24 h post stimulation. Data are shown as mean \pm SEM (n=3).

Since the previous results could show binding of the DI genome to RIG-I and suggested a strong effect on interferon induction, it was of further interest to determine the specific size the immunostimulatory RNA has and if there are differences between the viral stocks P0 and P5.

To address this question, the RNA of HEK293T cells infected with either P0 or P5 was isolated and separated on an agarose gel. To separate the RNA according to size, the gel was size-dependently cut into ten fractions (Figure 6 A). The RNA of each fraction was re-isolated and used for re-transfection into 1205 Lu cells. The amount of IP-10 was measured 24 h post transfection by ELISA, representing the immunostimulatory effect of the transfected RNA (Figure 6 B, C).

RNAs of the fractions with long RNA molecules (>10 – 4 kb) showed induction of IP-10 for both viral stocks P0 and P5 although the total amount of IP-10 differed highly between these stocks. The overall strongest IP-10 induction was observed in the fraction containing RNA molecules of 4 – 6 kb for the P0 stock (Figure 6 B). This fits to the size of the detected DI genome (4719 bp) and as expected, this immunostimulatory effect was absent in the stock

with low level of DI genomes (P5) (Figure 6 C). To show that the RNA fragmentation according to size worked, cDNA of each fraction of P0 was generated and analyzed by qRT-PCR for the amount of DI genomes (Figure 6 D) and the N protein of VSV (Figure 6 E). The Ct-values were normalized to the initial RNA volume. Indeed, most of the DI genome (4719 bp) as well as RNA encoding the N protein (1326 bp) were detected in the expected fraction.

Together, these data confirmed that the DI genome is the main trigger of the immune response and indicate that the full-length genome (>10 kb) is also able to induce an immune response.

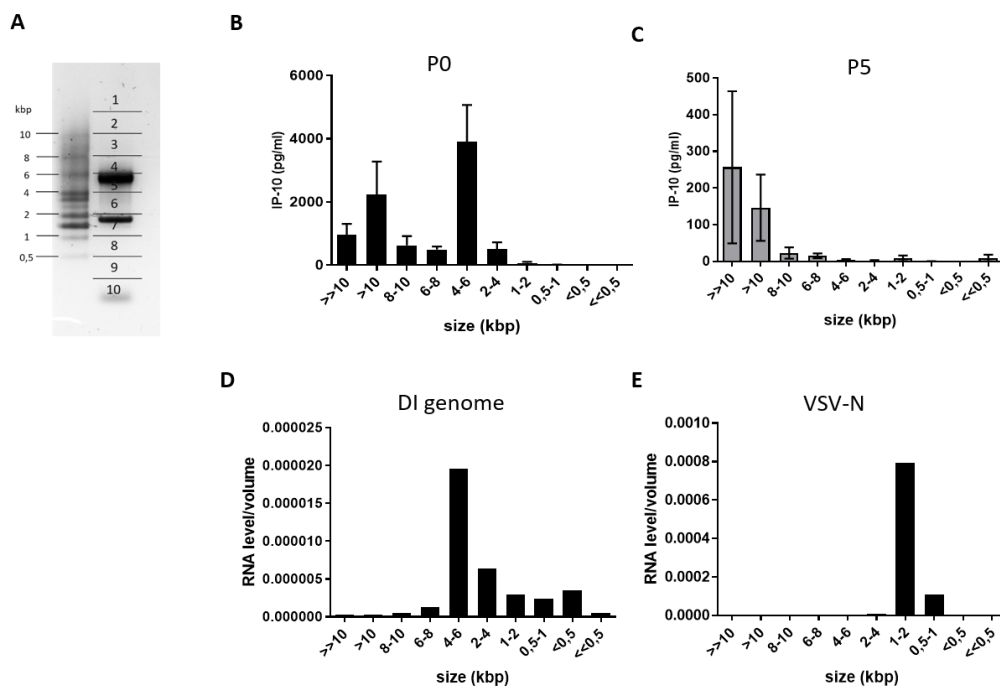


Figure 6: Size dependent profile of immunostimulatory RNA confirms the role of the DI genome. (A) RNA of HEK293T cells grown on 10 cm² dish and infected with VSV stock P0 or P5 for 24 h was isolated and separated on an agarose gel. The gel was size-dependently cut into ten fractions and RNA of each fraction was re-isolated. (B, C) 10 µl of each fraction was transfected into 1205Lu cells in a 96-well plate and the IP-10 concentration in the supernatant was measured 24 h after transfection by ELISA. Data are shown as mean ± SEM (n=3). The isolated RNA of each fraction of P0 was further transcribed into cDNA and the amount of (D) DI genome and (E) N protein was quantified by qRT-PCR and normalized to the initial RNA volume. The data show one representative experiment.

3.1.3 The defective interfering genome and Leader/N sequences of VSV are enriched after RIG-I immunoprecipitation

To validate the results of the RNA-fragmentation and the indicated role of the full-length genome as RIG-I ligand in the absence of DI genomes, the flag-RIG-I IP already done for the virus P0 by Andreas Linder was repeated for the stock P5 to compare the enriched genomic sequences by qRT-PCR.

The enrichment of each genomic part was calculated as ratio of flag-RIG-I expressing cells to the negative control (Flip-In) that do not express flag-RIG-I. Both viral stocks showed a comparable enrichment of the Leader/N sequences. That could either represent a so-called Leader/N readthrough transcript or the full-length genome. As expected, the enrichment of the DI genome was gone. The same was true for the L, L/trailer and trailer sequences, indicating that most of the enrichment in these sequences resulted from the DI genome (Figure 7).

In summary, the data could clearly show that in our standard stocks the DI genome is the main trigger of RIG-I. In the absence of DI genomes other VSV sequences, most likely Leader/N containing sequences such as read-throughs or the full-length genome, seem to bind to RIG-I but induce a much weaker interferon response.

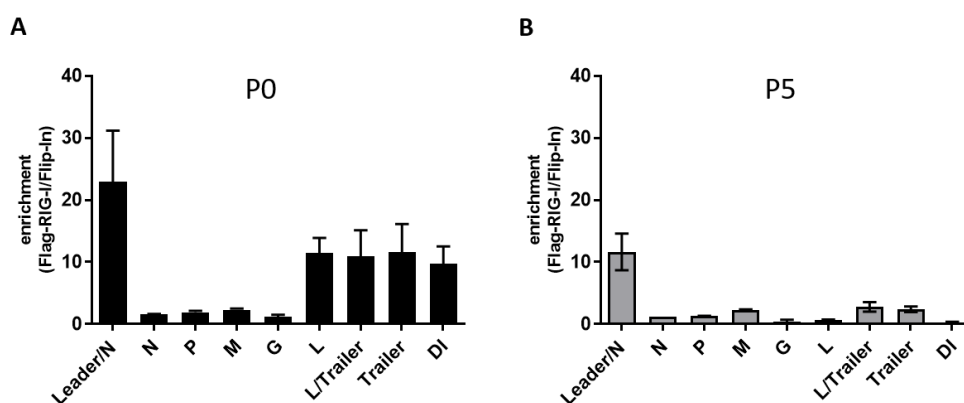


Figure 7: The DI genome and Leader/N sequences of VSV are enriched after RIG-I immunoprecipitation. HEK293T cells grown in 175 cm² flasks either overexpressing flag-RIG-I or not (Flip-In) were infected with either VSV stock (A) P0 or (B) P5 with an MOI = 1. 24 h later the cells were lysed and a flag-IP was performed. The co-immunoprecipitated RNA was isolated and analyzed for the indicated genomic segments by qRT-PCR. The relative enrichment represents the ratio of flag-RIG-I expressing cells to the negative control. Data are shown as mean \pm SEM (n=3 (A) and n=2 (B)).

3.2 Identification of potential MAVS interaction partners by APEX-mediated proximity-based labeling

3.2.1 MAVS-APEX fusion proteins display MAVS and APEX activity

The first requirement to use the method of proximity-based APEX-labeling for the analysis of the MAVS-associated proteome, was a fusion protein that combines the functions of MAVS and APEX. Since the fusion site of the proteins is critical to keep both protein functions intact, different sites of MAVS were chosen and tested for the integration of APEX (Figure 8 A). As a negative control, only the transmembrane (TM) domain of MAVS was fused to APEX. This construct should have the same localization in the mitochondrial membrane as MAVS and the enzymatic function of APEX but without the MAVS domains that integrate the molecule into the RIG-I signaling pathway. For every construct, besides APEX_N-MAVS, a second variant was generated that was flag-tagged at the N-terminus of APEX, thus allowing the detection of APEX. Furthermore, for the constructs, that contained APEX fused to the TM domain (APEX-TM and APEX₅₁₀-MAVS) a flexible linker (N`GGAAS`C) was introduced to allow proper protein folding.

To begin with, the constructs were tested for expression of the fusion protein. For that, 1205 Lu cells were used in which endogenous MAVS was knocked out using the CRISPR/Cas9 system (MAVS-KO). Each construct was transfected and analyzed by Western blot with a MAVS-specific antibody (Figure 8 B). As expected, MAVS expression was missing in the APEX-TM construct and all other constructs showed a MAVS specific band with an apparent size of approximately 110 kDa. Two of the constructs (APEX_NMAVS, APEX₈₄MAVS) showed an additional band, indicating that a part of the protein got cleaved, which could be due to improper folding. This is in line with the immunofluorescence staining that was done to control for correct localization of the constructs. Whereas the localization for the three constructs APEX₂₆₄MAVS, APEX₅₁₀MAVS and APEX-TM is restricted to mitochondria, the constructs showing additional bands in the Western blot also show cytoplasmic background staining (APEX_NMAVS, APEX₈₄MAVS) (Figure 8 C).

After demonstrating the correct expression and localization for three out of five constructs, they were analyzed for intact MAVS signaling. Again, the 1205Lu MAVS-KO cells were used to transfect the constructs. For induction of MAVS signaling 3p-RNA was used as a stimulus. 3p-RNA acts as a specific ligand for RIG-I, thus leading to activation of MAVS and its downstream signaling cascades. The measurement of IP-10 in the supernatant of cells 24h after 3p-RNA stimulation by ELISA was used as read-out for intact MAVS signaling. The two MAVS-APEX fusion constructs that possessed the expected expression pattern and localization showed an IP-10 production comparable with transfected wt-MAVS and as expected, APEX-TM was impaired for signaling (Figure 8 D).

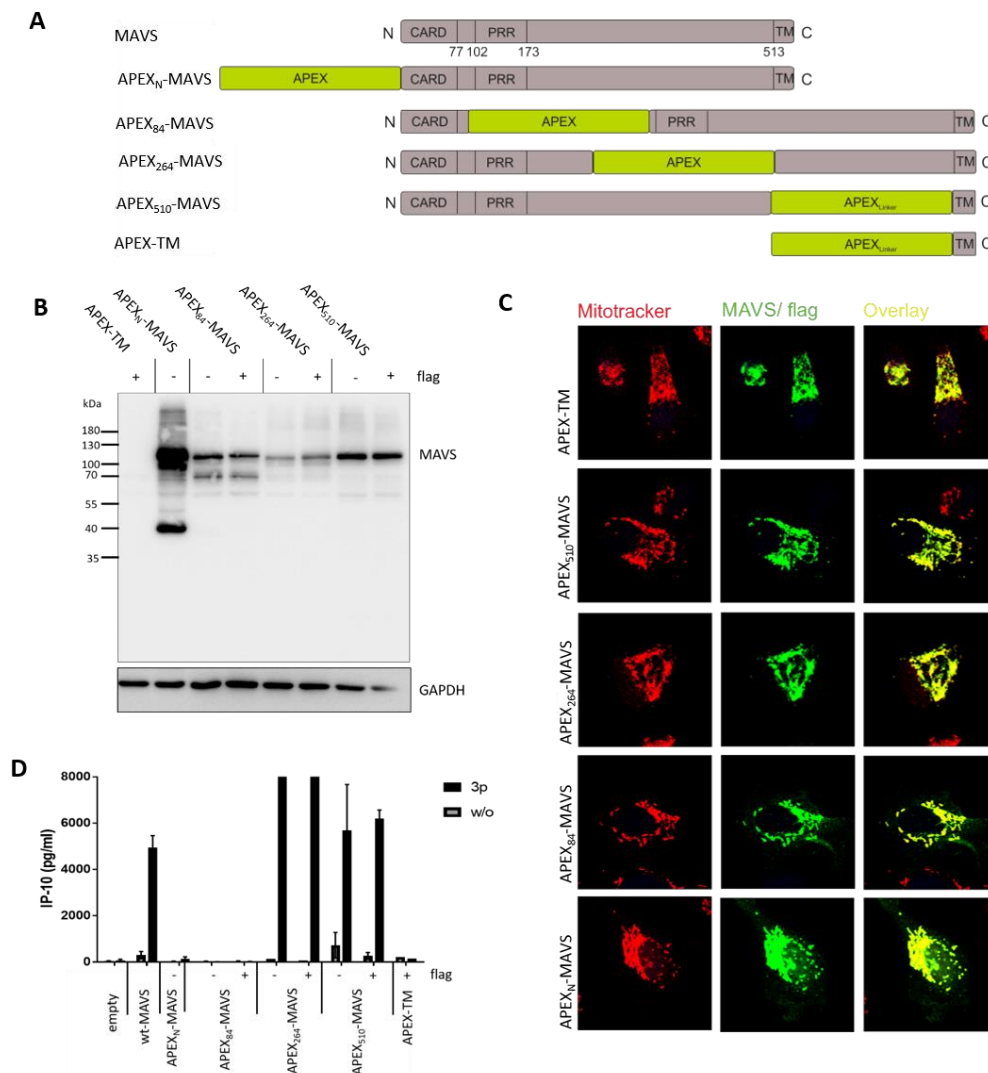


Figure 8: Different MAVS-APEX fusion proteins show intact MAVS localization and signaling. (A) Different MAVS-APEX fusion proteins were constructed by fusion of APEX to different sites of MAVS. 1205Lu MAVS knockout cells were transfected with 500 ng/ml of each construct for 24 h. (B) The size and expression pattern were analyzed by Western blot and (C) the localization by immunofluorescence and co-staining of mitochondria with Mitotracker red and MAVS or flag to detect the APEX-TM construct. (D) The function of MAVS signaling upon RLR activation was analyzed after stimulation with 500 ng/ml 3p-RNA via measurement of IP-10 in the supernatant by ELISA 24 h post stimulation. Data are shown as mean \pm SEM (n=2 to 3; except APEX₂₆₄MAVS and APEX-TM n=1).

In the next step, the functionality of APEX was analyzed. Again, 1205 Lu MAVS-KO cells were used for transfection of the constructs and 24 h post transfection the reaction of APEX was induced as described in 2.2.9.

The pattern and strength of biotinylation was analyzed by Western blot and immunofluorescence. As a positive control a plasmid was transfected that expresses APEX fused to a mitochondrial target sequence leading to localization into the mitochondrial matrix (mito-APEX). For this construct it was shown that biotinylation is highly restricted to the mitochondria (128). The expression pattern detected by Western blot with Streptavidin-HRP

is the same for all fusion constructs but differs from the pattern resulting from mito-APEX, indicating that they biotinylate a different set of proteins. Except for the APEX₈₄MAVS construct, all other fusion proteins are functional for APEX and show a comparable amount of biotinylation (Figure 9 A). The actual site of biotinylation within the cell was further analyzed by immunofluorescence using Streptavidin-FITC for detection of biotin. Herein, only these constructs were tested that had shown an intact MAVS signaling. Additionally, APEX-NES that expresses APEX unspecifically in the cytoplasm was used as a negative control. As expected, this construct biotinylates all cytoplasmic proteins, whereas the biotinylation induced by the mito-APEX construct is highly restricted to the mitochondria. All generated fusion proteins showed an enhanced biotinylation at the site of mitochondria with slight background biotinylation of cytoplasmic proteins.

In summary, two MAVS-APEX fusion constructs - APEX₂₆₄MAVS and APEX₅₁₀MAVS - as well as the negative control APEX-TM showed the expected properties concerning the activity of MAVS and APEX as well as the specificity of APEX no matter whether flag-tagged or untagged APEX was used.

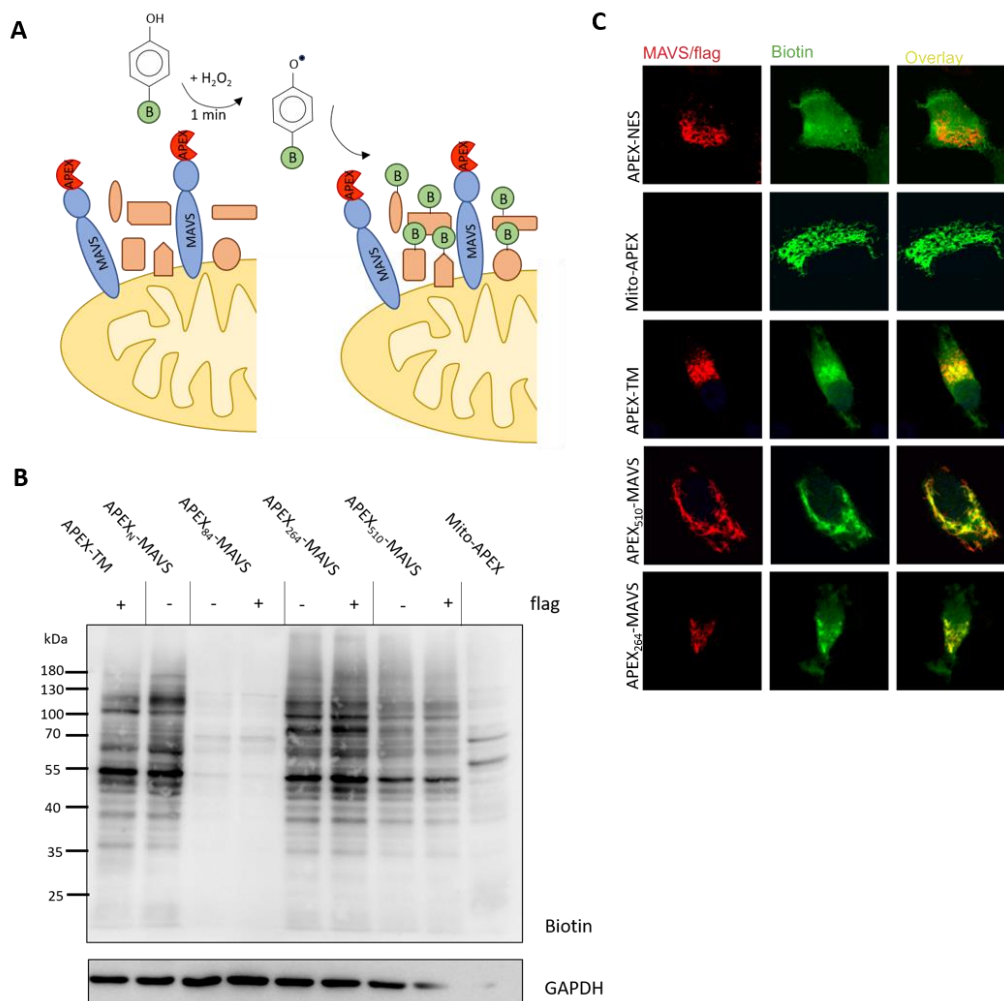


Figure 9: Different MAVS-APEX fusion proteins show specific APEX activity. (A) APEX activation is induced by addition of biotin phenol for 30 min and H_2O_2 for 1 min to the cell culture medium and is supposed to biotinylate all proteins in close proximity of the APEX-MAVS fusion protein. 1205 Lu MAVS-KO cells were transfected with 500 ng/ml of the indicated construct for 24 h. After activation of APEX for one minute (B) the pattern and strength of biotinylation was checked by Western blot with Streptavidin-HRP. (C) The localization of the subset of biotinylated proteins was analyzed by immunofluorescence using Streptavidin-FITC and MAVS-specific antibody or flag-specific antibody for detection of the APEX-TM construct.

3.2.2 Generation of a reproducible system by stable transduction of the fusion proteins

After confirming their intact functionalities, the constructs APEX₅₁₀MAVS and APEX-TM were used for further experiments. Since APEX is fused to the same site of the TM domain of MAVS in both constructs, these two constructs are suitable to distinguish MAVS-specific labeling from labeling due to localization in the outer mitochondrial membrane. Both constructs were cloned in a retroviral vector system that additionally encodes for a puromycin resistance. The construct of APEX₅₁₀MAVS was transduced for stable integration into the genome of 1205 Lu MAVS-KO cells and the APEX-TM construct into the wt background.

Hence, both cell lines are able to induce MAVS signaling. After transduction the cells were selected with puromycin for integration-positive cells.

Whereas for APEX-TM all transduced cells showed flag expression and the expected biotinylation pattern (Figure 10 D), for APEX₅₁₀MAVS only a few transduced cells showed MAVS expression and biotinylation. These cells were further sub-cultured into single cell clones and analyzed for MAVS expression (Figure 10 A) and signaling capacity measured by IP-10 in the cells supernatant 24 h after 3p-RNA stimulation (Figure 10 B). For further experiments clone 7 was picked showing MAVS expression and IP-10 induction comparable to wt cells. Furthermore, this clone was also functional for APEX, although the level of biotinylation differed between the cells in this population (Figure 10 C).

These results demonstrate that both cell lines are suitable tools for the envisioned pull-down experiments. Herein, the APEX-TM transduced cells will serve as negative control. Since they have endogenous MAVS, they are able to signal, but the biotinylation will not be MAVS-associated. It is the whole outer mitochondrial membrane, that is expected to be biotinylated in this cell line.

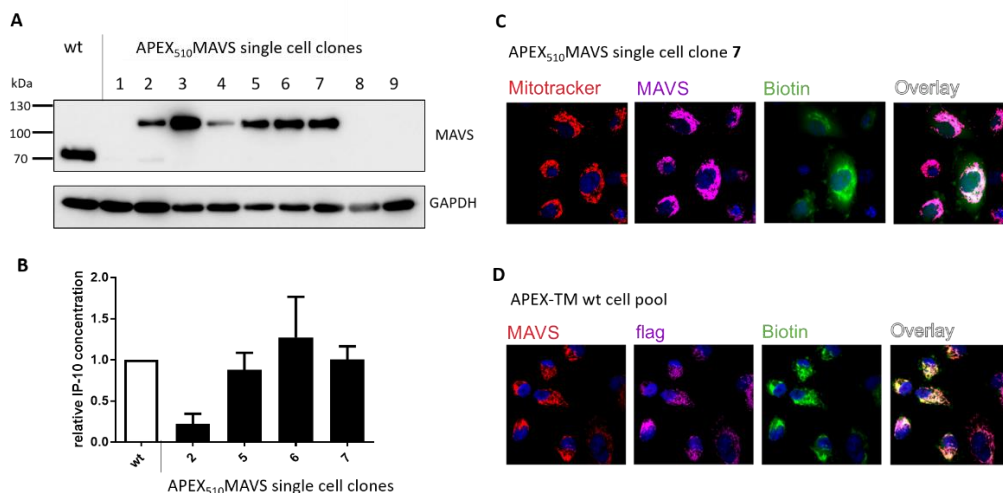


Figure 10: Generation of a reproducible system by stable transduction of the fusion proteins. The fusion construct APEX₅₁₀MAVS or APEX-TM were transduced into 1205 Lu MAVS-KO or 1205 Lu wt cells, respectively. After transduction of APEX₅₁₀MAVS single cell clones were analyzed for (A) expression level of MAVS and (B) IP-10 in the supernatant was measured by ELISA 24 h after 3p-RNA (500 ng/ml) stimulation (n=3). After activation of APEX reaction by addition of biotin phenol for 30 min and H₂O₂ for 1 min the reaction was stopped. The expression pattern of each construct was analyzed with either (C) MAVS-specific antibodies and co-staining with Mitotracker or (D) flag-specific antibodies and co-staining with MAVS-specific antibody. Biotinylated proteins were stained with Streptavidin-FITC.

3.2.3 APEX-MAVS specifically labels MAVS interaction partners upon RLR

activation

Since MAVS signaling is a highly dynamic process, it is of great importance to choose the right time point after signal activation to look for specific interaction partners.

In preliminary pull-down experiments, cells were stimulated by transfection of 500 ng/ml 3p-RNA and the APEX-mediated biotinylation was induced at different time points after stimulation. After stopping the reaction, the cells were lysed, and biotinylated proteins were pulled down with magnetic streptavidin beads. Bound proteins were eluted from the beads by heating, separated by Western blot and analyzed for RIG-I, TBK1 and TRAF3 that are well described interaction partners of MAVS (Figure 11). TBK1 and TRAF3 showed a clear enrichment after 60 min of stimulation whereas RIG-I was already detected in the unstimulated condition and did not get changed over time. Interestingly, the bait protein MAVS got decreased after stimulation. The house keeping protein GAPDH used as loading control is only hardly detectable after pull-down and did not get enriched after stimulation. In contrast, the control cell line APEX-TM wt showed no enrichment of any analyzed protein after 3p-RNA stimulation.

On the one hand that proved that MAVS interaction partners are detectable by APEX-MAVS (TBK1 and TRAF3). On the other hand, this indicated that APEX acts highly specific since it showed increased biotinylation of MAVS interaction partners after 3p-RNA stimulation only for the APEX-MAVS fusion protein but not for mitochondria localized APEX (APEX-TM).

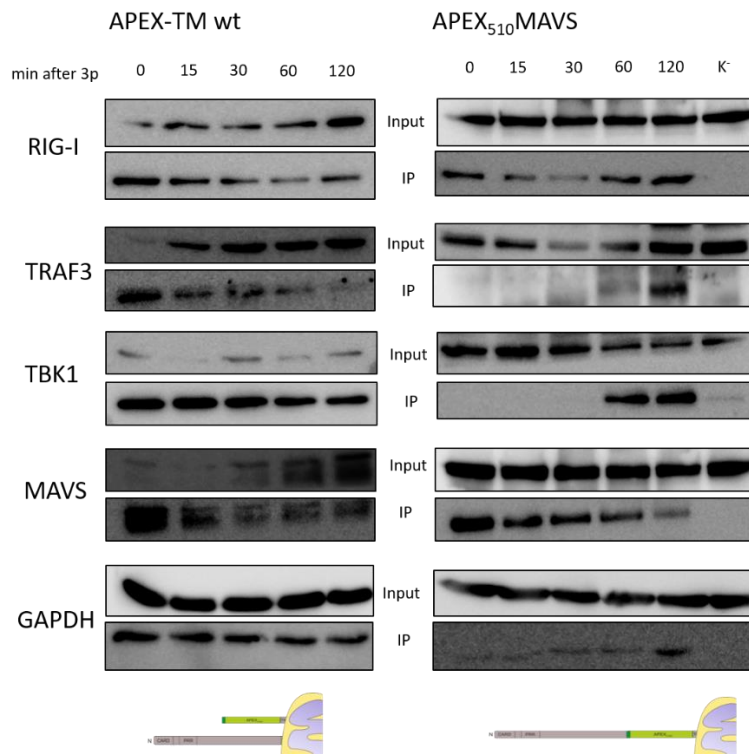


Figure 11: APEX-MAVS specifically biotinylates MAVS interaction partners after RLR signaling activation. An APEX₅₁₀MAVS expressing but wt-MAVS deleted cell line or APEX-TM expressing wt 1205 Lu cells were stimulated with 500 ng/ml of 3p-RNA. At indicated time points after stimulation the APEX reaction was induced or cells were left untreated (K⁻). Biotinylated proteins were pulled down with streptavidin beads and analyzed by Western blot for known MAVS interaction partners. One representative blot out of two independent experiments is shown.

Interestingly, the immunofluorescence staining of biotinylated proteins after 3p-RNA stimulation showed a specific dotted pattern that is also only detectable with the APEX-MAVS fusion protein but not in APEX-TM control condition. Since the Western blot showed that the biotinylated proteins are indeed MAVS interaction partners, the immunofluorescence staining indicated that the dotted pattern reflects MAVS signaling platforms that cannot be detected by staining MAVS (Figure 12). Thus, this method could be used further to specifically visualize and follow the activated MAVS signaling complexes.

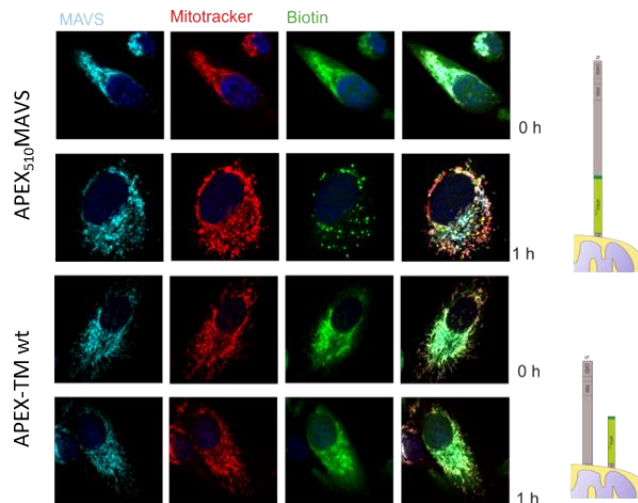


Figure 12: APEX-MAVS fusion protein induces a specific biotinylation pattern after RLR signaling activation. An APEX₅₁₀MAVS expressing but wt-MAVS deleted cell line or APEX-TM expressing wt 1205 Lu cells were stimulated with 500 ng/ml of 3p-RNA for 1h or left untreated. The APEX reaction was induced, stopped after 1 min and the cells were fixed and stained with MAVS-specific antibodies and streptavidin. Mitochondria were stained with Mitotracker red. One representative experiment out of three (APEX₅₁₀MAVS) or two (APEX-TM wt) is shown.

To further analyze, if this dotted pattern reflects MAVS oligomers and how they behave over time, the biotinylation pattern in APEX₅₁₀MAVS cells was followed over time after 3p-RNA stimulation and was co-stained with the MAVS-interacting protein TBK1 (Figure 13).

Indeed, especially 1h after 3p-RNA treatment there was a strong colocalization of biotin and TBK1 in a dotted pattern, supporting the data of the streptavidin pull-down. Up to 4 h after 3p-RNA treatment the dotted pattern stayed stable, whereas the co-localization with TBK1 decreased over time.

On the one hand, that further supports the interpretation that the biotinylated dots reflect MAVS oligomers that serve as a trigger for downstream signaling activation. On the other hand, it demonstrates that this method is suitable for kinetic studies of the signaling progress.

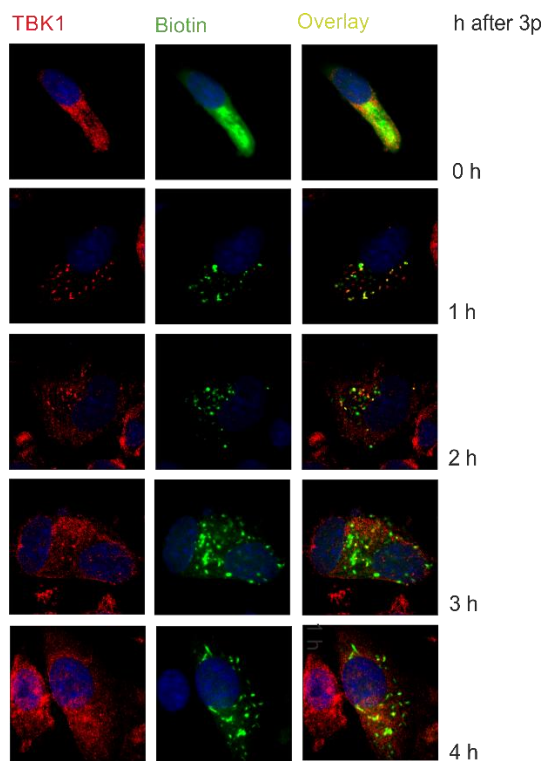


Figure 13: MAVS interaction partner TBK1 colocalizes with biotin at certain time points after RLR activation in an APEX₅₁₀MAVS expressing but wt-MAVS deleted cell line. The cells were stimulated for the indicated time points with 500 ng/ml of 3p-RNA. Subsequently the APEX reaction was induced and stopped after 1 min with quencher solution. The cells were fixed and stained for TBK1 and biotin. One representative experiment out of two is shown.

3.2.4 Mass spectrometry reveals new potential MAVS interaction partners

As the preliminary pull-down experiment showed, 60 min after stimulation MAVS interaction partners were clearly detectable. Because the early interactors of MAVS, that are necessary for induction of downstream signaling are of high interest, additionally the time point 15 min was chosen and compared to the unstimulated situation in the same cell line.

The streptavidin pull-down was performed in biological triplicates and the samples were further processed for liquid chromatography/ mass spectrometry (LC/MS) analysis in the group of Prof. Axel Imhof (Biomedical center, Munich). Each sample was measured in technical duplicates. The data analysis was performed with the software Perseus and done in cooperation with Prof. Axel Imhof.

First, the data sets were checked by quality control measures. For that, the overall number of detected proteins were compared, showing that in every sample of the respective cell line nearly the same amount of proteins was detected. Importantly, most of the detected proteins per condition were present in all replicates (Figure 14 A, B).

To analyze the differences between all samples of each cell line, a principal component analysis (PCA) was performed. The PCA is a method used to explain the variance of complex

data sets by reducing a big set of variables to smaller sets, the so-called principal factors. In fact, the more the samples cluster the more identical they are. For APEX₅₁₀MAVS this revealed that for component 1 all of the replicates cluster together and for component 2 the condition 60 min is different from the other conditions (Figure 14 C). For APEX-TM there were no clear variances between the conditions but more between the replicates (Figure 14 D). This indicated, that only the set of detected proteins after 60 min in APEX₅₁₀MAVS was different compared to 0 min or 15 min, while the other conditions did not differ. All in all, there was no outlier detected and the amount of proteins were comparable. Thus, the quality analyzes confirmed a valid data set the could be used for further analyzes.

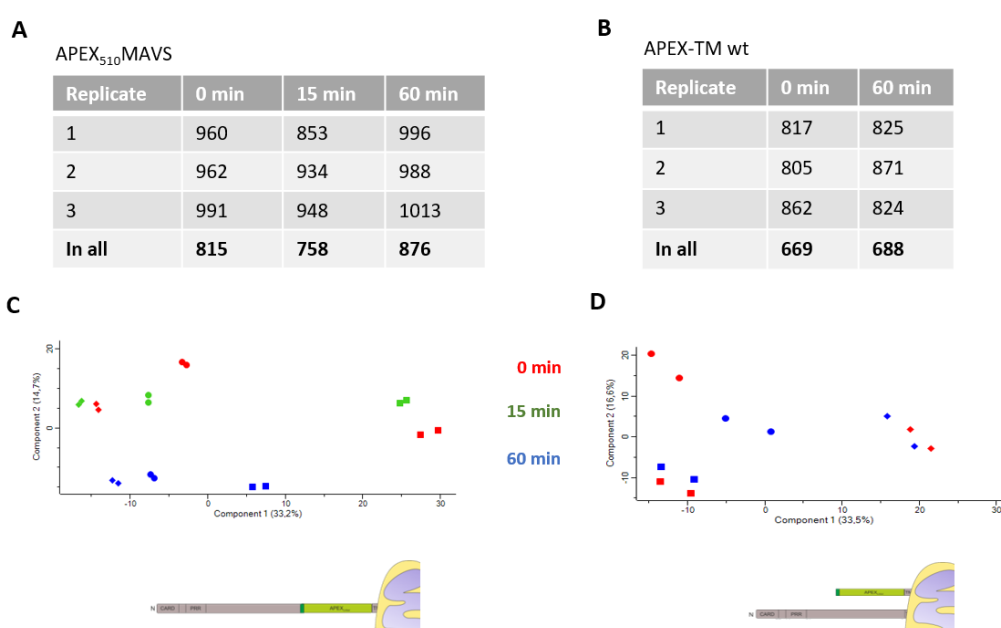


Figure 14: Evaluation of mass spectrometric data by principal component analysis shows a valid data set. The streptavidin pull-down after biotinylation of proteins by the APEX reaction of each condition were prepared in three biological replicates and measured in technical duplicates via LC-MS. The data sets were analyzed with the software Perseus for (A, B) the proteins identified in all replicates per condition and (C, D) by principal component analysis showing the clustering of all samples per cell line. Each symbol type reflects one replicate and each color one condition.

The most interesting question was, if there are any significant changes in protein abundance after RLR activation compared to the unstimulated condition. To determine the amount of protein in each sample the label-free quantification (LFQ) method was used. For identification of changes in LFQ intensities between two conditions a volcano plot was performed. In this analysis the difference in LFQ intensity for each detected protein is plotted together with the corresponding p-value. Every protein that is plotted outside the marked borderlines has significantly different LFQ intensities between the compared conditions.

Whereas the APEX₅₁₀MAVS cells stimulated for 15 min showed no significantly altered protein (Figure 15 A), after 60 min 31 proteins were found to be significantly enriched (Figure 15 B, Table 2 (appendix)). In contrast, the control cell line APEX-TM showed no significant change in protein abundance after 60 min of stimulation (Figure 15 C).

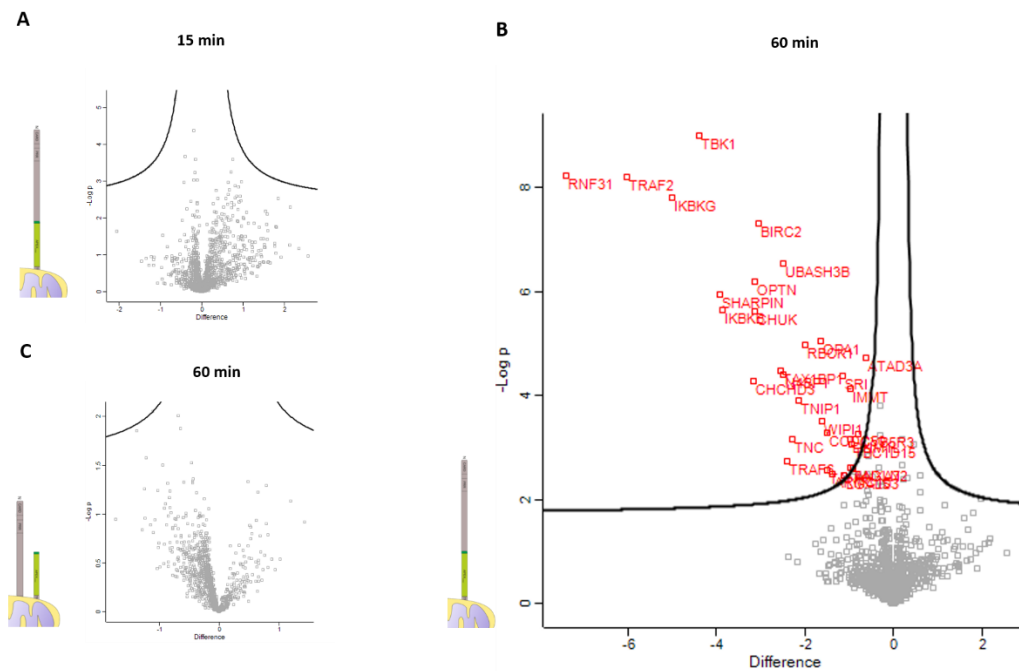


Figure 15: 31 significantly altered proteins were detected after 60 min of RLR activation in APEX₅₁₀MAVS cells. Label-free quantification (LFQ) determining the relative protein amount was used for calculating alteration in protein quantities. Significantly altered proteins were identified using the software Perseus and are depicted in a volcano plot after (A) 15 min or (B) 60 min of 3p-RNA stimulation compared to unstimulated for APEX₅₁₀MAVS or after (C) 60 min for APEX-TM wt.

The identified candidate proteins were further analyzed using the online tool string-db.org that searches for functional protein interaction networks. This revealed a subset of 14 proteins that cluster together with MAVS showing links that are derived from curated databases (Figure 16 A).

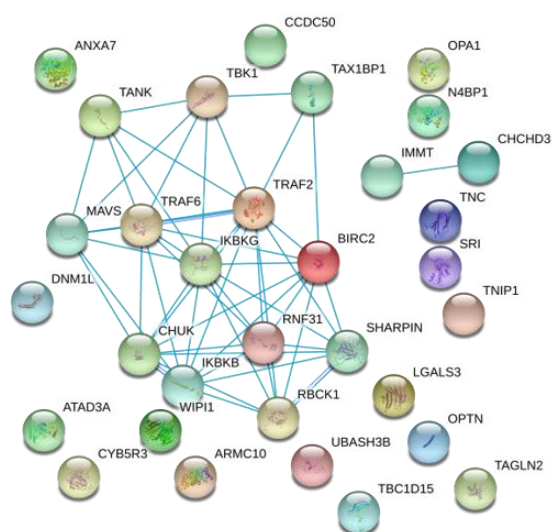
This is also reflected by the pathway analysis the string-db.org online tool provides. Here, the most significantly enriched biological processes in which the candidate proteins are involved were found to deal with innate immune signaling, such as NF κ B and PRR signaling. Reassuringly, the most significant KEGG pathway coming up is the RLR signaling pathway (Figure 16 B).

All in all, these analyzes convincingly showed that almost half of the identified proteins are known MAVS interaction partners. Since these proteins were not detectable with the control

cell line APEX-TM, the method works highly specific for MAVS and not only for a subcellular compartment, like the outer mitochondrial membrane.

All the other detected proteins that have no connection to this known MAVS network share no other common KEGG pathway. The main common feature is their localization at the mitochondria (11 out of 17 proteins). All these newly identified proteins, for which a connection to the RLR signaling is not yet known are highly interesting candidates to be further analyzed for their function in MAVS-dependent signaling.

A



B

| Biological Process (GO) | | | |
|-------------------------|--|-------------------|----------------------|
| pathway ID | pathway description | count in gene set | false discovery rate |
| GO:0043122 | regulation of I-kappaB kinase/NF-kappaB signaling | 11 | 2.79e-10 |
| GO:0043123 | positive regulation of I-kappaB kinase/NF-kappaB signaling | 10 | 5.45e-10 |
| GO:0002221 | pattern recognition receptor signaling pathway | 9 | 1.92e-09 |
| GO:0002757 | immune response-activating signal transduction | 11 | 1.3e-08 |
| GO:0002224 | toll-like receptor signaling pathway | 8 | 2e-08 |

| KEGG Pathways | | | |
|---------------|---------------------------------------|-------------------|----------------------|
| pathway ID | pathway description | count in gene set | false discovery rate |
| 04622 | RIG-I-like receptor signaling pathway | 8 | 3.12e-11 |
| 05160 | Hepatitis C | 7 | 1.35e-07 |
| 04064 | NF-kappa B signaling pathway | 6 | 3.17e-07 |
| 05222 | Small cell lung cancer | 6 | 3.17e-07 |
| 05168 | Herpes simplex infection | 7 | 4.61e-07 |

Figure 16: Identified proteins contain numerous known MAVS interaction partners but also reveal novel candidates. All significantly altered proteins together with MAVS were analyzed using the online tool <https://string-db.org> for functional protein association networks. (A) The links between the proteins are derived from curated databases. (B) The most significant biological processes and KEGG pathways the candidate proteins are involved in are listed.

3.2.5 Cell lines deficient in the newly identified potential MAVS-interaction proteins have a phenotype for antiviral signaling

As the proximity labeling experiment produced a list of 17 candidate proteins that are not (directly) described in MAVS-dependent signaling yet, different criteria were used to select the most interesting candidates within this list for further characterization. One important criterium was its described function, i.e. in which pathways it is involved, what are its interacting proteins and how does it act on the molecular level. Further the sub-cellular localization was considered (cytoplasm, inner or outer mitochondrial membrane, extracellular) as well as the significance level depicted in the volcano plot (Figure 15 B). Finally, a set of RNA sequencing data generated in our group was analyzed for the candidate proteins. Here, in 1205 Lu cells the total mRNA levels of unstimulated cells were compared to cells treated with 3p-RNA for 6h. The data were screened for any significant changes for the candidate proteins.

Based on these criteria, eight proteins were selected to be screened for their function in MAVS signaling, namely UBASH3B, CCDC50, N4BP1, Sorcin (SRI), WIP1, CHCHD3, Tenascin C (TNC C) and Optineurin (OPTN). Although OPTN is one of the proteins included in the protein network derived from the string database, its function in RLR signaling is still not clearly described. Thus, it works on the one hand as a positive control as there was the expectation to see an effect on MAVS signaling and on the other hand it is still of interest to reveal its mode of action in MAVS signaling.

To see if the proteins of interest have any effect on RLR signaling, knockout (KO) cells were generated using the CRISPR/Cas 9 gene editing system. Single cell clones (SCC) were considered as complete KO, if both alleles showed an out-of-frame mutation thus, causing an early stop codon and loss of the protein. For each protein two to five SCC were generated, with the exception of CHCHD3. Here, for all the analyzed SCC more than two alleles have been detected and at least one was still wildtype, indicating that a complete KO of this protein is lethal.

In a first functional screening approach, four different gene KOs (UBASH3B, OPTN, SRI, CCDC50) were analyzed. All SCC have been tested for their immune response upon stimulation with the MAVS-specific ligand 3p-RNA and a MAVS-independent PRR ligand pIC. By adding pIC onto the cells without transfection, it activates the TLR3 pathway. This was used as a control, because it activates a similar immune response via IRF3 as well as the NF κ B pathway but is independent of MAVS.

After stimulating the cells with the respective ligand for 6 h the supernatant was taken and the concentration of the cytokine IP-10 was measured via ELISA (Figure 17).

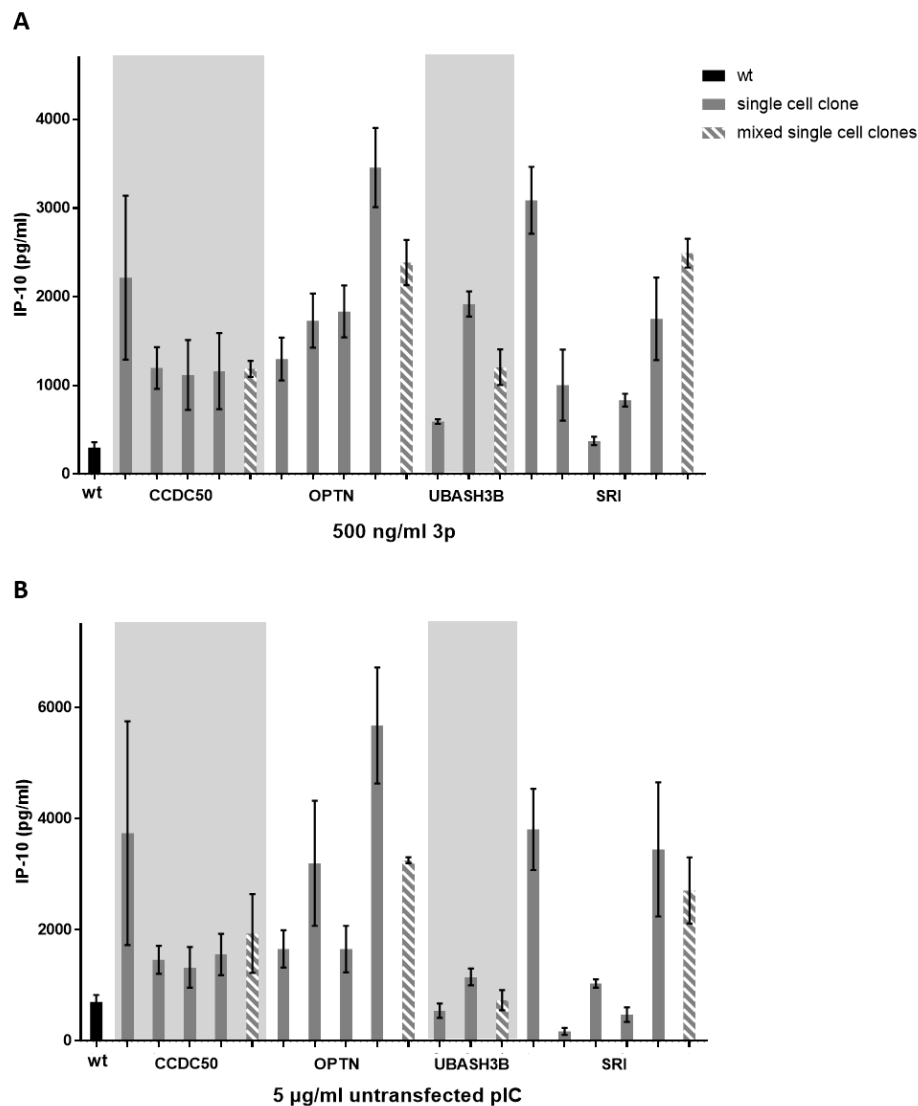


Figure 17: Analysis of the immune response in different gene knockouts. For each gene 2- 5 different single cell clones (grey) and a pool containing same amounts of each single cell clone (patterned) have been tested in comparison to 1205 Lu wt cells. The cells were grown in 96-well plate, stimulated with (A) 3p-RNA (500 ng/ml) or (B) untransfected pIC (5 µg/ml) for 6 h and IP-10 in the supernatant was measured by ELISA. Data are shown as mean \pm SEM from 2-5 independent experiments.

All KO cells showed an increased IP-10 release compared to the wt cells when stimulated with the RIG-I-specific ligand 3p-RNA. Upon stimulation with untransfected (ut) pIC only the CCDC50- and OPTN-KO cells showed a clear increase in IP-10 release that is consistent throughout the different SCC, whereas the UBASH3B-KO cells had IP-10 levels like wt cells. The SRI-KO SCC behaved differently with 2 clones showing an increase and 3 clones show lower or equal IP-10 amounts, but the mixed population showed a much higher IP-10 level than the wt cells.

This suggests, that all the proteins have a negative influence on the antiviral signaling, no matter if the signaling is MAVS-dependent or not. Only UBASH3B indicates an RLR-MAVS-

specific phenotype, since the cytokine release was only increased upon 3p-RNA stimulation but not with utpIC.

3.2.6 UBASH3B shows a negative regulatory function on RLR signaling

Considering this initial screening together with the set criteria, the decision was taken to look deeper into the role of UBASH3B. The considerations thereby were, that the ELISA data hinted towards an RLR-MAVS-specific phenotype, that it was the protein showing the most significant change in the volcano plot besides the known MAVS interactors and that its mRNA level was found to be significantly downregulated upon RLR-MAVS signaling activation. Furthermore, UBASH3B is described to modify different proteins post-translationally by dephosphorylation of ubiquitinated proteins. Post-translational modification is known to be an important feature that regulates MAVS activity.

To have a valid set of UBASH3B-KO cells, another round of CRISPR/Cas9 editing was performed. To exclude sgRNA-specific off-target effects, two sgRNAs targeting different sites of UBASH3B gene (sg1 and sg2) were used and SCC were screened by deep sequencing in the group of Prof. Veit Hornung (Gene center, Munich). The sequences were analyzed with the online tool *outknocker.org* giving the number of reads per sequencing as well as the type and amount of inserted mutation. Those clones having a homozygous or compound heterozygous out-of-frame mutations were further analyzed on Western blot for UBASH3B and Cas9 expression (Figure 18). Although the cells were only transiently transfected with the Cas9-encoding plasmid, some cells stably integrated its cDNA into their genome. Integration and constant expression of Cas9 and the sgRNA could later hinder the reconstitution of UBASH3B and could cause off-target effects. To avoid this, only SCC were chosen that were negative for UBASH3B as well as for Cas9. For each sgRNA five SCC that are marked in squares (Figure 18 A, B) and highlighted in bold (Figure 18 C) were used for further analysis.

As a control for the CRISPR/Cas9 treatment a cell pool was used that was transfected with a scrambled sgRNA that do not target any specific DNA site. Instead of single cell clones, all transfected cells were selected on puromycin and the whole remaining cell pool was used.

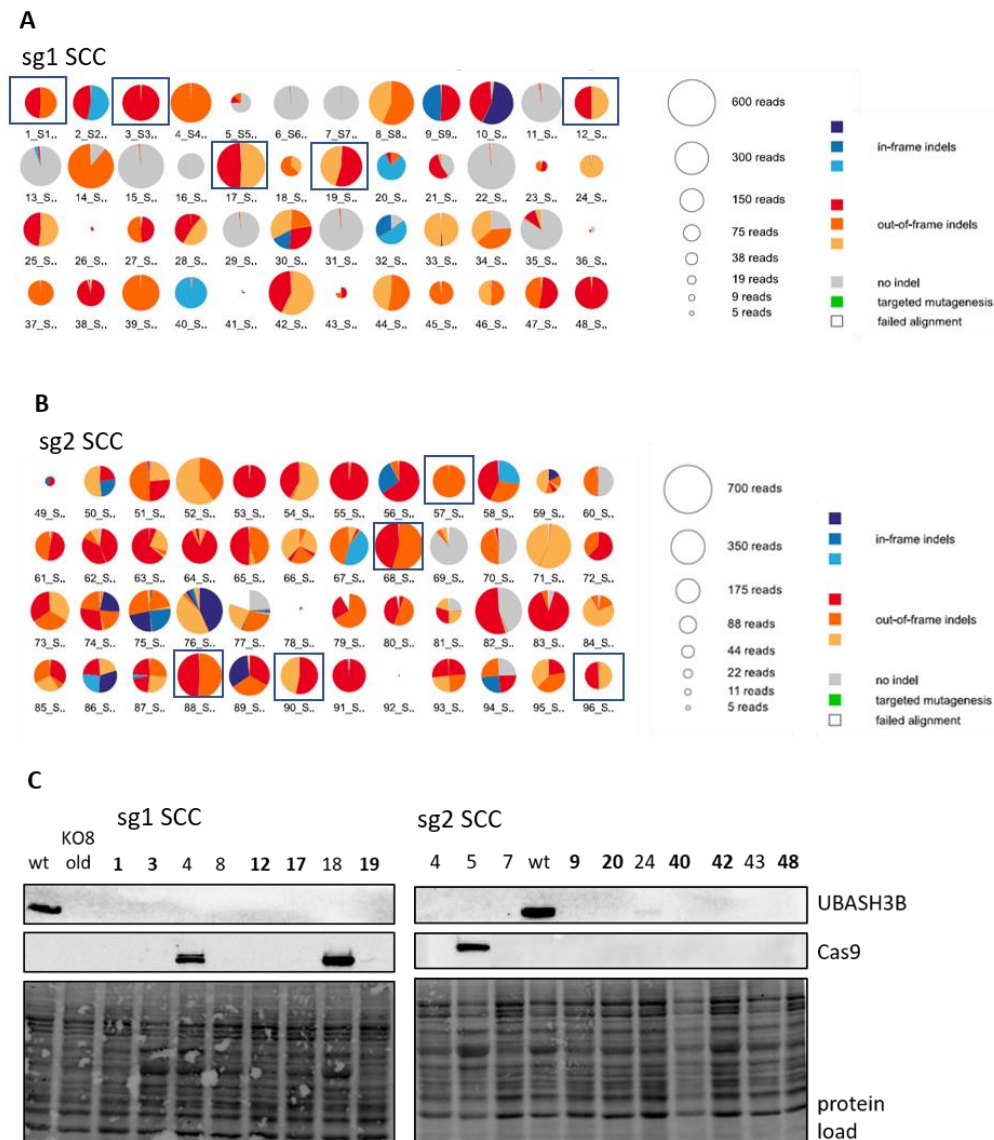


Figure 18: Generation of multiple UBASH3B-knockout cells in 1205 Lu cells. 1205 Lu cells were transfected with eSpCas9 plasmids either encoding sg1 or sg2. After puromycin selection and limiting dilution single cell clones were expanded and the CRISPR target site was (A, B) analyzed by deep sequencing and the online tool outknocker.org. (C) Clones showing homo- or heterozygous out-of-frame indels were further analyzed by Western blot for UBASH3B and Cas9. The clones highlighted in bold lacking UBASH3B and Cas9 were chosen for further experiments.

To confirm the results from the first two UBASH3B-KO SCC the new cell lines were also tested for their cytokine release upon 3p-RNA treatment. Again, the supernatant was taken 6 h after 3p-RNA stimulation, IP-10 and additionally IL-6 was measured. Whereas the promoter of IP-10 is driven by IRF3 and NFkB activation, the IL-6 production does not depend on IRF3 activation. Each SCC was either tested separately or in an equally mixed cell population of sg1 or sg2 derived cells or all SCC together (sg1+sg2). These pooled cells should minimize possible off-target effects in the SCC. Although each SCC produced different amounts of IP-10 and IL-6, most of the SCC produced more of the cytokine compared to wt or scrambled cells. The pool of KO clones generated with both sgRNAs induced more of each cytokine and

the effect was somewhat stronger for the KO cells generated with sg1 (Figure 19 A, B). This was in line with qRT-PCR data showing that both KO clone pools had increased mRNA levels for IP-10, IFN- β , IL-6 and IL-1 β compared to wt cells and cells treated with scrambled sgRNA. For IFN- β , there was already significantly more mRNA in the KO cells compared to the controls after 2 h of 3p-RNA treatment (Figure 19 D). For all the other cytokines the biggest difference was measured after 6 h, and after 12 h the difference in mRNA levels for IP-10 and IL-1 β were still increasing (Figure 19 C, F), whereas for IFN- β and IL-6 the levels equal again (Figure 19 D, E).

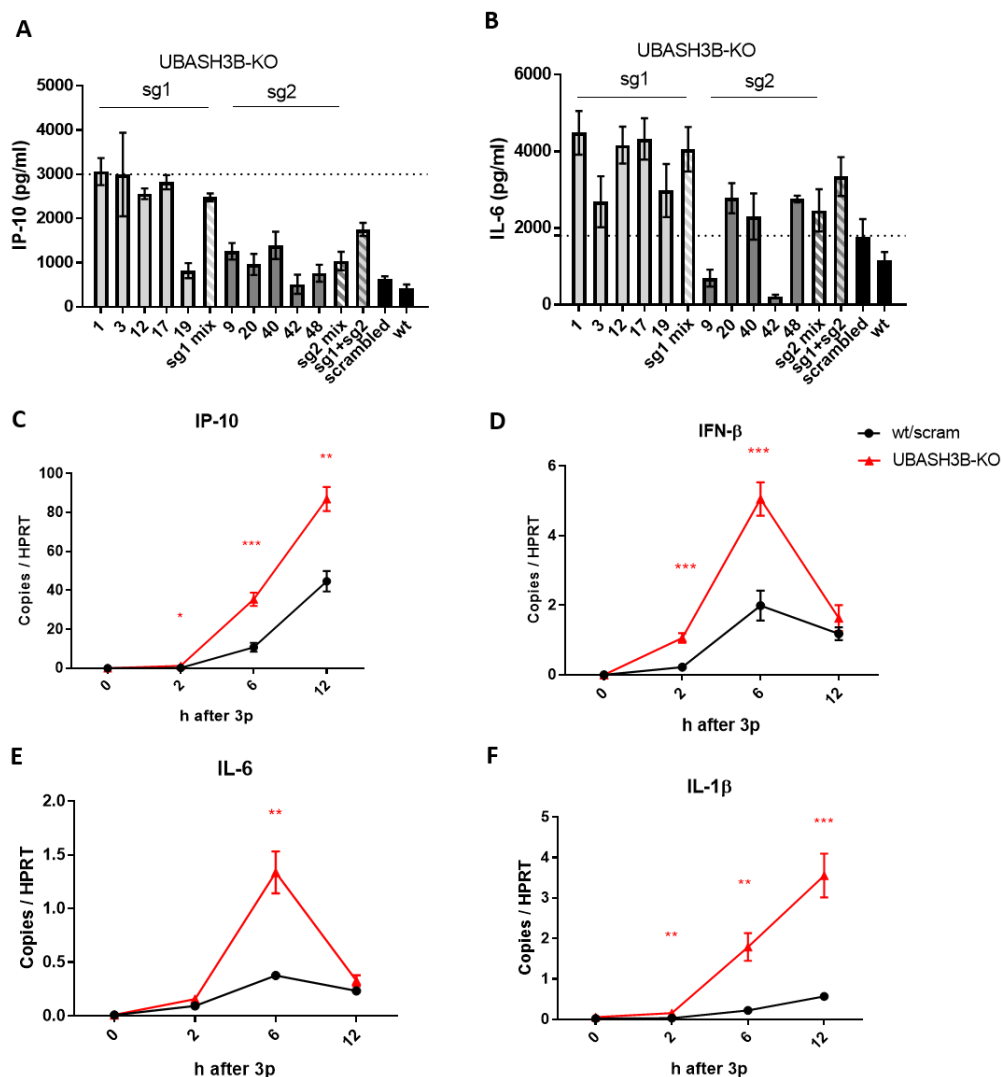


Figure 19: UBASH3B-knockout shows a phenotype on cytokine expression after RLR signaling activation. The UBASH3B-KO SCC generated with sg1 (5) or sg2 (5) were either separately tested or used as a mixed cell population of each sgRNA (sg1 mix; sg2 mix) or as mixed population of every SCC (sg1+sg2). As control 1205 Lu wt cells and a batch of scrambled sgRNA treated cells were used. The cells were plated in 96-well plate, stimulated for 6 h and the amount of (A) IP-10 and (B) IL-6 was measured in the cell's supernatant via ELISA. The dotted line shows the highest standard level of the assay. (C-F) For qRT-PCR each cell population (wt, scrambled, sg1 mix and sg2 mix) grown in 24-well plate were stimulated with 3p-RNA (500 ng/ml) for indicated time points. The RNA was isolated, transcribed into cDNA and analyzed for the mRNA level of the indicated cytokines via qRT-PCR. Subsequently, the data of UBASH3B-KO cells (sg1 mix, sg2 mix) and control cells (wt, scrambled) were pooled. Data are shown as mean \pm SEM from 3 (A-C) or 4 (D-F) independent experiments.

To have a closer look on the upstream signaling events prior to induction of the cytokines, the activation of MAVS itself and its downstream molecules were analyzed. For this, the mixed population of SCC of sg1 or sg2 were compared to the control wt or scrambled cells at different time points after 3p-RNA stimulation.

Upon activation, MAVS forms RIPA-insoluble oligomers causing a shift from the soluble into the insoluble fraction. Thus, activated and thereby aggregated MAVS can be found as a smear on Western blots in the pellet fraction of cell lysates after centrifugation. In both UBASH3B-KO cell pools (sg1 and sg2) MAVS oligomers were detected earlier and stronger upon 3p-RNA treatment (Figure 20 A, E) compared to UBASH3B-containing cells. The same was true for the analyzed downstream molecules. The activation of TBK1 was determined, since it directly interacts with MAVS and is crucial for downstream activation of the IRF3 pathway and is also described to be involved in the activation of the NF κ B signaling branch. The phosphorylation reflecting its activation was significantly higher in UBASH3B-deficient cells compared to wt cells after 3 and 6 h of 3p-RNA treatment (Figure 20 A, B). The analysis of further downstream molecules indicated that both main signaling branches were affected, because IRF3 as well as I κ B α (NF κ B-activation) showed stronger phosphorylation in the KO cells after signaling activation (Figure 20 C, D). For all these proteins the differences in its activation was only seen at early time points up to 6 h, whereas there was no difference anymore after 9 h. Interestingly, the protein level of UBASH3B decreased in the wt cells upon stimulation with 3p-RNA. This finding is in line with the mentioned RNA sequencing data of 1205 Lu cells done in collaboration with Dr. Lars König showing a significant decrease on mRNA level of UBASH3B upon 3p-RNA stimulation.

In summary, these data support the initial finding that UBASH3B-KO in 1205 Lu cells cause an enhanced immune response upon 3p-RNA stimulation measured by cytokine production. The kinetics further indicate, that the level of UBASH3B is especially important at the onset of signaling, since the early time points after stimulation were affected the most.

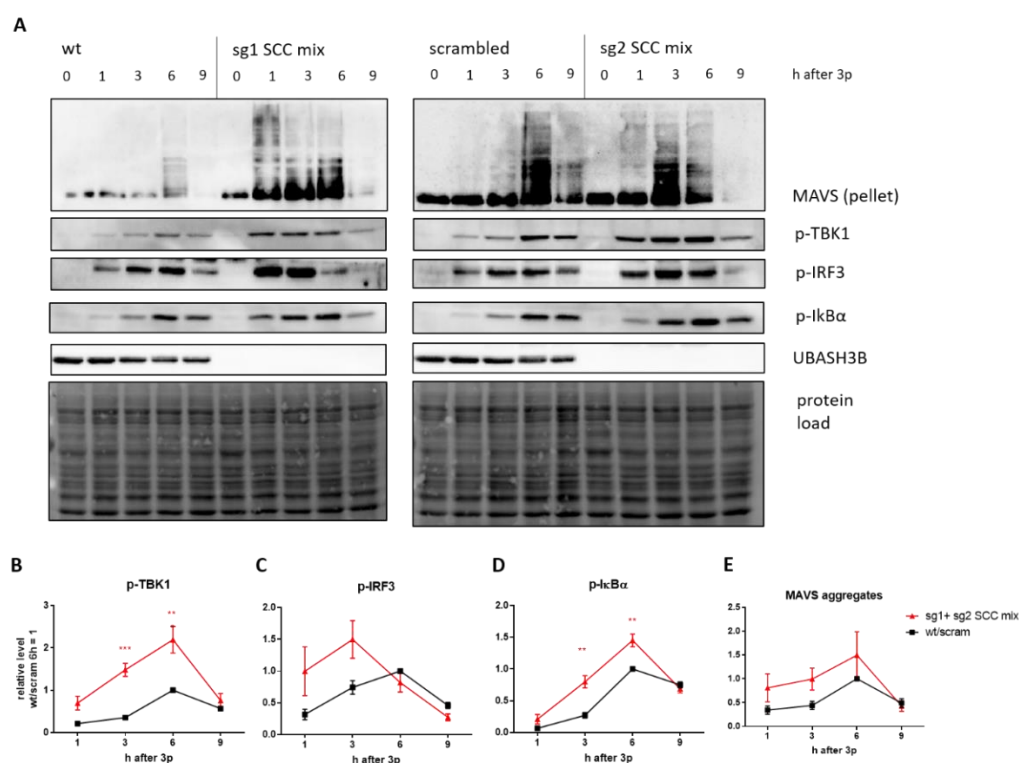


Figure 20: UBASH3B-knockout cells show an earlier and stronger activation of MAVS and its downstream molecules upon stimulation with 3p-RNA. 1205 Lu wt or scrambled cells as well as a mixed population of five SCC of either sg1 (sg1 SSC mix) or sg2 (sg2 SSC mix) were stimulated with 3p-RNA (500 ng/ml) for indicated time points. (A) The cells were lysed and the lysate and insoluble pellet were analyzed by Western blot for the indicated proteins. (B-E) The protein levels were quantified by calculating the intensities of the bands normalized to the total protein load with the software Image Lab. The data for sg1 and sg2 SCC mix or for control cells (wt and scrambled) were pooled and are shown as mean \pm SEM from 3 independent experiments.

Working with SCC, especially derived from a cancer cell line like the 1205 Lu, is prone to clonal variation in addition to the targeted gene deletion. We tried to control for those off-target effects by using different sgRNAs. But there is still the possibility of random mutations that arise from multiple division of a single cell in the process of the limiting dilution process. To circumvent this, batches of UBASH3B KO cells were generated with both sgRNAs. Here, the transfected cells were only selected with Puromycin and all surviving cells were cultivated as a batch. As a control, cells underwent the same procedure but were treated with scrambled sgRNA. Again, the cells were stimulated with 3p-RNA and tested for their IP-10 release via ELISA and the activation of MAVS and downstream molecules by Western blot. Both read-outs confirmed the findings from the SCC by showing a higher IP-10 production in both UBASH3B-KO batches compared to the scrambled cells (Figure 21 A) as well as a stronger activation of MAVS and the downstream molecules TBK1, IRF3 and I κ B α (Figure 21 B). The Western blot for UBASH3B further showed that both KO batches generated with sg1 or sg2 had a high knockout efficiency. There were still some cells expressing UBASH3B which could explain the smaller differences between KO cells and cells treated with scrambled sgRNA in

the IP-10 production as well as in the activation of the signaling molecules compared to SCC being complete KO.

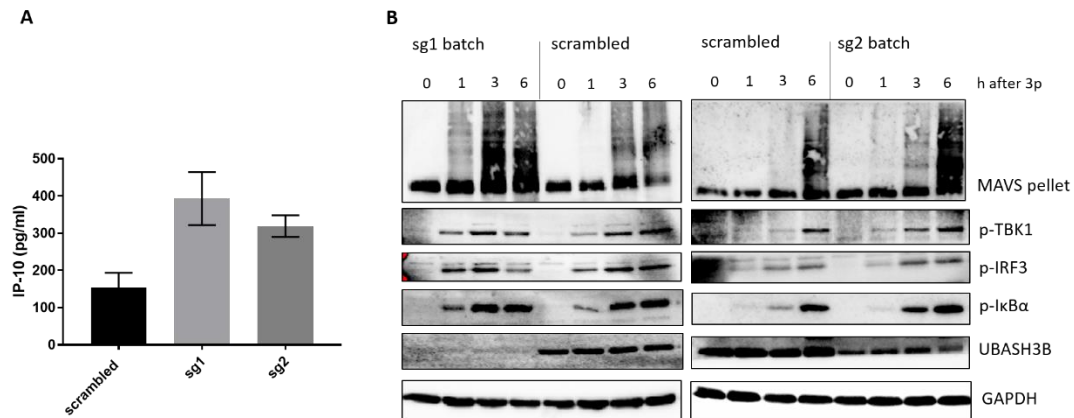


Figure 21: Batches of UBASH3B-knockout cells show the same phenotype as single cell UBASH3B knockout clones. 1205 Lu cells were treated with either UBASH3B-specific sgRNAs sg1 or sg2 or scrambled control sgRNA and cultivated as a cell batch. (A) The cells were stimulated with 3p-RNA (500 ng/ml) for 6 h and the amount of IP-10 was measured in the cell's supernatant via ELISA. Data are shown as mean \pm SEM from 3 independent experiments. (B) The cells were lysed after indicated time points of 3p-RNA stimulation and analyzed for the indicated proteins by Western blot. GAPDH was used as a loading control. Shown is one representative Western blot out of 3 independent experiments.

To see if the identified phenotype for UBASH3B-KO is only specific for 1205 Lu cells, additionally human fibroblasts were tested. These cells have some major differences to 1205 Lu cells, since they are derived from healthy donors and do not have the genetic instability of cancer cells and are therefore biallelic which makes it easier to distinguish between single or multiple cell clones. These primary cells were immortalized by transduction of the human telomerase reverse transcriptase (hTERT) that avoids the reduction of the telomeres.

These immortalized fibroblasts were treated with the UBASH3B-specific sgRNA sg1, expanded as SCC and analyzed by deep sequencing. Four SCC that were proven to be complete KO via DNA sequencing as well as on protein level were taken for analyzes of their phenotype in RLR signaling and were compared to wt cells.

Similar to the 1205 Lu cells, UBASH3B deficiency in these fibroblasts lead to a higher induction of IFN- β and IP-10 at the early time points (Figure 22 A, B). IL-1 β was significantly increased after 6 h (Figure 22 D) and although the differences for IL-6 were not significant, the KO cells tended to induce more IL-6 at all time points (Figure 22 C).

In line with the 1205 Lu cells, the UBASH3B-KO fibroblasts also showed a stronger and earlier MAVS activation. The same was true for the activation of I κ B α (p-I κ B α) (Figure 22 E). Unfortunately, p-TBK1 and p-IRF3 could not be detected in these cells.

All in all, the data of UBASH3B-KO cells provide evidence, that UBASH3B has a negative impact on the activation of MAVS and different downstream signaling pathways and is especially important at the onset of the signaling cascade. The observation of the same phenotype in two different cell lines suggests that the function of UBASH3B in RLR signaling is not cell type specific.

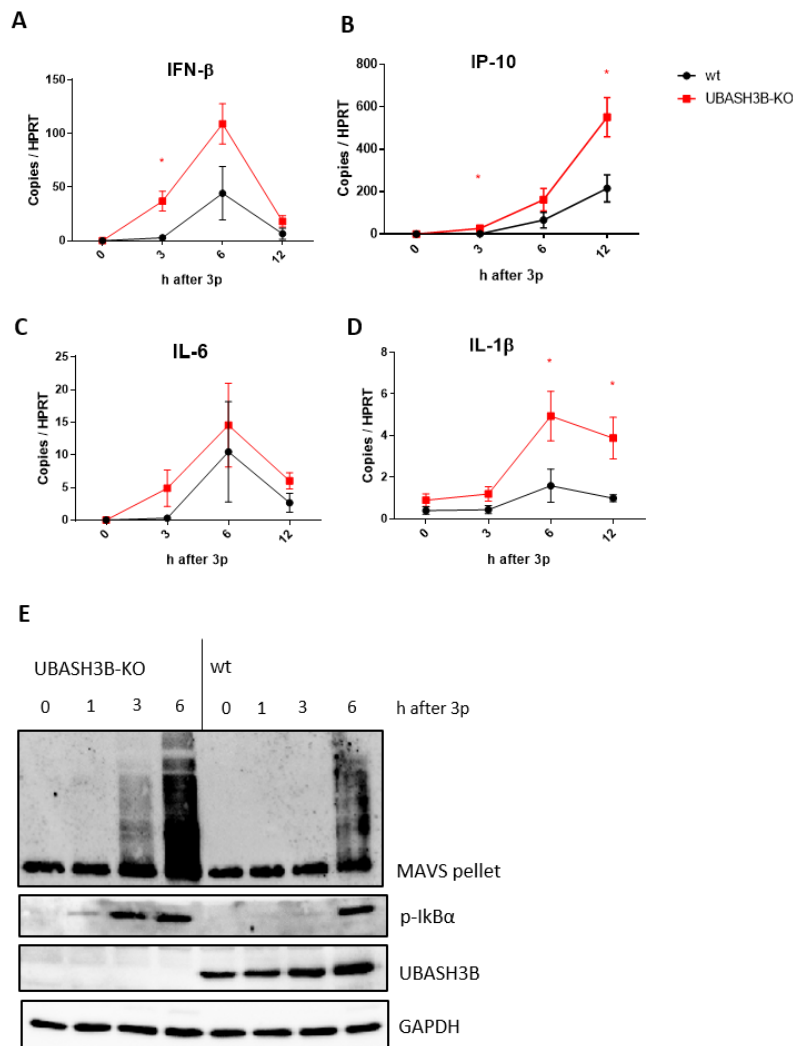


Figure 22: UBASH3B deficiency in human Fibroblasts has the same phenotype as in 1205 Lu cells. Four UBASH3B-KO SCC of human fibroblasts were used as equally mixed cell pool and compared to wt cells. The cells grown in a 24-well plate were stimulated for the indicated time points with 500 ng/ml of 3p-RNA. (A-D) Subsequently, the RNA was isolated, cDNA was synthesized and analyzed for expression of the indicated cytokines by qRT-PCR. Data are shown as mean \pm SEM from 3 independent experiments. (E) The cells were lysed and analyzed for the indicated proteins by Western blot. Shown is one representative Western blot out of 3 independent experiments.

3.2.7 Overexpression of UBASH3B has an inhibitory effect on RLR signaling in

HEK293T cells but not in 1205 Lu cells

To further confirm that the phenotype detected in the UBASH3B-KO cells was indeed caused by the lack of UBASH3B, this protein was overexpressed.

Firstly, UBASH3B was transiently overexpressed in 1205 Lu wt cells by transfection of two different plasmid concentrations. Although the protein was dose-dependently overexpressed, there was no effect on the formation of MAVS oligomers nor on the amount of phosphorylation of TBK1, IRF3 or I κ B α (Figure 23).

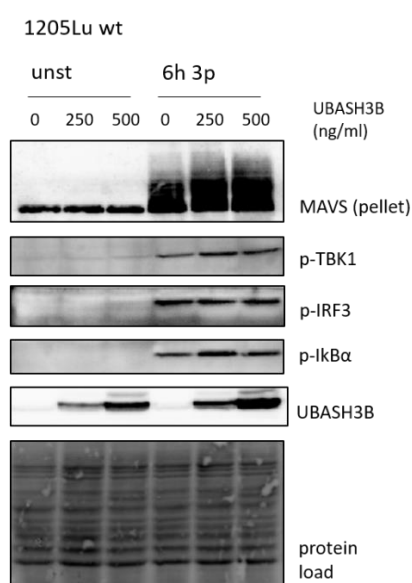


Figure 23: Transient Overexpression of UBASH3B in 1205 Lu cells has no effect on MAVS signaling. 1205 Lu wt cells were transiently overexpressed with increasing amounts UBASH3B. The empty vector pcDNA3 was used to keep the total amount of transfected DNA constant. 24 h after transfection the cells were stimulated with 3p-RNA (500 ng/ml) for 6h, the cells were lysed and analyzed on Western blot for the indicated proteins. The data show one representative blot out of two independent experiments.

1205 Lu cells have a low transfection efficiency and transfection itself can cause artefacts. To circumvent these limitations, the 1205 Lu wt cells and one UBASH3B-KO clone was stably transduced with a plasmid encoding UBASH3B under the control of a doxycycline-inducible promoter (pLVX system; see 2.2.6). The main advantage of this system is, that the same cell population can be used and different expression levels of UBASH3B can be induced depending on the doxycycline concentration used for induction (Figure 24 A).

However, the induction of two different UBASH3B level in the wt or in the KO background showed no altered activation of MAVS analyzed by oligomer formation on Western blot

(Figure 24 B) and no changes in cytokine induction measured by qRT-PCR (Figure 24 C – F), which led to the conclusion that the UBASH3B phenotype in 1205 Lu cells cannot be rescued.

Here, an interesting finding is, that not only endogenous UBASH3B as provided by the RNA sequencing data is downregulated upon 3p-RNA treatment but also UBASH3B transcribed from an artificially introduced vector system that lacks the endogenous promoter (Figure 24 G). This indicates that the mRNA level might not be regulated pre- but post-transcriptionally, meaning there is some factor induced by RLR signaling that destabilizes UBASH3B mRNA.

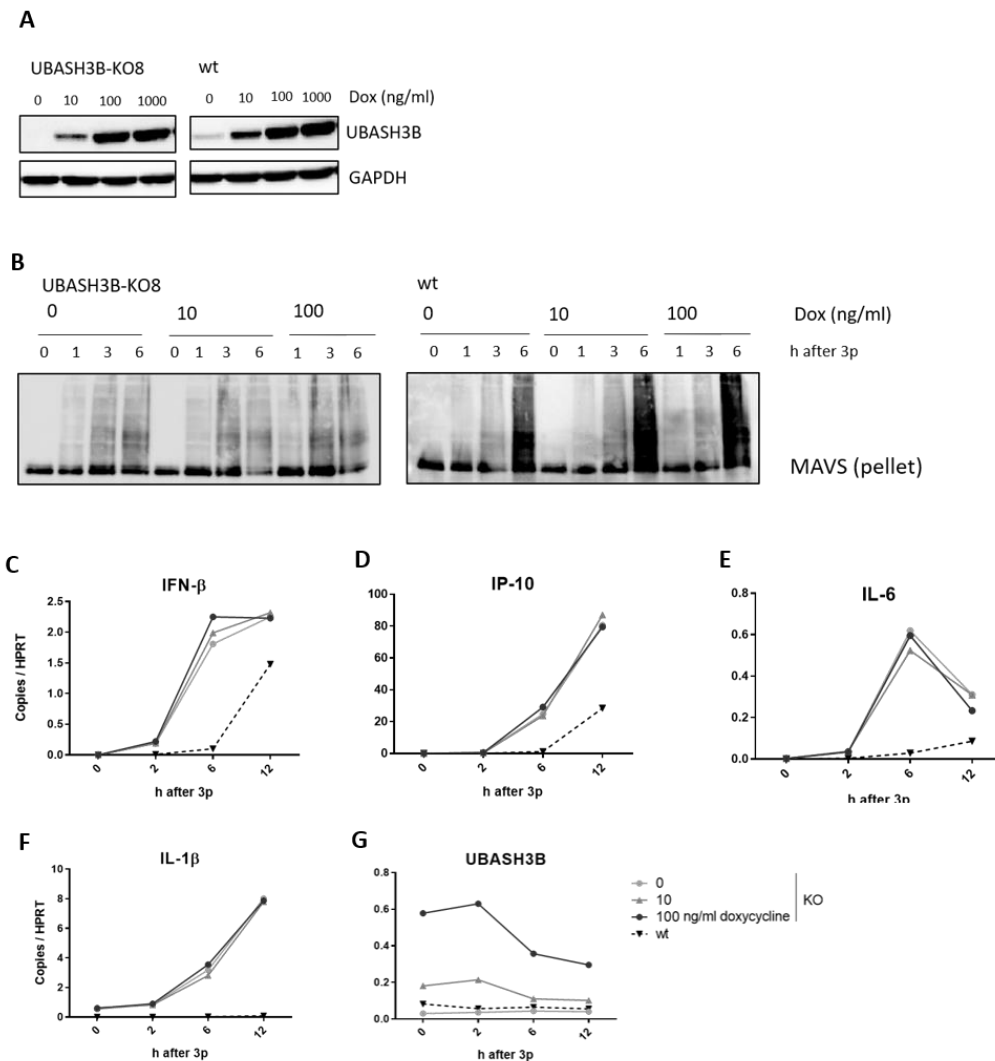


Figure 24: Stable, inducible overexpression of UBASH3B in 1205 Lu cannot rescue its phenotype. 1205 Lu wt or one UBASH3B-KO clone were stably transduced with UBASH3B using a doxycycline-inducible system. (A) Different concentrations of doxycycline were used to induce UBASH3B expression for 24 h. The cells were stimulated for indicated time points with 3p-RNA (500 ng/ml) and analyzed (B) via Western blot for MAVS aggregates in the pellet fraction or (C-G) mRNA levels of the indicated proteins were measured via qRT-PCR in the UBASH3B-KO background. Shown is one representative experiment out of two biological replicates.

Although an effect of UBASH3B overexpression on MAVS signaling in 1205 Lu cells was not detectable, HEK293T cells showed the expected phenotype in luciferase reporter assay.

Here, either RIG-I, MAVS, MAVS-K7/10R, TBK1 or IRF3-5D – a constitutive active IRF3 mutant – were overexpressed along with increasing amounts of UBASH3B or its mutant variant H391A. This mutation is described to highly decrease the phosphatase activity of UBASH3B (141). With overexpression of the respective signaling molecule the signaling cascade starts on the level of this molecule. The IFN- β promoter activity showed a dose dependent decrease when UBASH3B was overexpressed with RIG-I. This decrease was stronger and more significant when UBASH3B was co-expressed with MAVS or its mutant K7/10R. This MAVS mutant lacks the ubiquitination site at the lysine residue 7 and 10 and is therefore described to be incompetent for degradation (91). Furthermore, the UBASH3B mutant H391A showed the same effect as the wt variant, when co-expressed with MAVS. In contrast, overexpression of TBK1 or IRF3-5D did not show any UBASH3B-dependent regulation.

Together these results indicate, that UBASH3B targets the RLR signaling on the MAVS level. Further, the Ubiquitin-chains linked to lysine residues K7 and K10 do not seem to be the binding site of UBASH3B since mutation of the MAVS ubiquitination sites K7/10R that inhibit the ubiquitin-mediated degradation of MAVS do not seem to be important for the effect of UBASH3B on MAVS signaling. Also, the UBASH3B phosphatase domain does not seem to be important to exert the function of UBASH3B on MAVS.

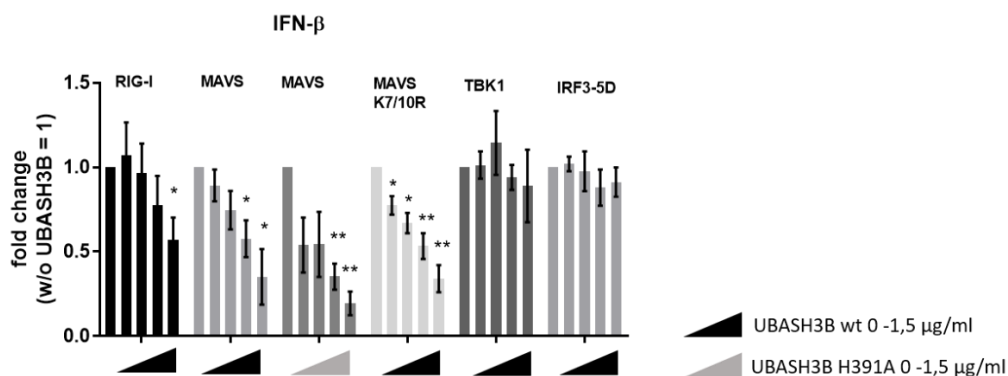


Figure 25: Overexpression of UBASH3B causes a MAVS-dependent downregulation of antiviral signaling in HEK293T cells. HEK293T cells grown in 96-well plate were transfected with increasing amounts of UBASH3B wt or the phosphatase-dead mutant UBASH3B H391A (0/250/500/1000/1500 ng/ml) together with 250 ng/ml of the indicated signaling protein and luciferase reporter plasmid for IFN- β 24 h after transfection, the luciferase activity was measured and normalized to the renilla activity. This relative activity was again normalized to the condition that lacks UBASH3B overexpression. This condition was used as reference to calculate the significance level. The data are shown as mean \pm SEM from 4 to 6 independent experiments.

To further investigate how UBASH3B mediates its inhibitory effect seen in HEK293T cells, MAVS was overexpressed together with increasing amounts of UBASH3B and the pellet fraction was analyzed for MAVS oligomers by Western blot. This experiment showed that indeed the amount of aggregated - and that implies activated MAVS - is decreased with increasing amounts of UBASH3B, whereas the amount of full-length MAVS in the lysate was not affected. Interestingly, the smaller transcript of MAVS – miniMAVS – showed a clear reduction in the presence of UBASH3B. In line with the luciferase assay, UBASH3B-dose dependently caused a decrease of the IFN response. For this, the induced expression of RIG-I as an ISG was used to reflect the strength of IFN induction. All these effects of UBASH3B were also observed with its phosphatase-mutant variant H391A, again indicating that its phosphatase function is not necessary for the observed effect on MAVS.

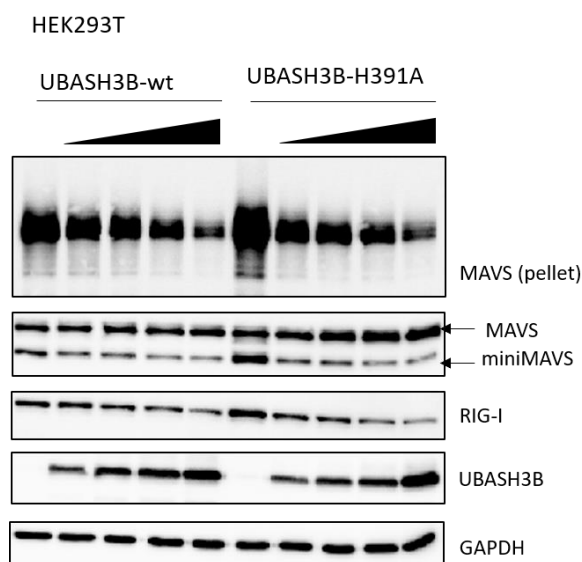


Figure 26: Overexpression of UBASH3B causes a decrease in MAVS activation in HEK293T cells. HEK293T grown in a 12-well plate were transfected with MAVS (250 ng/ml) along with increasing amounts of UBASH3B-wt or its phosphatase mutant H391A (0/250/500/1000/1500 ng/ml) for 24 h. The cells were lysed in RIPA buffer and after centrifugation of the lysate supernatants and the pellet, respectively were analyzed for the indicated proteins via Western blot. Shown is one representative blot out of three biological replicates.

3.2.8 The effect of UBASH3A/B deficiency on RLR signaling in murine bone marrow-derived macrophages varies depending on the strength of the RLR signal

In order to see, if UBASH3B also effects the RLR signaling in other species, our group got access to primary cells of UBASH3A/B double knockout cells. For this purpose, bone marrow from wt and UBASH3A/B double KO mice (a kind gift of Prof. Christian Brandts, university hospital, Frankfurt) was isolated and used to generate bone marrow-derived macrophages (BMDMs). UBASH3B only KO mice were not available to us. However, as UBASH3A expression is thought to be restricted to lymphocytes, we expected the effect of UBASH3B to be the dominant effect in macrophages.

The cells were stimulated with two different concentration of 3p-RNA (100 ng/ml or 500 ng/ml) and mRNA levels of IFN- β and IP-10 were measured at different time points via qRT-PCR (Figure 27). There was no difference for IP-10 and only a non-significant trend for higher induction of IFN- β in KO cells compared to wt cells when they were stimulated with 500 ng/ml 3p-RNA. However, when stimulated with low amounts of 3p-RNA (100 ng/ml) UBASH3A/B-double KO macrophages showed a significant increase in mRNA level at an early point after stimulation (3h) for IFN- β and at a late time point (12h) for IP-10. These results indicate that UBASH3B is likely to also play a role in the murine RLR signaling pathway, although the effect might be weaker than in human cells.

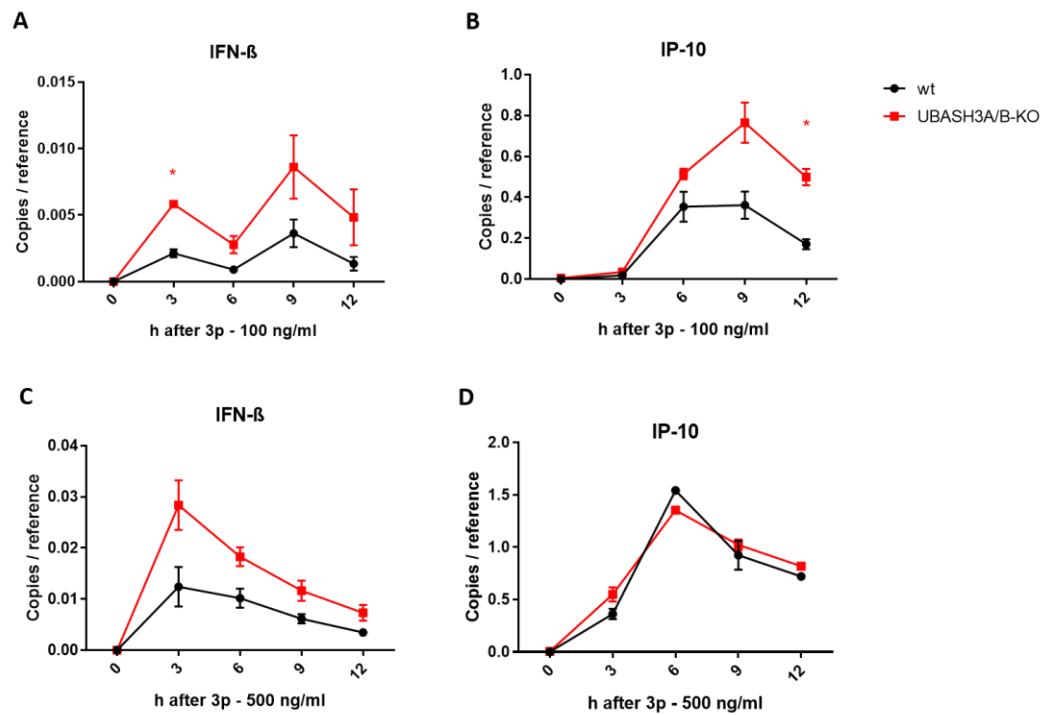


Figure 27: The effect of UBASH3A/B deficiency on RLR signaling in murine bone marrow derived macrophages varies depending on the strength of the RLR signal. BMDMs from wt or UBASH3A/B-KO mice were isolated, differentiated, plated in 96-well plate and stimulated for indicated time points with (A, B) 100 ng/ml or (C, D) 500 ng/ml of 3p-RNA. The isolated mRNA was analyzed via qRT-PCR for indicated cytokines and normalized to the house keeping genes actin and GAPDH (reference). Data are shown as mean \pm SEM from 3 individuals per genotype.

4 Discussion

4.1 The defective interfering genome is the main trigger of RIG-I during infection with VSV

In previous work of our group done by Andreas Linder, a specific DI genome was detected as a RIG-I ligand during infection with VSV by analyzing the RNA that co-immunoprecipitated with RIG-I 9 h after infection by next generation sequencing (NGS) (140). The present thesis could verify this finding by showing that the identified DI genome in our VSV stocks is mainly responsible for the induction of the immune response. VSV stocks without DI genomes seem to trigger the signaling via Leader/N readthrough transcripts.

The NGS analysis allowed precise reconstruction of the DI genome with a size of 4719 bp and a complementary trailer region of 55 bp. The complementary region can form base pairs, a characteristic feature of copyback DI genomes, which then would fulfill the requirements for a perfect RIG-I ligand: it is 5'triphosphorylated as it was shown in the thesis of Andreas Linder and has a short double stranded part (13,25).

As the particle size of DIs differ from full-length virus, DI genomes of VSV are well studied, due to the possibility to isolate them size-dependently by sucrose gradient and ultracentrifugation (142). However, the DI genome analyzed in this thesis was not described before. So far, five DI genomes of VSV are described in detail, that comprises one deletion DI, one snapback DI and three copyback DI genomes (143). It was already described that DI genomes are associated with an IFN response but so far, the precise mechanism for that have not been described for VSV. But in contrast to the copyback DI genome identified in this thesis, previous literature mainly described snapback DI RNA structures to induce an IFN response (144). Due to its long double-stranded part snapback DI genomes, however, rather carries features typical for an MDA5 ligand.

For VSV we describe for the first time that a DI genome is the dominant RIG-I trigger during the replication cycle. In the last years other groups revealed DI genomes from different RNA viruses as RIG-I ligands that also have a 5'copyback structure. Strahle et al. described copyback DI genomes of Sendai virus to be potent activators of IFN and could show that IFN induction depends on the replication of DI genomes. They also showed that these copyback DI particles are much more potent interferon inducers than DIs with an internal deletion (145). Later these copyback DI particles were found to specifically bind to RIG-I in NGS analysis, whereas full-length genomes have not been detected at all (33). In contrast to our study they used untagged endogenous RIG for their IP. In another approach RNA species were analyzed by NGS that are specifically associated with the nucleoprotein of measles (MV-N) and also found a copyback DI genome to be enriched. They could further show that the

IFN induction highly relies on binding of this DI genome to RIG-I (146). In line with that, DI genomes of MV were also found in RIG-I pull-downs after RNA-protein cross-linking and pull-down of endogenous RIG-I (147).

Hence, up to now copyback DI genomes are well described RIG-I ligands. However, the dependency on replication is still a matter of debate. Most of the studies investigating structural features of DI genomes that bind to RIG-I are done with in-vitro transcribed or isolated, naked DI genomes (148,149). The strong IFN activation by transfection of naked DI genomes was confirmed in our study. By transfection of size-fractionated RNA isolated from infected cells, we could show that the identified DI genome is responsible for most of the produced IFN (see Figure 6).

However, under physiological conditions the DI genome as well as the full-length genome are usually encapsidated by the N protein that should avoid the formation of secondary structures and in this way avoid detection by RIG-I. In the process of replication, the N protein is removed from DI genomes which could make them accessible for RIG-I. We also assume such replication-dependent detection from our data: The application of CHX, a translation inhibitor, that allows infection and primary transcription but no replication, showed complete blockage of DI genome accumulation as well as IFN induction (Figure 4). The replication-dependency of VSV DI genome detection was also shown in a study by Panda et al. (150). They developed a tool to independently investigate the effect of infection and replication by using a cell line that stably expresses the proteins N, P and L that are necessary for replication. They found, that the infection with DI particles is not sufficient to induce an IFN response but needs replication. In contrast, tenOever et al. showed that IFN induction is polymerase independent but only needs a certain threshold of ribonucleoprotein (RNP) to induce an immune response (151). Since we did not test higher viral titers for infection, it could be also possible that replication was just needed to reach this threshold.

However, how the detection by RIG-I would occur without replication is still unclear. One possibility could be that some DI genomes are not fully protected by the N protein and expose RNA sites that can form complementary structure, which could also explain the difference between our study, the studies of Panda et al. and of tenOever et al. In line with this hypothesis, Weber et al. claim, that the incoming RNPs of different segmented (-)ssRNA, like La Crosse virus (LACV) and Rift Valley Fever virus (RVFV) serve as RIG-I ligand, because they have complementary naked 3' and 5' ends that form panhandle structures (152). A mechanism that could also apply for copyback DI genomes. Another possible mechanism is given in a study showing, that ATP-dependent helicase activity of RIG-I itself is capable of removing viral proteins from the RNA for its detection (153).

Although we could clearly show, that a defined DI genome of VSV is the main trigger of RIG-I in the tested viral stock, further studies are needed to clarify if also encapsidated ones can be detected or if replication is truly needed.

4.2 RIG-I ligands in the absence of defective interfering genomes

While the DI genome could be detected as the main RIG-I ligand after infection with our VSV stocks, the question arose, if there are other ligands and what are the ligands, if DI genomes are absent. By serial dilution of the original viral stock we could eliminate the DI genome to the extent, that even after 24 h of infection it was barely detectable. However, this stock still induced an IFN response, although it was much weaker than with the original virus stock (Figure 5). That hinted towards additional immunostimulatory RNA species generated during VSV infection besides the DI genome. The data from the RNA fragmentation assay indicate that the full-length genome most likely is responsible for this immune response, because only the long RNA molecules that corresponds to the size of full-length genomes showed a slight immunostimulatory effect in the absence of DI genomes (Figure 6). We verified the correct size-dependent fragmentation by qRT-PCR assay and additionally shock-froze the RNA samples before loading on the gel. This should exclude secondary RNA structure formation that would lead to incorrect separation. Nevertheless, as discussed above, the immunostimulatory capacity measured in this assay relies on naked RNA, that can form secondary structures that do not naturally occur and serve as PAMP. Moreover, this assay only shows that long RNA molecules induce the immune response but does not look for the responsible receptor. Due to the length it could also be an MDA5 ligand.

The analysis of the RNA that co-immunoprecipitated with RIG-I after infection with DI-genome-low VSV stocks should have clarified this. This showed only a strong enrichment of leader/N sequences that could also hint towards the binding of the full-length genome. But in this case an equal enrichment of all other genome regions would be expected that was not detectable by qRT-PCR of different genomic regions (Figure 7). However, the data of Andreas Linder hints towards the binding of a small portion of full-length genome, since negative sensed RNA was found to be enriched by 3- to 5-fold along the whole genome after NGS analysis. Because the qRT-PCR assay used in the present study also detect mRNAs, the small amounts of genomic RNA could be simply underrepresented. Although the full-length genome might slightly contribute to RIG-I activation, the strong enrichment of the leader/N-readthrough speaks in favor of this RNA species being the main ligand of RIG-I in the absence of DI particles.

This result is in line with a study that identified RIG-I ligands during MV infection with NGS and found besides DI genomes leader/N readthroughs to be enriched (147). Another recent

study also found the leader/N readthrough to be the main inducer of IFN via RIG-I. They identified the leader/N RNA as a 1.8 kb long RNA that is 5'triphosphorylated and 3'polyadenylated. It associated with RIG-I in antiviral stress granules. They could show the same for two other non-segmented (-)ssRNA viruses, for VSV and Respiratory syncytial virus (RSV), indicating that this is a general mechanism of this virus family (154). Such readthrough RNAs are derived from transcription and thus are not wrapped by N proteins. Whether the leader/N RNA forms intramolecular double-stranded structures or pairs with the full-length genome was not addressed and would be an interesting question for further studies.

Our RNA fragmentation assay showed an immunostimulatory capacity only for the long fractions, which could be a result from binding of the readthrough to the full-length genome after RNA purification. The same finding was made by Rehwinkel et al., who used the same fragmentation assay after infection with Sendai virus or Influenza. They further used primer extension for identification, but this assay does not allow to distinguish between DI and full-length genome which could have led to the misinterpretation of the full-length genome as the main ligand for RIG-I (24). They lack the detailed analysis of RNA co-immunoprecipitated with RIG-I by NGS. Their interpretation is also contradicted by Baum et al. who could show by NGS analysis, that only DI genomes of Sendai virus but no full-length genome bind to RIG-I (33).

However, for influenza the finding of Rehwinkel et al. could also be due to its nature as a segmented (-)ssRNA virus. Weber et al. had shown that influenza genome segments can act as RIG-I ligands. They claim that the genome segments of influenza, even when they are protected by viral proteins can form a panhandle structure due to their high complementary termini, but that this is not the case for non-segmented (-)ssRNA viruses such as Sendai or VSV (152).

All in all, this led to the assumption that the leader/N readthrough of VSV could trigger RIG-I in the absence of DI genomes probably via formation of double-stranded intermediates by binding to the complementary full-length genome. To test this hypothesis, however, further experiments will be needed.

4.3 Physiological role of defective interfering genomes

The main finding of this part of the thesis is the strong contribution of DI genomes to the IFN response upon VSV infection. This poses the question, if and how this could be physiologically relevant.

Since more and more DI genomes are detected in human specimens (see 1.5) it is believed that they occur in natural infection and are not only cell culture artefacts. Because of their ability to induce IFN, they can restrict viral replication, thus limiting the outbreak of the

disease and induce a proper immune response. Although the physiological role of the accumulation of DI genomes after infection, i.e. if it also has advantages for the virus, is still not clear, DI genomes have gained much interest as a potential adjuvant in vaccines.

This potential of DI genomes was shown in a study that compares DI-low and DI-high viral stocks of a vaccine strain of MV (155). They found, that infection of monocyte-derived DCs with DI-high stocks induced more IFN that correlated with a greater DC maturation. They further showed, that the wt virus strain behaved similar as the vaccine strain, when the DI genomes were diluted out. This is one study demonstrating that DI genomes can highly contribute to vaccination efficiency as it was already shown for other viruses, like Sendai virus (29). It was further shown that a DI genome of Sendai is capable via the stronger activation of DCs to induce a stronger activation of naïve CD8⁺ T-cells and to enhance antibody production (156). For different live-attenuated vaccines, such as MV, poliovirus or influenza a high amount of DI genomes have been found (157). This further suggests a contribution to the efficacy of vaccination.

The identification and characterization of DI genomes of VSV, like the one identified in the present study can help to find a highly potent DI genome that can be used as an adjuvant for vaccines by triggering the RLR pathway. Moreover, as VSV is already used as a vector for different replication-competent vaccines, such as the vaccine against the Ebola virus (EBOV-VSV) (158), the determination of amount and type of DI genomes in these vaccines would be helpful to get more reproducible results on vaccination efficacy. VSV is further developed for oncolytic tumor therapy. Here, the efficacy of cell lysis and induction and reactivation respectively of immune responses against the tumor cells highly depends on the capacity of the virus to replicate and to induce cytokines, which is in turn influenced by the amount of DI genome. Thus, the determination and purposeful use of DI genomes could help to improve this therapy, which has to our knowledge not been investigated so far.

4.4 The specificity of APEX in the MAVS-APEX fusion protein

The second part of the thesis presented here focused on MAVS, the downstream adapter molecule of RIG-I and MDA5 and identified and characterized new interaction partners to gain further insights into the regulation of this antiviral pathway.

The list of MAVS interaction partners is constantly growing. So far most often conventional methods like co-immunoprecipitation and yeast-two-hybrid screens have been applied for their identification or verification. Since APEX-mediated labeling is applicable to living cells, it acts in the most physiological environment and has the ability to catch weak and transient interaction partners at a defined time point. This method is therefore highly promising to identify further important interactors, that have not yet been described in MAVS signaling.

At the time we started to use APEX, there were just two publications out describing the method in proof-of-principle studies. It was demonstrated that APEX is suitable for labeling subcellular proteomes that are enclosed by membranes, such as the mitochondrial matrix and the IMS (128,132). Thus, the first question that needed to be answered, was how specific the labeling was in the cytoplasmic part, where APEX is located when fused to MAVS.

The labeling radius of biotin phenoxyl radicals was suggested to be less than 20 nm. This number arose from electron microscopy experiments on fixed cells (159). Rhee et al. assumed that it can be even smaller in living cells, because of endogenous radical quenchers (e.g. glutathione). By fusion of APEX to localization sequences targeting the molecule to different organelles (i.e. nucleus, mitochondrial matrix, IMS, ER), they could show by confocal imaging and Western blot analysis, that each construct biotinylates different subsets of proteins in the expected compartment. Furthermore, they targeted APEX to different subcellular compartments, but with APEX facing the cytosol. Even these constructs displayed a distinct biotinylation pattern. This was the first hint that APEX works also specifically in the cytosolic part, when it is bound to a membrane (128).

With our constructs we could confirm this finding for cytosolic APEX: As expected, all APEX-MAVS constructs as well as the APEX-TM construct showed the same biotinylation pattern, since they all have the same localization at the OMM facing the cytosol. This was clearly distinct from the mito-APEX construct from the study of Rhee et al. that is localized in the mitochondrial matrix and was used by us as a control (128). While the improved APEX2 enzyme was used in our MAVS constructs, the mito-APEX construct bears the older version. This might explain the difference in biotinylation intensity that we observed (Figure 9).

Additionally, the confocal imaging supports the specificity of APEX, since the biotinylation was highly enriched at mitochondria, although it was not as restricted as for the control construct mito-APEX. Reasons for the observed background biotinylation could either be that the radical diffuses during the one minute the APEX reaction lasts and biotinylates a small fraction of distant proteins or that proximity labeled proteins diffuse in the cytosol after biotinylation. This question was already addressed by Hung et al., when they used IMS-targeted APEX, because the phenoxyl radicals are theoretically able to diffuse through the OMM. After MS analysis they found that also cytosolic proteins were biotinylated, mostly those that reside near the mitochondria. They concluded, that a small portion of the radicals diffuse and label cytosolic proteins (132). From this study we assume that this is also the case for our constructs.

Although the overall biotinylation pattern for APEX-TM and APEX₅₁₀MAVS was the same under homeostatic conditions, Western blot analysis of known MAVS interactors after streptavidin pull-down revealed, that both constructs biotinylate different proteins (Figure

11). Whereas for APEX-TM each protein was biotinylated in the unstimulated condition, TRAF3 and TBK1 were only detectable upon stimulation in APEX₅₁₀MAVS. Moreover, GAPDH was much more enriched for APEX-TM, indicating a stronger background biotinylation with this APEX-TM construct compared to APEX₅₁₀MAVS. Reasons for that may be the stronger enzyme activity of APEX in the APEX-TM construct due to a lack of steric hindrance by an N-terminal fusion protein. APEX within the APEX-TM construct is freely exposed into the cytosol, whereas in the APEX₅₁₀MAVS construct it is enclosed by the helicase and signaling domain of MAVS, which is likely to cause differences in the biotinylation capacity.

However, the most striking difference of both constructs was observed by confocal imaging upon 3p-RNA stimulation. Both, APEX₅₁₀MAVS and APEX-TM induced the same biotinylation pattern in the unstimulated condition. But 1 h after 3p-RNA treatment, APEX₅₁₀MAVS showed a completely different pattern with characteristic dots (Figure 12). Because this was not observed with APEX-TM, we assume that this pattern is specific for MAVS and not for any mitochondrial changes upon stimulation. Furthermore, this pattern was only observed upon MAVS activation with 3p-RNA, but not after stimulation with untransfected pIC, that signals independent of MAVS (data not shown). This further supports that it is a MAVS-specific change in the biotinylation pattern and represents activated polymerized MAVS and its associated signaling complex. The comparison of APEX-TM and APEX₅₁₀MAVS indicates, that APEX works not only specific for different subcellular sites but also for specific membrane bound proteins.

APEX₅₁₀MAVS thereby presents a new tool to study dynamics in MAVS signaling, that have not been possible before. So far, MAVS activation could only be detected with semi-denaturing detergent agarose gel electrophoresis (SDD-AGE) that allows to visualize MAVS polymers after lysing the cells. In contrast, simple MAVS staining in confocal microscopy cannot differentiate between monomeric or oligomerized MAVS. Thus, detection of MAVS activation with APEX can be applied to study the kinetics of MAVS activation and interaction progress with other molecules. We could show, that TBK1 is highly associated with the biotin dots after 1 h of stimulation and gets subsequently released, whereas the activated MAVS remains stable. This also further confirm that the biotin dots indeed reflect MAVS signaling complexes. This fits to the report from Pourcelot et al., showing that TBK-1 is activated in interaction with MAVS, but that activated TBK1 is mostly associated with the Golgi apparatus (160). We did not look for colocalization of TBK1 with the Golgi, but at least the dissociation from MAVS after activation is consistent with our result.

4.5 Control conditions for mass spectrometric analysis

Although, APEX₅₁₀MAVS seems to work specifically for MAVS associated proteins, there is some background biotinylation that needs to be eliminated in order to identify true positive interaction candidates. As it was shown in former APEX studies, choosing the right controls is crucial to gain high specificity.

In the initial APEX publication that identified the mitochondrial matrix proteome, a control that simply lacked the biotinylation process was sufficient to gain a specificity of > 94%, because the biotinylation is highly restricted to this membrane enclosed space (128). The same control for the mapping of the IMS proteome just gave a specificity of 40% for mitochondrial proteins. As discussed above, the permeability of the OMM for small molecules like the phenoxyl radicals produced by the APEX reaction leading to some cytosolic background has probably caused the reduced specificity. By including a second control, the APEX-NES that is unspecifically expressed in the cytosol, they were able to exclude the false positive cytosolic proteins and increased the specificity to 87% with prior mitochondrial annotation (132).

Independent from our study, more recently the group of Hung et al. published a paper where they used a construct (APEX2-OMM) that is exactly the same as our APEX-TM construct, meaning that APEX is fused to the TM domain of MAVS at the amino acid 510. The authors used this fusion protein to map the proteome of the OMM. Although they overall detect more than 4000 proteins, by again using APEX-NES as a spatial control, they were able to identify 137 proteins that are specific for the OMM (161). We could find 29 proteins from this list in each of our unstimulated APEX-TM replicates and 44 proteins of their OMM proteome were detected in at least one of our APEX-TM replicates. Reasons for this small number of overlapping proteins could be the amount of overall detected proteins. Whereas we detected approximately 800 proteins per replicate (see Figure 14B), Hung et al. detected more than 5000 proteins per replicate. As we used comparable amounts of protein for mass spectrometric analysis, it is unlikely that protein quantities caused this difference. One major difference between our analyses was the quantification method. Whereas we used label-free quantification, Hung et al. used SILAC (stable isotope labeling with amino acids in cell culture) for quantification. They further used another cell line (HEK293T) which could also cause the differences.

In the first study describing protein interaction networks with APEX it was further demonstrated, that even if the protein of interest changes its localization upon signaling activation, it is possible to identify true positive interactors by choosing the right control. They coupled APEX to a GPCR and could track it over time after activation. Similar to our APEX-TM, in their control condition APEX was fused to a respective localization sequence

(plasma membrane, endosome or cytosol) and was used for normalization at these time points when the GPCR was localized to this compartment. Since they used a well described GPCR they could confirm that this approach is specific and further revealed new interaction partners (137).

Similar to this study, we were not primarily interested in the proteomic composition of a steady-state situation, but rather in the proteomic alteration upon RLR activation. For this question, one obvious control was the unstimulated situation in the APEX₅₁₀MAVS cells. This should control for all background biotinylation and should only identify those proteins, that translocate into the vicinity of MAVS upon its activation. As a spatial control, we used the cell line APEX-TM in the unstimulated state and upon MAVS activation. This control was supposed to identify proteins that translocate to the mitochondria but independent of interaction with MAVS. Since we could not detect any significant changed protein in this control, all the proteins that are significantly altered in the APEX₅₁₀MAVS cells upon stimulation were considered to be MAVS-specific.

4.6 Analysis of the identified MAVS interaction network

The analysis of our MS data revealed 31 proteins that translocate to the MAVS signaling complex 1 h after stimulation with 3p-RNA. Since many interaction partners of MAVS are already well described, we expected to find some of these previously identified interaction partners in our assay.

Indeed, we were able to detect 11 proteins that are described as part of the MAVS signalosome. TBK1 showed the highest significance which is in line with the Western blot analysis (Figure 11) and with the literature, characterizing TBK1 as highly important for activation of downstream signaling. In contrast to the Western blot data, we could not detect TRAF3, but instead found TRAF2 and TRAF6 and all essential components to activate the NF κ B signaling branch (IKK α , IKK β , NEMO and TANK). Further proteins that are directly linked to the MAVS signalosome is the LUBAC complex consisting of HOIP (RNF31), HOIL (RBCK1) and SHARPIN, that were all significantly enriched. However, up to now, the actual role of the LUBAC complex in MAVS signaling is not clear. One report claims that it acts redundantly to TRAF molecules by transferring ubiquitin chains to MAVS if TRAF molecules are missing (79). In contrast, Belagnoui et al. described a negative regulatory function through ubiquitination of NEMO that subsequently inhibits MAVS-TRAF3 interaction (162). More recently TAX1BP1, also identified as interactor in our assay, was published to directly interact with MAVS and recruit AIP4 for MAVS degradation (163).

Although, several important proteins known to act downstream of MAVS were found within the candidate proteins, the essential upstream activator RIG-I was missing. In line with the

Western Blot data, it got biotinylated upon APEX activation, but the amount did not change after stimulation, no matter at which time point after stimulation. This raised the possibilities that RIG-I is not translocated to MAVS but is always in close surrounding and just needs an activating trigger or that activated RIG-I is not biotinylated because it binds to the CARD domain of MAVS that is distant from APEX. Since the predicted labeling radius of APEX should cover this distance, however, the latter possibility is not likely. Speaking in favor of the first hypothesis is, that in MS data of the control cell line APEX-TM RIG-I was not detected at all, although that contradicts the Western blot data (Figure 11). The common knowledge is, that RIG-I is translocated to MAVS (63,76), which speaks against our finding. However, this conclusion was always drawn after IP of RIG-I or after purification of mitochondrial membranes. It could be that only upon binding of the CARD domains of RIG-I and MAVS the interaction was strong enough to sustain the detection methods, whereas their sole proximity was not detectable with these methods. Since confocal microscopy could also not clearly show any redistribution upon RIG-I activation (data not shown) further experiments are needed to test this hypothesis.

Three additional proteins were detected after MS analysis that have an indirect link to the MAVS signaling platform and are described to play a role in NFkB activation (OPTN, BIRC2, TNIP1). Another three proteins are also linked to MAVS signaling but have not been within the cluster identified by the online tool *string-db* (Figure 16). N4BP1 is indirectly linked to MAVS through its interaction with AIP4 that in turn cause degradation of MAVS (93) and DRP1 and OPA1 are important for mitochondrial dynamics and have been shown to influence RLR signaling (98).

The remaining 14 proteins have no described connection to MAVS-dependent signaling yet. Interestingly, several proteins (IMMT, CHCHD3, ATAD3A) and OPA1 are located to the inner mitochondrial membrane (IMM) and together with TBC1D15 are important for mitochondrial morphology. Even though this needs to be further evaluated, if these proteins directly interact with MAVS or at least come in close proximity to MAVS due to mitochondrial rearrangement, the presence of these proteins in this data set supports the hypothesis that mitochondrial dynamics is a highly important process induced by as well as influencing MAVS activation as described in 1.8.

Taken together, we could convincingly show that APEX is suitable to detect MAVS interaction partners or at least proteins of the MAVS signaling complex. This makes it an interesting tool to further study MAVS signaling. To draw a dynamic picture of components of the MAVS signaling complex, the MS analysis could be repeated at later time points. Further interesting questions that could be tackled with the APEX method are, how physiological virus infection influences the signalosome and how it differs between viruses or whether there are any

differences in the kinetic and composition of the MAVS signalosome between activation via RIG-I and MDA5, respectively.

4.7 UBASH3B is a negative regulator of RIG-I like receptor signaling

UBASH3B, also known as Sts-1 (suppressor of T-cell signaling) or TULA-2 (T-cell ubiquitin ligand) is described as regulator of different cellular functions. It has three known functional domains: the ubiquitin-binding domain (UBA), a Src-homology 3 (SH3) domain and a histidine phosphatase domain, that is specific for tyrosine residues. Its mode of action is thought to be defined by these domains: UBASH3B binds via its UBA domain to ubiquitinated proteins, while the SH3 domain mediates the interaction with SH3-binding proteins. The active phosphatase domain then exerts its function on phosphorylated tyrosine residues. This protein family has a second member, UBASH3A (Sts-2, TULA), displaying the same function, but with a lower phosphatase activity. Furthermore, it is only expressed in lymphoid cells, whereas UBASH3B is ubiquitously expressed (164).

UBASH3B is described as a regulator for signaling receptors, like the T-cell receptor (TCR) and the epidermal growth factor receptor (EGFR). It has a negative regulatory function on TCR signaling by dephosphorylation of Zap-70 (165,166), whereas it has a stabilizing function on activated EGFR. Two groups showed, that it acts indirectly via dephosphorylation of the E3 ligase c-Cbl, a well described interaction partner of UBASH3B. C-Cbl was found to constantly interact with UBASH3B and upon ligand binding UBASH3B is recruited to the EGFR via c-Cbl. As the counter part of c-Cbl, which ubiquitinates and degrades EGFR, UBASH3B inhibits this degradation process (167,168).

Together with the data from MS (Figure 15) and the initial KO screen (Figure 17), these characteristics made UBASH3B a highly promising candidate in regulating MAVS, a membrane bound receptor, such as TCR or EGFR.

To analyze the function of UBASH3B, we decided to use a CRISPR/Cas9-mediated KO-based system. The invention of CRISPR/Cas9 has brought a revolutionary tool into the labs to easily knock out a gene of interest in cell culture. However, this method has some pitfalls one need to be aware of, when working with this system: The sgRNA can have off-target effects. If the sgRNA is not specific enough, it can bind to different loci and cause background mutations. To circumvent this, we used the online tool <http://chopchop.cbu.uib.no>, that predicts off-target effects, to design sgRNAs. We further used the enhanced Cas9 (eCas9), that has a mutation, allowing the cleavage of DNA only when the sgRNA is totally complementary to the target site (169). To further exclude off-target effects we used two different sgRNAs to generate KO clones.

The second major problem is not directly related to the CRISPR/Cas9 system, but to the process of generating single cell knockout clones that are used for KO studies. Especially when working with tumor-derived cell lines, such as the 1205 Lu cells, random mutations accumulate during the expansion process of generating SCC, that are not caused by sgRNA-mediated off-target. This was an observation we made in our group after exome sequencing of two different SCC generated with the same sgRNA. We further saw this phenomenon in the initial screen of different gene KOs, where some SCC carrying the same KO genotype concerning the target gene behaved differently (Figure 17). To avoid this error, we worked also with cell batches, that were treated with the CRISPR/Cas9 system and selected for Cas9 expression but were not subjected to the process of single cell cloning. A prerequisite to use this approach is a high efficiency of the sgRNA, that we could show by Western blot analysis. Additionally, we used knockout cell lines generated from patient derived fibroblasts, that were immortalized by transduction of hTERT. These cell lines have no tumorigenic background and therefore are supposed to be genetically more stable. This should reduce the accumulation of random mutations during SCC expansion. Fibroblasts are further described to be biallelic, a feature that makes it easier to identify genetically complete knockout SSC than in multiallelic tumor cell lines.

Consistently, both sgRNAs and clones derived from both cell lines (1205 Lu melanoma cells and immortalized fibroblasts) showed the same phenotype upon 3p-RNA stimulation: a higher induction of different cytokines and earlier and stronger MAVS activation, that was in line with earlier induction of the two signaling branches of IRF-3 and NFkB activation. These phenotypes were strongly observed at early time points after activation (up to 6 h), whereas at later time the KO and wt phenotypes converged again.

From these results we concluded a negative regulatory function for UBASH3B, that is especially important early on when the RLR signaling pathway is activated. Interestingly, already after 1 h of 3p-RNA stimulation, the time point the candidate proteins have been identified by our APEX screen, loss of UBASH3B had a direct impact on MAVS activation as shown by increased aggregate formation of MAVS. This was in line with the results obtained in HEK293T cells, showing that overexpression of UBASH3B along with MAVS decreased the IFN- and NFkB signaling in luciferase reporter assays (Figure 25) and also decreased the amount of MAVS aggregates (Figure 26). UBASH3B did not influence the signaling further downstream, at least not on the IRF3 signaling branch, as shown with the overexpression together with TBK1 or IRF3-5D.

These results suggest a direct interaction of UBASH3B with MAVS or one of the early interactors, like TRAF molecules that play a role on the activation of both, IFN and NFkB signaling path. Even more, preliminary IP assays verified the interaction of MAVS and UBASH3B (data not shown). These results could be further confirmed in the doctoral project

of Corinna Meyer-Gehlen. However, if this interaction is direct or via linking proteins still needs to be figured out.

One of the first crucial steps for MAVS activation is its ubiquitination by TRAF molecules. UBASH3B could possibly act, by binding to this ubiquitin chains and either dephosphorylates itself or another protein in the close surrounding leading to downregulation of the signaling.

To test if dephosphorylation is the mechanism, how UBASH3B downregulates MAVS signaling, we generated a phosphatase-dead mutant (H391A). This mutation is described to highly decrease the phosphatase activity (141). In our case this mutant behaved like the wt protein by reducing the antiviral signaling. Reasons for that could be, that this function of UBASH3B is not important and that just the binding is sufficient to e.g. recruit other signaling molecules that exerts the function. In this case UBASH3B would function as a bridging protein. Since we relied on the phenotype described in the literature for the H391A mutation and did not test for residual phosphatase activity in this mutant, it could be that some residual phosphatase activity is sufficient for the dephosphorylation. In further experiments it will be tested by MAVS-IP, if its tyrosine phosphorylation is different between wt and KO cells upon RLR activation. MAVS itself bears 10 tyrosine residues that would be possible targets for UBASH3B. In a study by Wen et al. the importance of all these residues were tested in mutation-based screen. They replaced every tyrosine by phenylalanine, leading to loss of this phosphorylation site by keeping the protein structure intact. Only the mutation Y9F was found to highly affect the immune response. Mechanistically, the loss of this phosphorylation impaired the binding of TRAF3 and TRAF6 (88). Up to now, the responsible kinase and phosphatase are unknown, which makes the T9 residue an interesting candidate to look for interaction with UBASH3B.

As mentioned above, UBASH3B constitutively interacts with c-Cbl, a protein that is also described in regulating the RLR pathway and could thus be an interesting link. It was found that c-Cbl is recruited to RIG-I via Siglec G and marks RIG-I by K-48 linked ubiquitination for degradation (170). Since UBASH3B counteracts c-Cbl activity, the KO of UBASH3B would decrease the activation of MAVS because more RIG-I would be degraded – the opposite effect of what we found. Thus, this mechanism does not seem to cause the phenotype.

Another described molecule that potentially links UBASH3B to MAVS is Src. This tyrosine kinase was found to be a substrate of UBASH3B (166). A recent study identified Src to be important for TBK1 phosphorylation at a specific tyrosine residue that facilitates its autophosphorylation and subsequent IRF3 activation. Interestingly, by performing in vitro GST-pull-down assays they found that Src and TBK1 do not interact directly. Instead, Src directly interacts with the proline-rich region of MAVS via its SH3 domain (171).

This mechanism would fit to the negative regulatory function of UBASH3B we observed: UBASH3B is a counterpart of Src, that inactivates it by dephosphorylation. Missing UBASH3B could lead to excessive Src activity that in turn leads to stronger activation of TBK1. Indeed, we could observe stronger phosphorylation in the KO cells upon RLR activation.

But part of the study of Li et al. do not fit to our observation: Li et al. showed that by chemical inhibition of Src the phosphorylation of I κ B α is not affected, whereas we also observed enhanced activation in the UBASH3B-KO. However, it may be that UBASH3B has an additional role on another kinase than Src, that regulates the NF κ B signaling. The hypothesis that UBASH3B mediates its effect on the RLR signaling via this Src-mediated phosphorylation could be tested by creating double KO cell lines in which the additional KO of Src should reverse the phenotype of the UBASH3B-KO (Figure 28).

Another interesting function of UBASH3B in the context of antiviral signaling is its influence on the interferon signaling. It was found, that the high level of IFN- α in B cells of patients with Systemic lupus erythematoses (SLE) correlated with increased level of UBASH3B. The authors could show that overexpression of UBASH3B in human B cells leads to increased expression of ISGs like OAS1, IFIT1 and IFI44 after IFN- α treatment. This effect also resulted from the interaction of UBASH3B with c-Cbl. They showed that c-Cbl inhibited the UBASH3B promoted STAT1 phosphorylation and concluded that UBASH3B enhances IFN- α -induced JAK-STAT signaling via c-Cbl (172). This finding could explain our observation that at later time points (9 and 12 h) after 3p-RNA stimulation the KO cells showed no enhanced signaling anymore as shown for the expression of IFN- β and IL-6 (Figure 19) as well as for the aggregation of MAVS and activation of TBK1, IRF3 and I κ B α (Figure 20). The RLR-dependent IFN induction starts approximately 6 h after signal activation leading to an autocrine mediated induction of JAK/STAT signaling. The positive regulatory function of UBASH3B in this interferon loop-pathway could then compensate for its opposite role in MAVS signaling.

Although most of the results fits to the hypothesis that UBASH3B directly or indirectly acts on MAVS to delay and reduce its activation, the main discrepancy is the missing reconstitution of the wt phenotype after UBASH3B overexpression in the 1205 Lu cells. In the experiment with transient overexpression of UBASH3B (see Figure 23), the missing effect could result from the low transfection efficiency. The 1205 Lu cells just reach a transfection rate of 20%, that might be too small to see the regulatory effect of UBASH3B. Instead, using HEK293T cells we could detect the inhibitory effect of UBASH3B, maybe because the transfection efficiency is much higher in these cells. Furthermore, we analyzed the data from RNA sequencing of the 1205 Lu cells for different splicing variants. There is just one isoform of UBASH3B expressed in these cells, hence overexpression of the wrong variant could not be the reason for the failed rescue.

Another explanation for the lacking rescue could be, that the insertion via exogenous DNA does not mimic the physiological amount and pattern of expression in one cell. To control for that, we generated a stable dox-inducible cell line with every cell expressing UBASH3B under control of a dox-inducible promoter. Although, we induced different amounts of UBASH3B and checked the expression pattern by confocal microscopy, showing a cytoplasmic distribution as for the endogenous protein (data not shown), we could not rescue the phenotype. The most likely explanation for this unexpected result comes from a recently published paper: By searching for small molecule inhibitors for UBASH3B, Zhou et al. found that doxycycline was one of the most effective compound to inhibit phosphatase activity of UBASH3B (173). The half maximal inhibitory concentration (IC_{50}) is 4.1 μ M (1.8 ng/ml), which is much less than dosages we used (10 and 100 ng/ml) for UBASH3B induction. Since the effect of UBASH3B on MAVS might be dependent on its phosphatase function, it is likely that the inhibition via doxycycline caused the lack of reconstitution. Thus, it is necessary to use another system for induction of UBASH3B expression to show that the knockout phenotype is reversible.

However, the dose dependent overexpression revealed another interesting phenomenon: Although we could not detect any effect on the immune signaling, UBASH3B mRNA, even though it was exogenous introduced with the help of the pLVX vector using the dox-inducible promoter, was down-regulated upon 3p-RNA stimulation. This indicates a post-transcriptional regulation of the mRNA by a factor that is induced upon RLR signaling activation. It could be that an ISG that is induced upon 3p-RNA stimulation and drives mRNA degradation of UBASH3B or that a microRNA is induced which can destabilize the mRNA. It is further possible that the promoter activity is influenced, here most likely by the doxycycline concentration. Since the unstimulated condition was incubated with doxycycline as long as the sample stimulated for 12 h with 3p-RNA, we can rule out, that the reduction of doxycycline in the medium over time caused the effect.

By analyzing TCGA (The cancer genome atlas) data, a recent study found that the expression level of UBASH3B is negatively correlated with its methylation state (174). This modification could also explain our observation although nothing is known about the regulation of this methylation. The authors speculate that the Estrogen receptor 1 (ESR1) could be a regulator, since the UBASH3B mRNA level inversely correlated with ESR1 protein level. The lack of Estrogen receptor together with increased UBASH3B level is one hallmark of triple-negative breast cancer (TNBC). It was found that UBASH3B has a direct oncogenic function by enhancing the EGFR signaling leading to uncontrolled cell proliferation (175).

The finding, that RLR signaling activation can decrease UBASH3B level, leads to the hypothesis that 3p-RNA treatment could be an efficient therapy against TNBC. On the one hand the RLR activation could induce tumor-specific apoptosis and subsequently adaptive

immunity to fight the cancer as it was already shown for several tumor entities. On the other hand, the additional decrease of UBASH3B could reduce its tumorigenic character.

Moreover, UBASH3B is an interesting therapeutic target to treat different infectious diseases. In mice lacking both homologues UBASH3A and UBASH3B it was found that they are profoundly more resistant to fungal infection with *Candida albicans* as well as to bacterial infection with *Francisella tularensis* (176,177). The better survival corresponds to stronger induction of different proinflammatory cytokines at early time points after infection (e.g. IL-4, IL-10, IL-13 in the spleen after *F. tularensis* infection and IP-10 in the kidney after *C. albicans* infection). The authors hypothesize that UBASH3A and UBASH3B negatively control innate immune signaling pathways. In their model UBASH 'tips the balance of effector activation in such a way as to favor improved host cell responses and enhanced microbial clearance' (176). This is exactly what we also observed in the UBASH3B single KO in human cell lines after mimicking a viral infection with 3p-RNA with MAVS being this effector. To figure out, if viral infection in the double-KO mice also shows a phenotype, we initially stimulated BMDMs with 3p-RNA. We observed a slight effect with increased IP-10 and IFN- β induction in the KO cells when using small amounts of 3p-RNA (100 ng/ml). With higher concentration (500 ng/ml) these differences between KO and wt were less pronounced (see Figure 27). Thus, BMDMs showed the expected phenotype, but to a less extent compared to human cells. The study of Parashar et al. indicates that BMDMs might not be the best cell population to study the function of UBASH3B. They also used these cells for *F. tularensis* infection ex vivo and could not find any differences in bacterial clearance but found that monocytes could restrict the growth (176). Therefore, it would be interesting to test also this cell population with 3p-RNA stimulation and to infect UBASH3A/3B double- and single KO mice with a virus that signals via MAVS, such as VSV. That would help to find out, if UBASH3B has a physiological role during virus infection.

All in all, with loss-of-function experiments and overexpression we were able to show, that UBASH3B has a negative regulatory function on the RLR pathway. From the data we assume that UBASH3B influences the signaling on the level of MAVS. To elucidate the mechanism, however, further experiments are needed to, e.g. clarify if MAVS is targeted directly or if there are any bridging protein involved. Since the phenotype of UBASH3B-KO shows that it has a modulatory influence mainly at the onset of signaling, it needs to be figured out if this function is relevant in a physiological context, like a virus infection in vivo.

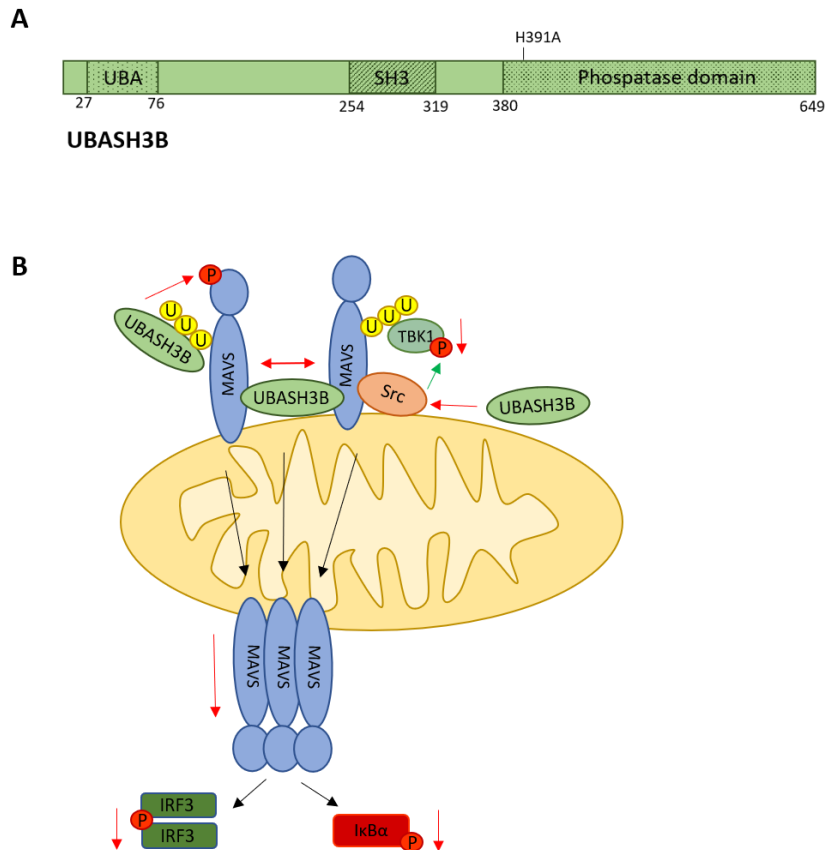


Figure 28: Possible mechanism how UBASH3B downregulates RLR signaling. (A) Schematic representation of UBASH3B with its functional domains: the ubiquitin-binding domain (UBA), the SH3 and phosphatase domain, as well as the point mutation that was used to diminish the phosphatase activity. (B) Downregulation of MAVS activity could be caused by direct binding of ubiquitin chains of MAVS thereby dephosphorylating MAVS tyrosine residues, by modification of other MAVS interactors causing the inhibition of MAVS aggregation or via the interaction of UBASH3B with Src that would lead to less TBK1 phosphorylation. Finally, UBASH3B leads to formation of less MAVS aggregates and subsequently less activation of IRF3 and I κ B α . For further description see 4.7.

5 Summary

The induction of an adequate innate immune response after viral infection is crucial to constrain viral replication and to activate the adaptive immune system. RIG-I-like receptors (RLRs) detect viral RNA patterns in the cytosol and are crucial for detection of many RNA viruses. RLR ligands are under development as vaccine adjuvants and as anti-tumor agents. Conversely, gain-of-function mutations in the RLR pathway have been identified as the cause of inborn autoinflammatory syndromes.

The detected RNA pattern and many important players of the RLR signaling pathway have been already defined. However, the actual RNA species that trigger RIG-I in the natural course of infection are less characterized and it is still incompletely understood how this signaling is orchestrated and downmodulated to induce a balanced immune response.

We therefore set out to identify the ligands of RIG-I during infection with vesicular stomatitis virus (VSV) as a model virus of the *Mononegavirales*, that are known to be mainly detected by RIG-I. In a former project of our group, we had been able to show that one defined copy-back DI genome associated with RIG-I. After analysis of RIG-I bound RNA by deep sequencing the precise sequence of this DI genome was identified and showed perfect characteristics of a RIG-I ligand with a short double-stranded part and a 5'triphosphate moiety.

In the work presented here we could extend this data and show that the identified DI genome replicates in the course of infection. Through serial dilution of the viral stock, the DI genomes were diluted out allowing the comparison of DI-high versus DI-low viral stocks. This revealed that DI-high stocks were much more potent in inducing an interferon (IFN) response. An RNA fragmentation assay further showed that the RNA with the highest immunostimulatory capacity in our DI-high stocks has a size that matches the size of the identified DI genome (4719 bp), confirming that the binding of the DI genome to RIG-I triggers the antiviral signaling. In the absence of DI genomes, the RNA fragmentation assay and RIG-I IP indicated that leader/N readthrough sequences and - to a smaller extent - the VSV full-length genome induces the immune response via RIG-I.

In the second part the thesis focused on MAVS, the downstream adapter molecule of RIG-I that is crucial for signal transduction. It is a central signaling hub in this pathway since the signaling of RIG-I and MDA5 culminates here and bifurcates downstream into different signaling branches like the IFN- or NFκB pathway or autophagy. We aimed at a better understanding of the regulatory mechanism by searching for novel MAVS interaction partners.

Using the method of proximity-based APEX-mediated live cell tagging we were able to show that APEX when fused to the cytosolic part of MAVS is highly suitable to identify MAVS interaction partners. We identified 31 proteins in the proximity of MAVS 60 min after RLR

activation with triphosphate RNA (3p-RNA) that were significantly enriched in comparison to the unstimulated control. Within this data set we found eleven proteins that are well described as part of the MAVS signaling platform, such as the crucial downstream molecules TBK1, TRAF2, TRAF6 and the IKK kinases IKK α , β , γ (NEMO). Further six of the identified proteins are indirectly linked to MAVS, e.g. through interaction with described binding partners of MAVS, such as OPTN or TNIP1.

UBASH3B, one of the proteins that were enriched 60 min after stimulation with 3p-RNA but had no known link to MAVS so far was chosen to be analyzed in more detail, because it was the most significantly enriched protein besides known interactors and an initial knockout screen indicated a MAVS-specific phenotype.

Using two different sgRNAs and two different human cell lines (1205 Lu melanoma cells, immortalized human fibroblasts) with up to five single cell clones we could show that the loss of UBASH3B caused an enhanced immune response upon 3p-RNA stimulation measured by cytokine induction (e.g. IP-10, IL-6) especially at early time points after signal activation. The analysis of MAVS activation via its aggregate formation further showed earlier and more MAVS aggregation in the absence of UBASH3B, that was in line with earlier activation of TBK1, IRF3 and I κ B α . These data indicate that UBASH3B is a negative regulator by inhibiting the formation of MAVS aggregates early after activation.

All in all, the present thesis contributes to a better understanding of the antiviral RLR pathway by describing natural RIG-I ligands and by identification of novel MAVS interaction partners that in proof-of-concept studies indeed seem to play a role in the RLR pathway.

6 Zusammenfassung

Das Auslösen einer angemessenen Antwort des angeborenen Immunsystems nach einer Virusinfektion ist entscheidend, um die Virusreplikation einzuschränken und das adaptive Immunsystem zu aktivieren. RIG-I-like Rezeptoren (RLRs) erkennen virale RNA-Muster im Zytosol und sind für die Erkennung vieler RNA-Viren von entscheidender Bedeutung. RLR-Liganden sind als Adjuvantien für Impfstoffe und als Tumorthherapie in der Entwicklung. Umgekehrt wurden *Gain-of-function*-Mutationen in RLR-Proteinen als Ursache für angeborene auto-inflammatorische Syndrome identifiziert.

Obwohl die erforderlichen RNA Eigenschaften, um den Rezeptor zu aktivieren und viele wichtige Moleküle des RLR-Signalwegs bereits definiert sind, sind die konkreten RNA-Spezies, die RIG-I im natürlichen Verlauf einer Infektion aktivieren, weniger charakterisiert. Weiterhin ist noch unvollständig verstanden, wie dieser Signalweg reguliert wird, um eine adäquate Immunantwort auszulösen und überschießende Reaktionen zu vermeiden.

Ziel dieser Arbeit war es deshalb, die Liganden von RIG-I während der Infektion mit dem Vesikulären Stomatitis-Virus (VSV) als Modellvirus der *Mononegavirales* zu identifizieren, von dem bekannt ist, dass er hauptsächlich durch RIG-I erkannt wird. In einem früheren Projekt unserer Gruppe hatten wir zeigen können, dass ein definiertes *Copy-back* DI-Genom von VSV mit RIG-I assoziiert. Nach der Analyse von RIG-I-gebundener RNA mittels *Deep Sequencing* wurde die genaue Sequenz dieses DI-Genoms identifiziert und zeigte perfekte Eigenschaften eines RIG-I-Liganden mit einem kurzen doppelsträngigen Teil und einer 5'-Triphosphat-Gruppe.

In der hier vorgestellten Arbeit konnten wir diese Daten ergänzen und zeigen, dass sich das identifizierte DI-Genom während der Infektion repliziert. Durch serielle Verdünnung des Virusstamms wurden die DI-Genome heraus verdünnt, was den Vergleich von DI-reichen mit DI-armen-Virusstämmen ermöglichte. Dies zeigte, dass DI-reiche Stocks eine viel stärkere Interferonantwort auslösten. Ein RNA-Fragmentierungs-Assay zeigte weiterhin, dass die RNA mit der höchsten immunstimulierenden Kapazität in unseren DI-reichen Stocks eine Größe aufweist, die der Größe des identifizierten DI-Genoms entspricht (4719 bp). Dies bestätigte, dass die Bindung des DI-Genoms an RIG-I den antiviralen Signalweg auslöst. In Abwesenheit von DI-Genomen zeigten der RNA-Fragmentierungs-Assay und die RIG-I-Co-Immunopräzipitation, dass auch Leader/N-Sequenzen und zu einem kleineren Teil das VSV-Volllängen-Genom die Immunantwort über RIG-I induzieren.

Im zweiten Teil konzentrierte sich die Arbeit auf MAVS, welches das stromabwärts gelegene Adaptermolekül von RIG-I ist und für die Signaltransduktion eine entscheidende Bedeutung einnimmt. Es bildet eine zentrale Schaltstelle in diesem Signalweg, bei der die Signale von RIG-I und MDA5 zusammenlaufen und stromabwärts in verschiedene Richtungen, wie den

IFN- oder NF κ B-Weg oder die Autophagie weitergegeben werden. Um die Mechanismen der Regulation an dieser Schaltstelle besser zu verstehen, war es das Ziel weitere MAVS-Interaktionspartner zu identifizieren.

Mit der Methode des APEX-vermittelten Markierens benachbarter Proteine in lebenden Zellen konnten wir zeigen, dass APEX, wenn es mit dem zytosolischen Teil von MAVS fusioniert ist, sehr gut geeignet ist, um MAVS-Interaktionspartner zu identifizieren. Wir konnten 60 Minuten nach der RLR-Signalaktivierung mittels Triphosphat-RNA (3p-RNA) 31 Proteine in der Nähe von MAVS identifizieren, die im Vergleich zur unstimulierten Kontrolle signifikant angereichert waren. In diesem Datensatz fanden wir elf Proteine, die als Teil der MAVS-Signalplattform bereits gut beschrieben sind, wie die stromabwärts gelegenen Moleküle TBK1, TRAF2, TRAF6 und die IKK-Kinasen IKK α , β , γ (NEMO). Weitere sechs der identifizierten Proteine sind indirekt in der Literatur als mit MAVS verbunden beschrieben, d.h. durch Interaktion mit beschriebenen Bindungspartnern von MAVS, wie OPTN oder TNIP1.

UBASH3B, eines der Proteine, die 60 Minuten nach der Stimulation mit 3p-RNA angereichert waren und bisher nicht als Interaktoren von MAVS in der Literatur beschrieben waren, wurde zur detaillierteren Analyse ausgewählt, da es neben den bekannten Interaktoren das Protein mit der signifikantesten Anreicherung war. Weiterhin wiesen erste Versuche mit Knockout-Zellen auf einen MAVS-spezifischen Phänotyp hin.

Unter Verwendung zweier verschiedener sgRNAs und zweier humaner Zelllinien (1205 Lu-Melanomzellen und immortalisierte humane Fibroblasten) mit jeweils bis zu fünf verschiedenen Einzel-Zellklonen konnten wir zeigen, dass der Verlust von UBASH3B nach 3p-RNA-Stimulation eine verstärkte Immunantwort hervorrief, die anhand von Zytokinbildung (z.B. IP-10, IL-6) gemessen wurde. Dieser Effekt war insbesondere zu frühen Zeitpunkten nach der Signalaktivierung nachweisbar. Die Analyse der MAVS-Aktivierung über ihre Aggregatbildung zeigte weiterhin eine frühere und stärkere MAVS-Aggregation bei Fehlen von UBASH3B, die mit der früheren Aktivierung von TBK1, IRF3 und I κ B α einherging. Anhand dieser Daten vermuten wir, dass UBASH3B ein Negativ-Regulator des RLR-Signalweges ist, indem er die Bildung von MAVS-Aggregaten früh nach der Signalaktivierung hemmt. Es sind jedoch weitere Studien erforderlich, um den genauen Mechanismus der Signalmodulation aufzuklären.

Zusammengefasst trägt die vorliegende Arbeit zu einem besseren Verständnis des antiviralen RLR-Signalwegs bei, indem natürliche RIG-I-Liganden beschrieben und neue MAVS-Interaktionspartner identifiziert wurden, von denen gezeigt werden konnte, dass sie tatsächlich im RLR-Signalweg funktionell eine Rolle spielen.

7 References

1. Janeway CA. Approaching the asymptote?: Evolution and revolution in immunology. *Cold Spring Harbor Symposia on Quantitative Biology*. 1989;54:1–13.
2. Brubaker SW, Bonham KS, Zanoni I, Kagan JC. Innate immune pattern recognition: a cell biological perspective. *Annu Rev Immunol*. 2015;33:257–90.
3. Lester SN, Li K. Toll-like receptors in antiviral innate immunity. *J Mol Biol*. 2014;426:1246–64.
4. Takeuchi O, Akira S. Pattern recognition receptors and inflammation. *Cell*. 2010;140:805–20.
5. Chen G, Shaw MH, Kim Y-G, Nuñez G. NOD-like receptors: role in innate immunity and inflammatory disease. *Annu Rev Pathol*. 2009;4:365–98.
6. Geijtenbeek TBH, Gringhuis SI. Signalling through C-type lectin receptors: shaping immune responses. *Nat Rev Immunol*. 2009;9:465–79.
7. Brunette RL, Young JM, Whitley DG, Brodsky IE, Malik HS, Stetson DB. Extensive evolutionary and functional diversity among mammalian AIM2-like receptors. *J Exp Med*. 2012;209:1969–83.
8. Gray EE, Winship D, Snyder JM, Child SJ, Geballe AP, Stetson DB. The AIM2-like receptors are dispensable for the interferon response to intracellular DNA. *Immunity*. 2016;45:255–66.
9. Sun L, Wu J, Du F, Chen X, Chen ZJ. Cyclic GMP-AMP synthase is a cytosolic DNA sensor that activates the type I interferon pathway. *Science*. 2013;339:786–91.
10. Kawai T, Akira S. Toll-like receptor and RIG-I-like receptor signaling. *Ann N Y Acad Sci*. 2008;1143:1–20.
11. Yoneyama M, Kikuchi M, Natsukawa T, Shinobu N, Imaizumi T, Miyagishi M, Taira K, Akira S, Fujita T. The RNA helicase RIG-I has an essential function in double-stranded RNA-induced innate antiviral responses. *Nat Immunol*. 2004;5:730–7.
12. Fujita T, Onoguchi K, Onomoto K, Hirai R, Yoneyama M. Triggering antiviral response by RIG-I-related RNA helicases. *Biochimie*. 2007;89:754–60.
13. Hornung V, Ellegast J, Kim S, Brzózka K, Jung A, Kato H, Poeck H, Akira S, Conzelmann KK, Schlee M, Endres S, Hartmann S. 5'-Triphosphate RNA is the ligand for RIG-I. *Science*. 2006;314:994–7.

14. Schmidt A, Schwerdt T, Hamm W, Hellmuth JC, Cui S, Wenzel M, Hoffmann FS, Michallet MC, Besch R, Hopfner KP, Endres S, Rothenfusser S. 5-triphosphate RNA requires base-paired structures. *Proc Natl Acad Sci U S A*. 2009;106:12067–72.
15. Goubau D, Schlee M, Deddouche S, Pruijssers AJ, Zillinger T, Goldeck M, Schuberth C, Van der Veen, Annemarie G, Fujimura T, Rehwinkel J, Iskarpatyoti JA, Barchet W, Ludwig J, Dermody TS, Hartmann G, Reis e Sousa C. Antiviral immunity via RIG-I-mediated recognition of RNA bearing 5'-diphosphates. *Nature*. 2014;514:273-275
16. Pichlmair A, Schulz O, Tan CP, Rehwinkel J, Kato H, Takeuchi O, Akira S, Way M, Schiavo G, Reis e Sousa C. Activation of MDA5 Requires Higher-Order RNA Structures. *J Virol*. 2009;83:10761–9.
17. Züst R, Cervantes-Barragan L, Habjan M, Maier R, Neuman BW, Ziebuhr J, Szretter KJ, Baker SC, Barchet W, Diamond MS, Siddell SG, Ludewig B, Thiel V. Ribose 2'-O-methylation provides a molecular signature for the distinction of self and non-self mRNA dependent on the RNA sensor Mda5. *Nat Immunol*. 2011;12:137–43.
18. Komuro A, Horvath CM. RNA- and Virus-Independent Inhibition of Antiviral Signaling by RNA Helicase LGP2. *J Virol*. 2006;80:12332–42.
19. Rothenfusser S, Goutagny N, DiPerna G, Gong M, Monks BG, Schoenemeyer A, Yamamoto M, Akira S, Fitzgerald KA. The RNA helicase Lgp2 inhibits TLR-independent sensing of viral replication by retinoic acid-inducible gene-I. *J Immunol* 2005;175:5260–8.
20. Bruns AM, Leser GP, Lamb RA, Horvath CM. The innate immune sensor LGP2 activates antiviral signaling by regulating MDA5-RNA interaction and filament Assembly. *Mol Cell*. 2014;55:771-81.
21. Bruns AM, Pollpeter D, Hadizadeh N, Myong S, Marko JF, Horvath CM. ATP hydrolysis enhances RNA recognition and antiviral signal transduction by the innate immune sensor, laboratory of genetics and physiology 2 (LGP2). *J Biol Chem*. 2013;288:938–46.
22. Satoh T, Kato H, Kumagai Y, Yoneyama M, Sato S, Matsushita K, Tsujimura T, Fujita T, Akira S, Takeuchi O. LGP2 is a positive regulator of RIG-I- and MDA5-mediated antiviral responses. *Proc Natl Acad Sci U S A*. 2010;107:1512–7.
23. Kato H, Takeuchi O, Sato S, Yoneyama M, Yamamoto M, Matsui K, Uematsu S, Jung A, Kawai T, Ishii KJ, Yamaguchi O, Otsu K, Tsujimura T, Koh C-S, Reis e Sousa, Caetano, Matsuura Y, Fujita T, Akira S. Differential roles of MDA5 and RIG-I helicases in the recognition of RNA viruses. *Nature*. 2006;441:101–5.

24. Rehwinkel J, Tan CP, Goubau D, Schulz O, Pichlmair A, Bier K, Robb N, Vreede F, Barclay W, Fodor E, Reis e Sousa, Caetano. RIG-I detects viral genomic RNA during negative-strand RNA virus infection. *Cell*. 2010;140:397–408.
25. Schlee M, Roth A, Hornung V, Hagmann CA, Wimmenauer V, Barchet W, Coch C, Janke M, Mihailovic A, Wardle G, Juranek S, Kato H, Kawai T, Poeck H, Fitzgerald KA, Takeuchi O, Akira S, Tuschl T, Latz E, Ludwig J, Hartmann G. Recognition of 5' triphosphate by RIG-I helicase requires short blunt double-stranded RNA as contained in panhandle of negative-strand virus. *Immunity*. 2009;31:25–34.
26. Loo Y-M, Fornek J, Crochet N, Bajwa G, Perwitasari O, Martinez-Sobrido L, Akira S, Gill MA, García-Sastre A, Katze MG, Gale M. Distinct RIG-I and MDA5 signaling by RNA viruses in innate immunity. *J Virol*. 2008;82:335–45.
27. Gitlin L, Barchet W, Gilfillan S, Cella M, Beutler B, Flavell RA, Diamond MS, Colonna M. Essential role of mda-5 in type I IFN responses to polyriboinosinic:polyribocytidylic acid and encephalomyocarditis picornavirus. *Proc Natl Acad Sci U S A*. 2006;103:8459–64.
28. Ikegame S, Takeda M, Ohno S, Nakatsu Y, Nakanishi Y, Yanagi Y. Both RIG-I and MDA5 RNA helicases contribute to the induction of alpha/beta interferon in measles virus-infected human cells. *J Virol*. 2010;84:372–9.
29. Yount JS, Gitlin L, Moran TM, Lopez CB. MDA5 Participates in the Detection of Paramyxovirus Infection and Is Essential for the Early Activation of Dendritic Cells in Response to Sendai Virus Defective Interfering Particles. *J Immunol*. 2008;180:4910–8.
30. Ablasser A, Bauernfeind F, Hartmann G, Latz E, Fitzgerald KA, Hornung V. RIG-I-dependent sensing of poly(dA:dT) through the induction of an RNA polymerase III-transcribed RNA intermediate. *Nat Immunol*. 2009;10:1065–72.
31. Dixit E, Kagan JC. Intracellular pathogen detection by RIG-I-like receptors. *Adv Immunol*. 2013;117:99–125.
32. Habjan M, Andersson I, Klingström J, Schümann M, Martin A, Zimmermann P, Wagner V, Pichlmair A, Schneider U, Mühlberger E, Mirazimi A, Weber F. Processing of genome 5' termini as a strategy of negative-strand RNA viruses to avoid RIG-I-dependent interferon induction. *PLoS ONE*. 2008;3:e2032.
33. Baum A, Sachidanandam R, Garcia-Sastre A. Preference of RIG-I for short viral RNA molecules in infected cells revealed by next-generation sequencing. *Proc Natl Acad Sci U S A*. 2010;107:16303–8.

34. Plumet S, Herschke F, Bourhis J-M, Valentin H, Longhi S, Gerlier D. Cytosolic 5'-triphosphate ended viral leader transcript of measles virus as activator of the RIG I-mediated interferon response. *PLoS ONE*. 2007;2:e279.
35. Killip MJ, Young DF, Gatherer D, Ross CS, Short, J. A. L., Davison AJ, Goodbourn S, Randall RE. Deep sequencing analysis of defective genomes of parainfluenza virus 5 and their role in interferon induction. *J Virol*. 2013;87:4798–807.
36. Weber M, Weber F. RIG-I-like receptors and negative-strand RNA viruses: RLRly bird catches some worms. *Cytokine Growth Factor Rev*. 2014;25:621–8.
37. Abraham G BAK. Sequential transcription of the genes of vesicular stomatitis virus. *Proc Natl Acad Sci U S A*. 1976;73:1504–8.
38. Ball LA. Transcriptional mapping of vesicular stomatitis virus in vivo. *J Virol*. 1977;21:411–4.
39. Gerlier D, Lyles DS. Interplay between Innate Immunity and Negative-Strand RNA Viruses: towards a Rational Model. *Microbiol Mol Biol Rev*. 2011;75:468–90.
40. Barr JN, Whelan SP, Wertz GW. Transcriptional control of the RNA-dependent RNA polymerase of vesicular stomatitis virus. *Biochimica et Biophysica Acta (BBA) - Gene Structure and Expression*. 2002;1577:337–53.
41. Blumberg BM, Leppert M, Kolakofsky D. Interaction of VSV leader RNA and nucleocapsid protein may control VSV genome replication. *Cell*. 1981;23:837–45.
42. Lazzarini RA, Keene JD, Schubert M. The origins of defective interfering particles of the negative-strand RNA viruses. *Cell*. 1981;26:145-54.
43. Pathak KB, Nagy PD. Defective interfering RNAs: Foes of viruses and friends of virologists. *Viruses*. 2009;1:895–919.
44. Henle W HG. Interference of inactive virus with the propagation of virus of influenza. *Science*. 1943;98:87-9.
45. Magnus P. Propagation of the PR8 strain of influenza A virus in chick embryos. II. The formation of incomplete virus following inoculation of large doses of seed virus. *Acta Pathol Microbiol Scand*. 1951;278–93.
46. Huang AS. Defective Interfering Viruses. *Annu Rev Microbiol*. 1973;27:101-17.
47. Marriott AC, Dimmock NJ. Defective interfering viruses and their potential as antiviral agents. *Rev Med Virol*. 2010;20:51–62.
48. Perrault J. Origin and replication of defective interfering particles. *Curr Top Microbiol Immunol*. 1981;93:151-207.

49. Marcus PI SM. Defective interfering particles with covalently linked [+/-]RNA induce interferon. *Nature*. 1977;266:815–9.
50. López CB. Defective viral genomes: critical danger signals of viral infections. *J Virol*. 2014;88:8720–3.
51. Li D, Lott WB, Lowry K, Jones A, Thu HM, Aaskov J, Coffey LL. Defective interfering viral particles in acute Dengue infections. *PLoS ONE*. 2011;6:e19447.
52. Saira K, Lin X, DePasse JV, Halpin R, Twaddle A, Stockwell T, Angus B, Cozzi-Lepri A, Delfino M, Dugan V, Dwyer DE, Freiberg M, Horban A, Losso M, Lynfield R, Wentworth DN, Holmes EC, Davey R, Wentworth DE, Ghedin E. Sequence analysis of In vivo defective interfering-like RNA of influenza A H1N1 pandemic virus. *J Virol*. 2013;87:8064–74.
53. Nüesch JP, de Chastonay J, Siegl G. Detection of defective genomes in hepatitis A virus particles present in clinical specimens. *J Gen Virol*. 1989;70:3475–80.
54. Yeh CT, Lu SC, Chu CM, Liaw YF. Molecular cloning of a defective hepatitis C virus genome from the ascitic fluid of a patient with hepatocellular carcinoma. *J Gen Virol*. 1997;78:2761–70.
55. Schlee M, Hartmann G. The chase for the RIG-I ligand--recent advances. *Mol Ther*. 2010;18:1254–62.
56. Kato H, Fujita T. RIG-I-like receptors and autoimmune diseases. *Curr Opin Immunol*. 2015;37:40–5.
57. Kowalinski E, Lunardi T, McCarthy AA, Louber J, Brunel J, Grigorov B, Gerlier D, Cusack S. Structural basis for the activation of innate immune pattern-recognition receptor RIG-I by viral RNA. *Cell*. 2011;147:423–35.
58. Saito T, Hirai R, Loo Y-M, Owen D, Johnson CL, Sinha SC, Akira S, Fujita T, Gale M. Regulation of innate antiviral defenses through a shared repressor domain in RIG-I and LGP2. *Proc Natl Acad Sci U S A*. 2007;104:582–7.
59. Maharaj NP, Wies E, Stoll A, Gack MU. Conventional protein kinase C- α (PKC- α) and PKC- β negatively regulate RIG-I antiviral signal transduction. *J Virol*. 2012;86:1358–71.
60. Sun Z, Ren H, Liu Y, Teeling JL, Gu J. Phosphorylation of RIG-I by casein kinase II inhibits its antiviral response. *J Virol*. 2011;85:1036–47.

61. Wies E, Wang MK, Maharaj NP, Chen K, Zhou S, Finberg RW, Gack MU. Dephosphorylation of the RNA sensors RIG-I and MDA5 by the phosphatase PP1 is essential for innate immune signaling. *Immunity*. 2013;38:437–49.
62. Gack MU, Shin YC, Joo C-H, Urano T, Liang C, Sun L, Takeuchi O, Akira S, Chen Z, Inoue S, Jung JU. TRIM25 RING-finger E3 ubiquitin ligase is essential for RIG-I-mediated antiviral activity. *Nature*. 2007;446:916–20.
63. Liu HM, Loo Y-M, Horner SM, Zornetzer GA, Katze MG, Gale M. The mitochondrial targeting chaperone 14-3-3 ϵ regulates a RIG-I translocon that mediates membrane association and innate antiviral immunity. *Cell Host Microbe*. 2012;11:528–37.
64. Oshiumi H, Matsumoto M, Hatakeyama S, Seya T. Riplet/RNF135, a RING finger protein, ubiquitinates RIG-I to promote interferon-beta induction during the early phase of viral infection. *J Biol Chem*. 2009;284:807–17.
65. Kuniyoshi K, Takeuchi O, Pandey S, Satoh T, Iwasaki H, Akira S, Kawai T. Pivotal role of RNA-binding E3 ubiquitin ligase MEX3C in RIG-I-mediated antiviral innate immunity. *Proc Natl Acad Sci U S A*. 2014;111:5646–51.
66. Wang W, Jiang M, Liu S, Zhang S, Liu W, Ma Y, Zhang L, Zhang J, Cao X. RNF122 suppresses antiviral type I interferon production by targeting RIG-I CARDs to mediate RIG-I degradation. *Proc Natl Acad Sci U S A*. 2016;113:9581–6.
67. Arimoto K-i, Takahashi H, Hishiki T, Konishi H, Fujita T, Shimotohno K. Negative regulation of the RIG-I signaling by the ubiquitin ligase RNF125. *Proc Natl Acad Sci U S A*. 2007;104:7500–5.
68. Friedman CS, O'Donnell MA, Legarda-Addison D, Ng A, Cárdenas WB, Yount JS, Moran TM, Basler CF, Komuro A, Horvath CM, Xavier R, Ting AT. The tumour suppressor CYLD is a negative regulator of RIG-I-mediated antiviral response. *EMBO reports*. 2008;9:930–6.
69. Cui J, Song Y, Li Y, Zhu Q, Tan P, Qin Y, Wang HY, Wang R-F. USP3 inhibits type I interferon signaling by deubiquitinating RIG-I-like receptors. *Cell Res*. 2014;24:400–16.
70. Liu Y, Olganier D, Lin R. Host and viral modulation of RIG-I-mediated antiviral immunity. *Front Immunol*. 2016;7:662.
71. Kawai T, Takahashi K, Sato S, Coban C, Kumar H, Kato H, Ishii KJ, Takeuchi O, Akira S. IPS-1, an adaptor triggering RIG-I- and Mda5-mediated type I interferon induction. *Nat Immunol*. 2005;6:981–8.

72. Meylan E, Curran J, Hofmann K, Moradpour D, Binder M, Bartenschlager R, Tschopp J. Cardif is an adaptor protein in the RIG-I antiviral pathway and is targeted by hepatitis C virus. *Nature*. 2005;437:1167–72.
73. Seth RB, Sun L, Ea C-K, Chen ZJ. Identification and characterization of MAVS, a mitochondrial antiviral signaling protein that activates NF- κ B and IRF3. *Cell*. 2005;122:669–82.
74. Xu L-G, Wang Y-Y, Han K-J, Li L-Y, Zhai Z, Shu H-B. VISA is an adapter protein required for virus-triggered IFN-beta signaling. *Molecular Cell*. 2005;19:727–40.
75. Dixit E, Boulant S, Zhang Y, Lee AS, Odendall C, Shum B, Hacohen N, Chen ZJ, Whelan SP, Fransen M, Nibert ML, Superti-Furga G, Kagan JC. Peroxisomes are signaling platforms for antiviral innate immunity. *Cell*. 2010;141:668–81.
76. Horner SM, Liu HM, Park HS, Briley J, Gale M. Mitochondrial-associated endoplasmic reticulum membranes (MAM) form innate immune synapses and are targeted by hepatitis C virus. *Proc Natl Acad Sci U S A*. 2011;108:14590–5.
77. Saha SK, Pietras EM, He JQ, Kang JR, Liu SY, Oganessian G, Shahangian A, Zarnegar B, Shiba TL, Wang Y, Cheng G. Regulation of antiviral responses by a direct and specific interaction between TRAF3 and Cardif. *EMBO J*. 2006;3257–63.
78. Tang ED, Wang C. Y. TRAF5 is a downstream target of MAVS in antiviral innate immune signaling. *PLoS ONE*. 2010;5:e9172.
79. Liu S, Chen J, Cai X, Wu J, Chen X, Wu YT. MAVS recruits multiple ubiquitin E3 ligases to activate antiviral signaling cascades. *Elife*. 2013;2:e00785.
80. Shi Y, Yuan B, Qi N, Zhu W, Su J, Li X, Qi P, Zhang D, Hou F. An autoinhibitory mechanism modulates MAVS activity in antiviral innate immune response. *Nat Comms*. 2015;6:7811.
81. Zhao T, Yang L, Sun Q, Arguello M, Ballard DW, Hiscott J, Lin R. The NEMO adaptor bridges the nuclear factor-kappaB and interferon regulatory factor signaling pathways. *Nat Immunol*. 2007;8:592–600.
82. Fang R, Jiang Q, Zhou X, Wang C, Guan Y, Tao J, Xi J, Feng J-M, Jiang Z. MAVS activates TBK1 and IKK ϵ through TRAFs in NEMO dependent and independent manner. *PLoS Pathog*. 2017;13:e1006720.
83. Liu S, Cai X, Wu J, Cong Q, Chen X, Li T, Du F, Ren J, Wu Y, Grishin N, Chen ZJ. Phosphorylation of innate immune adaptor proteins MAVS, STING, and TRIF induces IRF3 activation. *Science*. 2015;347:aaa2630.

84. Belgnaoui SM, Paz S, Hiscott J. Orchestrating the interferon antiviral response through the mitochondrial antiviral signaling (MAVS) adapter. *Curr Opin Immunol*. 2011;23:564–72.
85. Vitour D, Dabo S, Ahmadi Pour M, Vilasco M, Vidalain P-O, Jacob Y, Mezel-Lemoine M, Paz S, Arguello M, Lin R, Tangy F, Hiscott J, Meurs EF. Polo-like kinase 1 (PLK1) regulates interferon (IFN) induction by MAVS. *J Biol Chem*. 2009;284:21797–809.
86. Yan B-R, Zhou L, Hu M-M, Li M, Lin H, Yang Y, Wang Y-Y, Shu H-B. PKACs attenuate innate antiviral response by phosphorylating VISA and priming it for MARCH5-mediated degradation. *PLoS Pathog*. 2017;13:e1006648.
87. Song T, Wei C, Zheng Z, Xu Y, Cheng X, Yuan Y, Guan K, Zhang Y, Ma Q, Shi W, Zhong H. c-Abl tyrosine kinase interacts with MAVS and regulates innate immune response. *FEBS Lett*. 2010;584:33–8.
88. Wen C, Yan Z, Yang X, Guan K, Xu C, Song T, Zheng Z, Wang W, Wang Y, Zhao M, Zhang Y, Xu T, Dou J, Liu J, Xu Q, He X, Wei C, Zhong H. Identification of tyrosine-9 of MAVS as critical target for inducible phosphorylation that determines activation. *PLoS ONE*. 2012;7:e41687.
89. Xiang W, Zhang Q, Lin X, Wu S, Zhou Y, Meng F, Fan Y, Shen T, Xiao M, Xia Z, Zou J, Feng X-H, Xu P. PPM1A silences cytosolic RNA sensing and antiviral defense through direct dephosphorylation of MAVS and TBK1. *Sci Adv*. 2016;2:e1501889.
90. Liu B, Zhang M, Chu H, Zhang H, Wu H, Song G, Wang P, Zhao K, Hou J, Wang X, Zhang L, Gao C. The ubiquitin E3 ligase TRIM31 promotes aggregation and activation of the signaling adaptor MAVS through Lys63-linked polyubiquitination. *Nat Immunol*. 2017;18:214–24.
91. Castanier C, Zemirli N, Portier A, Garcin D, Bidère N, Vazquez A, Arnoult D. MAVS ubiquitination by the E3 ligase TRIM25 and degradation by the proteasome is involved in type I interferon production after activation of the antiviral RIG-I-like receptors. *BMC Biol*. 2012;10:44.
92. Yoo Y-S, Park Y-Y, Kim J-H, Cho H, Kim S-H, Lee H-S, Kim T-H, Sun Kim Y, Lee Y, Kim C-J, Jung JU, Lee J-S, Cho H. The mitochondrial ubiquitin ligase MARCH5 resolves MAVS aggregates during antiviral signalling. *Nat Commun*. 2015;6:7910.
93. You F, Sun H, Zhou X, Sun W, Liang S, Zhai Z, Jiang Z. PCBP2 mediates degradation of the adaptor MAVS via the HECT ubiquitin ligase AIP4. *Nat Immunol*. 2009;10:1300–8.

94. Allen IC, Moore CB, Schneider M, Lei Y, Davis BK, Scull MA, Gris D, Roney KE, Zimmermann AG, Bowzard JB, Ranjan P, Monroe KM, Pickles RJ, Sambhara S, Ting JP. NLRX1 Protein Attenuates Inflammatory Responses to Infection by Interfering with the RIG-I-MAVS and TRAF6-NF- κ B Signaling Pathways. *Immunity*. 2011;34:854–65.
95. Arnoult D, Soares F, Tattoli I, Castanier C, Philpott DJ, Girardin SE. An N-terminal addressing sequence targets NLRX1 to the mitochondrial matrix. *J Cell Sci*. 2009;122:3161–8.
96. Liu X-Y, Wei B, Shi H-X, Shan Y-F, Wang C. Tom70 mediates activation of interferon regulatory factor 3 on mitochondria. *Cell Res*. 2010;20:994–1011.
97. Yasukawa K, Oshiumi H, Takeda M, Ishihara N, Yanagi Y, Seya T, Kawabata S, Koshiba T. Mitofusin 2 inhibits mitochondrial antiviral signaling. *Sci Signal*. 2009;2:ra47.
98. Castanier C, Garcin D, Vazquez A, Arnoult D. Mitochondrial dynamics regulate the RIG-I-like receptor antiviral pathway. *EMBO Rep*. 2009;11:133–8.
99. Koshiba T, Yasukawa K, Yanagi Y, Kawabata S. Mitochondrial membrane potential is required for MAVS-mediated antiviral signaling. *Sci Signal*. 2011;4:ra7.
100. Tal MC, Sasai M, Lee HK, Yordy B, Shadel GS, Iwasaki A. Absence of autophagy results in reactive oxygen species-dependent amplification of RLR signaling. *Proc Natl Acad Sci U S A*. 2009;106:2770–5.
101. Soucy-Faulkner A, Mukawera E, Fink K, Martel A, Jouan L, Nzengue Y, Lamarre D, Vande Velde C, Grandvaux N. Requirement of NOX2 and reactive oxygen species for efficient RIG-I-mediated antiviral response through regulation of MAVS expression. *PLoS Pathog*. 2010;6:e1000930.
102. Zhao Y, Sun X, Nie X, Sun L, Tang T-s, Chen D, Sun Q, Iwasaki A. COX5B Regulates MAVS-mediated Antiviral Signaling through Interaction with ATG5 and Repressing ROS Production. *PLoS Pathog*. 2012;8:e1003086.
103. Sun X, Sun L, Zhao Y, Li Y, Lin W, Chen D, Sun Q. MAVS maintains mitochondrial homeostasis via autophagy. *Cell Discov*. 2016;2:16024.
104. Cheng J, Liao Y, Xiao L, Wu R, Zhao S, Chen H, Hou B, Zhang X, Liang C, Xu Y, Yuan Z. Autophagy regulates MAVS signaling activation in a phosphorylation-dependent manner in microglia. *Cell Death Differ*. 2017;24:276–87.
105. Jin S, Cui J. BST2 inhibits type I IFN (interferon) signaling by accelerating MAVS degradation through CALCOCO2-directed autophagy. *Autophagy*. 2018;14:171–2.

106. Brubaker SW, Gauthier AE, Mills EW, Ingolia NT, Kagan JC. A bicistronic MAVS transcript highlights a class of truncated variants in antiviral immunity. *Cell*. 2014;156:800–11.
107. Qi N, Shi Y, Zhang R, Zhu W, Yuan B, Li X, Wang C, Zhang X, Hou F. Multiple truncated isoforms of MAVS prevent its spontaneous aggregation in antiviral innate immune signalling. *Nat Commun*. 2017;8:15676.
108. Lakhdari O, McAllister CS, Wang M, Minev I, Prince LS, Eckmann L, Kagnoff MF. TLR3 signaling is downregulated by a MAVS isoform in epithelial cells. *Cell Immunol*. 2016;310:205–210.
109. Ishikawa H, Barber GN. STING is an endoplasmic reticulum adaptor that facilitates innate immune signalling. *Nature*. 2008;455:674–8.
110. Zhong B, Yang Y, Li S, Wang Y-Y, Li Y, Diao F, Lei C, He X, Zhang L, Tien P, Shu H-B. The adaptor protein MITA links virus-sensing receptors to IRF3 transcription factor activation. *Immunity*. 2008;29:538–50.
111. Rice GI, Del Toro Duany Y, Jenkinson EM, Forte GMA, Anderson BH, Ariaudo G, Bader-Meunier B, Baildam EM, Battini R, Beresford MW, Casarano M, Chouchane M, Cimaz R, Collins AE, Cordeiro NJV, Dale RC, Davidson JE, Waele L de, Desguerre I, Faivre L, Fazzi E, Isidor B, Lagae L, Latchman AR, Lebon P, Li C, Livingston JH, Lourenço CM, Mancardi MM, Masurel-Paulet A, McInnes IB, Menezes MP, Mignot C, O'Sullivan J, Orcesi S, Picco PP, Riva E, Robinson RA, Rodriguez D, Salvatici E, Scott C, Szybowska M, Tolmie JL, Vanderver A, Vanhulle C, Vieira JP, Webb K, Whitney RN, Williams SG, Wolfe LA, Zuberi SM, Hur S, Crow YJ. Gain-of-function mutations in IFIH1 cause a spectrum of human disease phenotypes associated with upregulated type I interferon signaling. *Nat Genet*. 2014;46:503–9.
112. Rutsch F, MacDougall M, Lu C, Buers I, Mamaeva O, Nitschke Y, Rice GI, Erlandsen H, Kehl HG, Thiele H, Nürnberg P, Höhne W, Crow YJ, Feigenbaum A, Hennekam RC. A specific IFIH1 gain-of-function mutation causes Singleton-Merten syndrome. *Am J Hum Genet*. 2015;96:275–82.
113. Jang M-A, Kim EK, Now H, Nguyen NTH, Kim W-J, Yoo J-Y, Lee J, Jeong Y-M, Kim C-H, Kim O-H, Sohn S, Nam S-H, Hong Y, Lee YS, Chang S-A, Jang SY, Kim J-W, Lee M-S, Lim SY, Sung K-S, Park K-T, Kim BJ, Lee J-H, Kim D-K, Kee C, Ki C-S. Mutations in DDX58, which encodes RIG-I, cause atypical Singleton-Merten syndrome. *Am J Hum Genet*. 2015;96:266–74.

114. Zaki M, Thoenes M, Kawalia A, Nürnberg P, Kaiser R, Heller R, Bolz HJ. Recurrent and prolonged infections in a child with a homozygous IFIH1 nonsense mutation. *Front Genet.* 2017;8:130.
115. Lamborn IT, Jing H, Zhang Y, Drutman SB, Abbott JK, Munir S, Bade S, Murdock HM, Santos CP, Brock LG, Masutani E, Fordjour EY, McElwee JJ, Hughes JD, Nichols DP, Belkadi A, Oler AJ, Happel CS, Matthews HF, Abel L, Collins PL, Subbarao K, Gelfand EW, Ciancanelli MJ, Casanova J-L, Su HC. Recurrent rhinovirus infections in a child with inherited MDA5 deficiency. *J Exp Med.* 2017;214:1949-1972.
116. Asgari S, Schlapbach LJ, Anchisi S, Hammer C, Bartha I, Junier T, Mottet-Osman G, Posfay-Barbe KM, Longchamp D, Stocker M, Cordey S, Kaiser L, Riedel T, Kenna T, Long D, Schibler A, Telenti A, Tapparel C, McLaren PJ, Garcin D, Fellay J. Severe viral respiratory infections in children with IFIH1 loss-of-function mutations. *Proc Natl Acad Sci U S A.* 2017;114:8342-8347.
117. Pothlichet J, Niewold TB, Vitour D, Solhonne B, Crow MK, Si-Tahar M. A loss-of-function variant of the antiviral molecule MAVS is associated with a subset of systemic lupus patients. *EMBO Mol Med.* 2011;3:142–52.
118. Buskiewicz IA, Montgomery T, Yasewicz EC, Huber SA, Murphy MP, Hartley RC, Kelly R, Crow MK, Perl A, Budd RC, Koenig A. Reactive oxygen species induce virus-independent MAVS oligomerization in systemic lupus erythematosus. *Sci Signal.* 2016;9:ra115.
119. Li K, Qu S, Chen X, Wu Q, Shi M. Promising Targets for Cancer Immunotherapy: TLRs, RLRs, and STING-Mediated Innate Immune Pathways. *Int J Mol Sci.* 2017;18:
120. Poeck H, Besch R, Maihoefer C, Renn M, Tormo D, Morskaya SS, Kirschnek S, Gaffal E, Landsberg J, Hellmuth J, Schmidt A, Anz D, Bscheider M, Schwerd T, Berking C, Bourquin C, Kalinke U, Kremmer E, Kato H, Akira S, Meyers R, Häcker G, Neuenhahn M, Busch D, Ruland J, Rothenfusser S, Prinz M, Hornung V, Endres S, Tüting T, Hartmann G. 5'-triphosphate-siRNA: turning gene silencing and Rig-I activation against melanoma. *Nat Med.* 2008;14:1256–63.
121. Fukuhara H, Ino Y, Todo T. Oncolytic virus therapy: A new era of cancer treatment at dawn. *Cancer Sci.* 2016;107:1373–9.
122. Melzer MK, Lopez-Martinez A, Altomonte J. Oncolytic vesicular stomatitis virus as a viro-immunotherapy: Defeating cancer with a "hammer" and "anvil". *Biomedicines.* 2017;5:
123. Westermarck J, Ivaska J, Corthals GL. Identification of protein interactions involved in cellular signaling. *Mol Cell Proteomics.* 2013;12:1752–63.

124. Brückner A, Polge C, Lentze N, Auerbach D, Schlattner U. Yeast two-hybrid, a powerful tool for systems biology. *Int J Mol Sci.* 2009;10:2763–88.
125. Wodak SJ, Vlasblom J, Turinsky AL, Pu S. Protein-protein interaction networks: the puzzling riches. *Curr Opin Struct Biol.* 2013;23:941–53.
126. Rees JS, Li X-W, Perrett S, Lilley KS, Jackson AP. Protein neighbors and proximity proteomics. *Mol Cell Proteomics.* 2015;14:2848–56.
127. Kim DI, Roux KJ. Filling the void: Proximity-based labeling of proteins in living cells. *Trends Cell Biol.* 2016;26:804–817.
128. Rhee H-W, Zou P, Udeshi ND, Martell JD, Mootha VK, Carr SA, Ting AY. Proteomic mapping of mitochondria in living cells via spatially restricted enzymatic tagging. *Science.* 2013;339:1328–31.
129. Martell JD, Deerinck TJ, Sancak Y, Poulos TL, Mootha VK, Sosinsky GE, Ellisman MH, Ting AY. Engineered ascorbate peroxidase as a genetically encoded reporter for electron microscopy. *Nat Biotechnol.* 2012;30:1143–8.
130. Hung V, Udeshi ND, Lam SS, Loh KH, Cox KJ, Pedram K, Carr SA, Ting AY. Spatially resolved proteomic mapping in living cells with the engineered peroxidase APEX2. *Nat Protoc.* 2016;11:456–75.
131. Lam SS, Martell JD, Kamer KJ, Deerinck TJ, Ellisman MH, Mootha VK, Ting AY. Directed evolution of APEX2 for electron microscopy and proximity labeling. *Nat Meth.* 2014;12:51–4.
132. Hung V, Zou P, Rhee H-W, Udeshi ND, Cracan V, Svinkina T, Carr SA, Mootha VK, Ting AY. Proteomic mapping of the human mitochondrial intermembrane space in live cells via ratiometric APEX tagging. *Mol Cell.* 2014;55:332–41.
133. Mick DU, Rodrigues RB, Leib RD, Adams CM, Chien AS, Gygi SP, Nachury MV. Proteomics of primary cilia by proximity labeling. *Dev Cell.* 2015;35:497–512.
134. Hwang J, Espenshade PJ. Proximity-dependent biotin labelling in yeast using the engineered ascorbate peroxidase APEX2. *Biochem J.* 2016;473:2463–9.
135. Jing J, He L, Sun A, Quintana A, Ding Y, Ma G, Tan P, Liang X, Zheng X, Chen L, Shi X, Zhang SL, Zhong L, Huang Y, Dong M-Q, Walker CL, Hogan PG, Wang Y, Zhou Y. Proteomic mapping of ER-PM junctions identifies STIMATE as a regulator of Ca²⁺ influx. *Nat Cell Biol.* 2015;17:1339–47.
136. Hung V, Lam SS, Udeshi ND, Svinkina T, Guzman G, Mootha VK, Carr SA, Ting AY. Proteomic mapping of cytosol-facing outer mitochondrial and ER membranes in living human cells by proximity biotinylation. *eLife.* 2017;6:

137. Lobingier BT, Hüttenhain R, Eichel K, Miller KB, Ting AY, Zastrow M v., Krogan NJ. An approach to spatiotemporally resolve protein interaction networks in living cells. *Cell*. 2017;169:350-360.e12.
138. Zhen Y, Haugsten EM, Singh SK, Wesche J. Proximity labeling by a recombinant APEX2-FGF1 fusion protein reveals interaction of FGF1 with the proteoglycans CD44 and CSPG4. *Biochemistry*. 2018;57:3807-3816.
139. Myers SA, Wright J, Peckner R, Kalish BT, Zhang F, Carr SA. Discovery of proteins associated with a predefined genomic locus via dCas9-APEX-mediated proximity labeling. *Nat Methods*. 2018;15:437-439.
140. Linder A. Charakterisierung der Liganden von retinoic acid inducible gene I in Vesicular-stomatitis-Virus-infizierten Zellen. Dissertation, LMU München: Medizinische Fakultät. 2017.
141. Agrawal R, Carpino N, Tsygankov A. TULA proteins regulate activity of the protein tyrosine kinase Syk. *J Cell Biochem*. 2008;104:953-64.
142. Frensing T. Defective interfering viruses and their impact on vaccines and viral vectors. *Biotechnology Journal*. 2015;10:681-9.
143. Meier E, Harmison GG, Keene JD, Schubert M. Sites of copy choice replication involved in generation of vesicular stomatitis virus defective-interfering particle RNAs. *J Virol*. 1984;51:515-21.
144. Marcus PI, Gaccione C. Interferon induction by viruses. XIX. Vesicular stomatitis virus—New Jersey: High multiplicity passages generate interferon-inducing, defective-interfering particles. *Virology*. 1989;171:630-3.
145. Strahle L, Garcin D, Kolakofsky D. Sendai virus defective-interfering genomes and the activation of interferon-beta. *Virology*. 2006;351:101-11.
146. Komarova AV, Combredet C, Sismeiro O, Dillies M-A, Jagla B, Sanchez David RY, Vabret N, Coppée J-Y, Vidalain P-O, Tangy F. Identification of RNA partners of viral proteins in infected cells. *RNA Biol*. 2013;10:944-56.
147. Runge S, Sparrer, Konstantin M. J., Lässig C, Hembach K, Baum A, García-Sastre A, Söding J, Conzelmann K-K, Hopfner K-P, Mossman KL. In vivo ligands of MDA5 and RIG-I in measles virus-Infected cells. *PLoS Pathog*. 2014;10:e1004081.
148. Xu J, Mercado-López X, Grier JT, Kim W-K, Chun LF, Irvine EB, Del Toro Duany Y, Kell A, Hur S, Gale M, Raj A, López CB. Identification of a natural viral RNA motif that optimizes sensing of viral RNA by RIG-I. *mBio*. 2015;6:

149. Patel JR, Jain A, Chou Y-y, Baum A, Ha T, García-Sastre A. ATPase-driven oligomerization of RIG-I on RNA allows optimal activation of type-I interferon. *EMBO reports*. 2013;14:780–7.
150. Panda D, Dinh PX, Beura LK, Pattnaik AK. Induction of interferon and interferon signaling pathways by replication of defective interfering particle RNA in cells constitutively expressing vesicular stomatitis virus replication proteins. *J Virol*. 2010;84:4826–31.
151. tenOever BR, Sharma S, Zou W, Sun Q, Grandvaux N, JULKUNEN I, Hemmi H, Yamamoto M, Akira S, Yeh WC, Lin R, Hiscott J. Activation of TBK1 and IKKε kinases by vesicular stomatitis virus infection and the role of viral ribonucleoprotein in the development of interferon antiviral immunity. *J Virol*. 2004;78:10636–49.
152. Weber M, Gawanbacht A, Habjan M, Rang A, Borner C, Schmidt AM, Veitinger S, Jacob R, Devignot S, Kochs G, García-Sastre A, Weber F. Incoming RNA virus nucleocapsids containing a 5'-triphosphorylated genome activate RIG-I and antiviral signaling. *Cell Host Microbe*. 2013;13:336–46.
153. Yao H, Dittmann M, Peisley A, Hoffmann H-H, Gilmore RH, Schmidt T, Schmid-Burgk JL, Hornung V, Rice CM, Hur S. ATP-dependent effector-like functions of RIG-I-like receptors. *Mol Cell*. 2015;58:541–548.
154. Oh S-W, Onomoto K, Wakimoto M, Onoguchi K, Ishidate F, Fujiwara T, Yoneyama M, Kato H, Fujita T. Leader-containing uncapped viral transcript activates RIG-I in antiviral stress granules. *PLoS Pathog*. 2016;12:e1005444.
155. Shivakoti R, Siwek M, Hauer D, Schultz K. L. W., Griffin DE. Induction of dendritic cell production of type I and Type III Interferons by wild-type and vaccine strains of measles virus: Role of defective Interfering RNAs. *J Virol* 2013;87:7816–27.
156. Martínez-Gil L, Goff PH, Hai R, García-Sastre A, Shaw ML, Palese P. A Sendai virus-derived RNA agonist of RIG-I as a virus vaccine adjuvant. *J Virol*. 2013;87:1290–300.
157. Vasou A, Sultanoglu N, Goodbourn S, Randall RE, Kostrikis LG. Targeting pattern recognition receptors (PRR) for vaccine adjuvantation: From synthetic PRR agonists to the potential of defective interfering particles of viruses. *Viruses*. 2017;9:
158. Jones SM, Feldmann H, Ströher U, Geisbert JB, Fernando L, Grolla A, Klenk H-D, Sullivan NJ, Volchkov VE, Fritz EA, Daddario KM, Hensley LE, Jahrling PB, Geisbert TW. Live attenuated recombinant vaccine protects nonhuman primates against Ebola and Marburg viruses. *Nat Med*. 2005;11:786–90.

159. Mayer G, Bendayan M. Biotinyl-tyramide: a novel approach for electron microscopic immunocytochemistry. *J Histochem Cytochem.* 1997;45:1449–54.
160. Pourcelot M, Zemirli N, Silva Da Costa L, Loyant R, Garcin D, Vitour D, Munitic I, Vazquez A, Arnoult D. The Golgi apparatus acts as a platform for TBK1 activation after viral RNA sensing. *BMC Biol.* 2016;14:69.
161. Hung V, Lam SS, Udeshi ND, Svinkina T, Guzman G, Mootha VK, Carr SA, Ting AY. Proteomic mapping of cytosol-facing outer mitochondrial and ER membranes in living human cells by proximity biotinylation. *eLife.* 2017;6:
162. Belgnaoui SM, Paz S, Samuel S, Goulet M-L, Sun Q, Kikkert M, Iwai K, Dikic I, Hiscott J, Lin R. Linear ubiquitination of NEMO negatively regulates the interferon antiviral response through disruption of the MAVS-TRAF3 complex. *Cell Host Microbe.* 2012;12:211–22.
163. Choi YB, Shembade N, Parvatiyar K, Balachandran S, Harhaj EW. TAX1BP1 Restrains Virus-Induced Apoptosis by Facilitating Itch-Mediated Degradation of the Mitochondrial Adaptor MAVS. *Mol Cell Biol.* 2017;37:
164. Tsygankov AY. TULA-family proteins: a new class of cellular regulators. *J Cell Physiol.* 2013;228:43–9.
165. Carpino N, Turner S, Mekala D, Takahashi Y, Zang H, Geiger TL, Doherty P, Ihle JN. Regulation of ZAP-70 activation and TCR signaling by two related proteins, Sts-1 and Sts-2. *Immunity.* 2004;20:37–46.
166. Mikhailik A, Ford B, Keller J, Chen Y, Nassar N, Carpino N. A phosphatase activity of Sts-1 contributes to the suppression of TCR signaling. *Mol Cell.* 2007;27:486–97.
167. Kowanetz K, Crosetto N, Haglund K, Schmidt MHH, Heldin C-H, Dikic I. Suppressors of T-cell receptor signaling Sts-1 and Sts-2 bind to Cbl and inhibit endocytosis of receptor tyrosine kinases. *J Biol Chem.* 2004;279:32786–95.
168. Feshchenko EA, Smirnova EV, Swaminathan G, Teckchandani AM, Agrawal R, Band H, Zhang X, Annan RS, Carr SA, Tsygankov AY. TULA: an SH3- and UBA-containing protein that binds to c-Cbl and ubiquitin. *Oncogene.* 2004;23:4690–706.
169. Slaymaker IM, Gao L, Zetsche B, Scott DA, Yan WX, Zhang F. Rationally engineered Cas9 nucleases with improved specificity. *Science.* 2016;351:84–8.
170. Chen W, Han C, Xie B, Hu X, Yu Q, Shi L, Wang Q, Li D, Wang J, Zheng P, Liu Y, Cao X. Induction of Siglec-G by RNA viruses inhibits the innate immune response by promoting RIG-I degradation. *Cell.* 2013;152:467–78.

-
171. Li X, Yang M, Yu Z, Tang S, Wang L, Cao X, Chen T. The tyrosine kinase Src promotes phosphorylation of the kinase TBK1 to facilitate type I interferon production after viral infection. *Sci Signal*. 2017;10:
 172. Dong G, You M, Fan H, Ding L, Sun L, Hou Y. STS-1 promotes IFN- α induced autophagy by activating the JAK1-STAT1 signaling pathway in B cells. *Eur J Immunol*. 2015;45:2377–88.
 173. Zhou W, Yin Y, Smith E, Chou J, Shumate J, Scampavia L, Spicer TP, Carpino N, French JB. Discovery and characterization of two classes of selective inhibitors of the suppressor of the TCR signaling family of proteins. *ACS Infect Dis*. 2019;5:250–9.
 174. Ketao Jin, Huanrong Lan, Junyu Zhang, Jieqing Lv, Yuan Chen, Kang Yu. UBASH3B promotes tamoxifen resistance and could be negatively regulated by ESR1. *Oncotarget*. 2017;9:8326-8333.
 175. Lee ST, Feng M, Wei Y, Li Z, Qiao Y, Guan P, Jiang X, Wong CH, Huynh K, Wang J, Li J, Karuturi KM, Tan EY, Hoon DSB, Kang Y, Yu Q. Protein tyrosine phosphatase UBASH3B is overexpressed in triple-negative breast cancer and promotes invasion and metastasis. *Proc Natl Acad Sci U S A*. 2013;110:11121–6.
 176. Parashar K, Kopping E, Frank D, Sampath V, Thanassi DG, Carpino N. Increased Resistance to intradermal francisella tularensis LVS infection by inactivation of the Sts phosphatases. *Infect Immun*. 2017;85:
 177. Naseem S, Frank D, Konopka JB, Carpino N. Protection from systemic *Candida albicans* infection by inactivation of the Sts phosphatases. *Infect Immun*. 2015;83:637–45.

8 Appendices

8.1 List of identified candidate proteins

Table 2: List of identified candidate proteins. The proteins are listed in the order of their significance level beginning with the most significant. Proteins in bold back are known as part of the MAVS signaling complex. Proteins highlighted in bold grey have an indirect connection to MAVS.

| P-value (-Logp) | Difference (LFQ intensity) | Gene name |
|--------------------|-------------------------------|--------------------------------------|
| 9,005013374 | -4,380057653 | TBK1 |
| 8,240475337 | -7,393762906 | RNF31 |
| 8,207464697 | -6,012409846 | TRAF2 |
| 7,816895025 | -4,99873956 | IKBKG (NEMO) |
| 7,30927026 | -3,044510841 | BIRC2 |
| 6,539345024 | -2,495058378 | UBASH3B |
| 6,18272406 | -3,121424357 | OPTN |
| 5,940226096 | -3,910493533 | SHARPIN |
| 5,647112211 | -3,873440742 | IKBKB (IKKβ) |
| 5,614276172 | -3,129470825 | CHUK (IKKα) |
| 5,038177645 | -1,653711637 | OPA1 |
| 4,984357487 | -2,000564575 | RBCK1 |
| 4,721023467 | -0,629809697 | ATAD3A |
| 4,481846556 | -2,546969414 | TAX1BP1 |
| 4,414132706 | -2,48865668 | N4BP1 |
| 4,37275035 | -1,147908211 | SRI |
| 4,28042528 | -3,163050334 | CHCHD3 |
| 4,12899366 | -0,97087129 | IMMT |
| 3,902281941 | -2,139049848 | TNIP1 |
| 3,494645291 | -1,627751668 | WIPI1 |
| 3,284339545 | -1,493394534 | CCDC50 |
| 3,247751353 | -0,796626409 | CYB5R3 |
| 3,149360636 | -2,290521304 | TNC |
| 3,147355109 | -0,972751935 | DNM1L (DRP1) |
| 3,062151132 | -0,940523465 | TBC1D15 |
| 2,734228071 | -2,407656352 | TRAF6 |
| 2,605307632 | -0,92519029 | ANXA7 |
| 2,599994702 | -0,970018705 | TAGLN2 |
| 2,566233406 | -1,489706675 | TANK |
| 2,491821171 | -1,36869367 | ARMC10 |
| 2,449905255 | -1,127365112 | LGALS3 |

8.2 List of quantitative reverse transcriptase PCR primers and probes

Table 3: List of qRT-PCR primer and probes. The primers were designed using the online assay design center of Roche Universal probe library (UPL) and obtained from Metabion. The assays without a UPL probe were designed manually and the probes were obtained from Molbiol.

| Target gene | Forward primer (5'→3') | Reverse primer (5'→3') | probe |
|---------------|----------------------------|-----------------------------|-----------------------------|
| human | | | |
| HPRT | tgaccttgattttttgcatacc | cgagcaagacgttcagtcct | UPL #73 |
| IFN-β | cgacactgttcgtgttgta | gaggcacaacaggagagcaa | UPL #25 |
| IL-1β | ctgtctcgcgtgttgaaaga | ttgggtaattttgggatctaca | UPL #78 |
| IL-6 | gatgagtacaaaagtcctgatcca | ctgcagccactggttctgt | UPL #40 |
| IP-10 | gaaagcagtttagcaaggaaaggt | gacatatactccatgtagggaagtga | UPL #34 |
| UBASH3B | gctggacgtgctcctctc | agtcacatgctgcctgaaca | UPL #69 |
| murine | | | |
| β-actin | ggagcagaaggagattactgc | ccaccgatccacacagagta | UPL #63 |
| GAPDH | agcttgtcatcaacgggaag | tttgatgttagtggggtctcg | UPL #9 |
| IFN-β | tccagaatgtctttctgtcttca | gacgtacaacaatagtctcattcca | UPL #67 |
| IL-1β | tgagcaccttctttccttca | catctcggagcctgtagtgc | UPL #62 |
| IL-6 | tgatggatgctacaaactgg | ttcatgtactccaggtagctatgg | UPL #6 |
| IP-10 | atcagcaccatgaaccaag | cctatggcctcattctcac | UPL #3 |
| VSV | | | |
| Leader/N | cgaagacaaacaaaccattattatca | gttgtcaatgattctcttgactgtaac | UPL #2 |
| N | cgaagacaaacaaaccattattatca | tctgcaacttctcggttcaa | UPL #85 |
| P | gcagagtgcacattgaagc | agttatctggcgctccttcat | UPL #7 |
| M | gcgaaggcagggcttatt | gctctggtacattgagcatgg | UPL #60 |
| G | tggttcgagatggctgataa | acttgacccttctgggcatt | UPL #71 |
| L | cctttagaaggggaattggaagaa | tctgccgacttgataggattg | UPL #62 |
| L/trailer | catgaggagactccaaac | gacgaagaccacaaaacc | tcttggtgtttttttttatc tgg |
| Trailer | ggctttgatccttaagacc | gacgaagaccacaaaacc | tcttggtgtttttttttatc tgg |
| DI genome | cgcgggacgaagaccacaaaa | gccgtttgataacttctttggtg | tcttggtgtttttttttatc tgg |

8.3 List of sgRNAs and its oligonucleotides

Table 4: List of sgRNAs and its oligonucleotides. The sgRNAs were designed with the online tool <http://chopchop.cbu.uib.no> and the corresponding oligonucleotides flanked by the BbsI restriction sites (*in italic*) were ordered by Metabion.

| Target gene | sgRNA | Oligo top strand (5'→3') | Oligo bottom strand (5'→3') |
|----------------|------------------------------|---------------------------|----------------------------------|
| CCDC50 | gtaactatctgcataagcacg gg | caccgtaactatctgcataagcac | <i>aaacgtgcttatgcagatagttac</i> |
| CHCHD3 | gatgttgctttccagctttcg g | caccgatgttgctttccagcttt | <i>aaacaaagctggaaaagcaacatc</i> |
| N4BP1 | gaccttgcacagtaaccgaa gg | caccgaccttgcacagtaaccga | <i>aaactcgggttactgatgcaaggtc</i> |
| OPTN | gatttgaggagctttcggcct gg | caccgatttgaggagctttcggcc | <i>aaacggccgaaagctcctcaaac</i> |
| SRI | gcagcaaagtaaccatacag cgg | caccgcagcaaagtaaccatacag | <i>aaacctgtatggttactttgctgc</i> |
| TNC | gttgccccgaccgctacaga agg | caccgttgccccgaccgctacaga | <i>aaactctgtagcggtcggggcaac</i> |
| UBASH3B sg1 | gacgacgtatagagctccag ggg | caccgacgacgtatagagctccag | <i>aaacctggagctctatacgtcgtc</i> |
| UBASH3B sg2 | ggctggctgttgaccctcagc gg | caccggctggctgttgaccctcag | <i>aaacctgaggggtcaacagccagcc</i> |
| WIPI1 | gcctgaggcattgaagggtga tgg | caccgcctgaggcattgaagggtga | <i>aaactcaccttcaatgcctcaggc</i> |

8.4 List of primers for target site amplification

Table 5: List of primers for target site amplification. The listed primers were obtained from Metabion and expected amplicon size is given with the expected fragment after T7 digestion.

| Target gene | Forward primer (5'→3') | Reverse primer (5'→3') | Amplicon (T7 cleaved) (bp) |
|-------------|-------------------------|------------------------|----------------------------|
| CCDC50 | tgtaagcagtcacatctggcatt | tgccacacatctaaatgtaccc | 425 (170/255) |
| CHCHD3 | taaaggagtagtgctgtggggt | ggattcaagagtgggaagagaa | 520 (330/190) |
| N4BP1 | acagaaacatgaagtctggggt | tacgtaattgcaacattgctcc | 480 (170/310) |
| OPTN | tcctggtatctcaagatggctt | cagatgacctttctgattccc | 650 (150/400) |
| SRI | tggttacctagtttgactca | aagcaaagggactcagtaccac | 500 (250/250) |
| TNC | acaaatggttctcaagccagat | tggtgagacacagaggcttggt | 540 (160/380) |
| UBASH3B sg1 | atgccaatgttaagtagcagca | ctgaattaggaggagatggtgg | 420 (180/240) |
| UBASH3 sg2 | ttaatggccaaatgctactcct | ccagtactcccaaacacaaca | 365 (95/270) |
| WIPI1 | gagggagaaaggagaaaagagg | attccaggcagaagacatcaat | 550 (400/150) |

8.5 List of abbreviations

| | |
|-------------------------------|--|
| 3p-RNA | Triphosphate RNA |
| Aa | Amino acid |
| ALR | AIM2-like-receptors |
| APEX | Ascorbate peroxidase |
| ATP | Adenosine triphosphate |
| BHK | Baby hamster kidney |
| BMDM | Bone marrow-derived macrophage |
| BME | β -Mercaptoethanol |
| Bp | Base pair |
| BSA | Bovine serum albumine |
| CARD | Caspase recruitment domain |
| cDNA | Complementary DNA |
| CHX | Cycloheximide |
| CLR | C-type-lectine receptor |
| CTD | Carboxy-terminal domain |
| DI | Defective interfering |
| DNA | Desoxyribonucleic acid |
| Dox | Doxycycline |
| Ds | Double stranded |
| ECL | Enhanced chemiluminescence |
| e.g. | Exempli gratia |
| EGFR | Epidermal growth factor receptor |
| ELISA | Enzyme-linked immunosorbent assay |
| EMCV | Encephalomyocarditis virus |
| ER | Endoplasmic reticulum |
| FCS | Fetal calf serum |
| FITC | Fluorescein isothiocyanate |
| FL | Full-length |
| GM-CSF | Granulocyte-macrophage colony-stimulating factor |
| GPCR | G-protein-coupled receptor |
| h | Hour |
| H ₂ O ₂ | Hydrogen peroxide |
| HEK | Human embryonic kidney |
| Hpi | Hours post infection |
| HRP | Horse radish peroxidase |
| hTERT | Human telomerase reverse transcriptase |
| i.e. | Id est |
| IFN | Interferon |
| IKK α | I κ B kinase α |
| IL-6 | Interleukin 6 |
| IMM | Inner mitochondrial membrane |
| IMS | Mitochondrial intermembrane space |
| IP | Immunoprecipitation |
| IP-10 | Interferon γ induced protein 10 |
| IRF3 | Interferon regulatory factor 3 |
| ISG | Interferon-stimulated gene |
| Kb | Kilo base pair |

| | |
|----------|---|
| KDa | Kilo Dalton |
| KEGG | Kyoto encyclopedia of genes and genomes |
| KO | Knockout |
| LC/MS | Liquid chromatography/ mass spectrometry |
| LFQ | Label-free quantification |
| LGP2 | Laboratory of genetics and physiology 2 |
| M | Molar |
| MAM | Mitochondria-associated membranes |
| MAVS | Mitochondrial antiviral signaling protein |
| M-CSF | Macrophage colony-stimulating factor |
| MDA5 | Melanoma differentiation antigen 5 |
| Min | Minute |
| MOI | Multiplicity of infection |
| mRNA | Messenger RNA |
| MS | Mass spectrometry |
| MV | Measles virus |
| NEMO | NFκB essential modulator |
| NES | Nuclear export sequence |
| NFκB | Nuclear factor κ B |
| NGS | Next generation sequencing |
| NLR | NOD-like receptors |
| nt | Nucleotide |
| OMM | Outer mitochondrial membrane |
| OPTN | Optineurin |
| P- | Phospho- |
| PAMP | Pathogen-associated molecular pattern |
| PBS | Phosphate-buffered saline |
| PCA | Principal component analysis |
| PCR | Polymerase chain reaction |
| pIC | Polyinosinic:polycytidylic acid |
| PPI | Protein protein interaction |
| PRR | Pattern recognition receptor |
| PVDF | Polyvinyliden fluoride |
| qRT-PCR | Quantitative reverse transcriptase PCR |
| RIG-I | Retinoic acid inducible gene I |
| RLR | RIG-I-like receptor |
| RNA | Ribonucleic acid |
| RNP | Ribonucleoprotein |
| ROS | Reactive oxygen species |
| RT | Room temperature |
| SCC | Single cell clone |
| SDS | Sodium dodecyl sulfate |
| SDS-PAGE | SDS polyacrylamide gel electrophoresis |
| Sec | Second |
| SEM | Standard error of mean |
| sgRNA | Single-guide RNA |
| SRI | Sorcin |
| Ss | Single-stranded |

| | |
|----------------|--|
| STING | Stimulator of interferon genes |
| TANK | TRAF family member associated NFκB activator |
| TBK1 | TANK binding kinase 1 |
| TBS | Tris-buffered saline |
| TCR | T-cell receptor |
| Tet | Tetracycline |
| TIM | TRAF-interacting motifs |
| TLR | Toll-like receptors |
| TM | Transmembrane |
| TNBC | Triple-negative breast cancer |
| TNC | Tenascin C |
| TRAF | TNF receptor-associated factor |
| Ut | Untransfected |
| UTR | Untranslated region |
| VSV | Vesicular stomatitis virus |
| Wt | Wildtype |
| Y2H | Yeast-two-hybrid |
| $\Delta\psi_m$ | Mitochondrial membrane potential |

9 Acknowledgement

Firstly, I would like to thank Prof. Dr. med. Simon Rothenfußer for the supervision of my thesis. He continuously supported my work with discussions, ideas and motivation and also left enough room for realization of own ideas.

I also thank Prof. Dr. med. Stefan Endres for the opportunity to work in the Division of Clinical Pharmacology and for creating a unique and motivating work environment.

Further, my sincere thanks go to our collaboration partners Prof. Dr. Axel Imhof and Natalia Kochanova for mass spectrometric analysis and for their help in data analysis.

I thank Dr. rer. biol. hum. Dharmendra Pandey for introducing me into the lab work and for showing me the secrets of successful experiments in molecular biology.

Finally, I want to thank all co-students and technicians who created an inspiring and lively atmosphere in the daily lab life.

10 Curriculum vitae

Work experience

02/2014 – 09/2018 **PhD student, Ludwig-Maximilian-Universität München, Munich, Germany**

Division of Clinical Pharmacology, University Hospital

- Research group of Prof. Simon Rothenfußer
- PhD thesis: *Identification and characterization of activators and modulators in the antiviral RIG-I-like receptor pathway*

11/2013 – 01/2014 **Student assistant, University of Leipzig, Germany**

Department of Ophthalmology

- Screening of knockout mice via PCR

10/2011 – 09/2012 **Student assistant, Fraunhofer institute of cell therapy and immunology, Leipzig, Germany**

- Research on ischemia: cell culture, behavioral tests with rats

02/2011 – 05/2011 **Student assistant, University of Leipzig, Germany**

Department of Otorhinolaryngology

- Cancer research: cell culture, qRT-PCR, ELISA, immunofluorescence

10/2009 – 04/2010 **Student assistant, University of Leipzig, Germany**

Department of Ophthalmology

- generation of DNA constructs: PCR, cloning, transfection

Education

10/2011 – 10/2013 **Master studies in Biology, University of Leipzig, Germany**

- Focus: cell biology and genetics
- Master thesis: *Involvement of mitochondria-mediated apoptosis in rubella virus-induced cell death (1,3)*
- Degree: Master of Science (1,3)

10/2007 – 09/2010 Bachelor studies in Biology, University of Leipzig, Germany

- Bachelor thesis: *Generation of DNA constructs for conditional expression of murine pigment-epithelium-associated factor (mPEDF)* (1,3)
- degree: Bachelor of Science (1,9)

09/2000 – 06/2007 Spreeland-Gymnasium, Cottbus, Germany

- Degree: A-Level ("Allgemeine Hochschulreife") (1,3)

Honors

02/2014 – 09/2014 Stipend awarded by the DFG Graduate School 2012 "Oligonucleotides in cell biology and therapy"

04/2015 – 08/2017 Stipend awarded by the "Studienstiftung des deutschen Volkes"

Further Skills

Languages German (native)
 English (fluent)
 Latin (Latinum)
 French (basic)

Computer Microsoft Office (excellent skills in power point and excel), Prism GraphPad (statistical data analysis), Adobe Photoshop and Illustrator (image processing), Endnote (scientific referencing)

Publications

1. Posel C, Scheibe J, Kranz A, **Bothe V**, Quente E, Frohlich W, Lange F, Schabitz WR, Minnerup J, Boltze J, Wagner DC. *Bone marrow cell transplantation time-dependently abolishes efficacy of granulocyte colony-stimulating factor after stroke in hypertensive rats.* Stroke; 2014; 45:2431-7.

2. Claus C, Manssen L, Hübner D, Roßmark S, **Bothe V**, Petzold A, Große C, Reins M, Mankertz, A, Frey Teryl K, Liebert Uwe G. *Activation of the mitochondrial apoptotic signaling platform during rubella virus infection.* Viruses; 2015; 12: 6108–6126.